

## TABLE OF CONTENTS

<b>1. CHAPTER 1 - INTRODUCTION</b> .....	1
<b>2. CHAPTER 2 - METHODOLOGY</b> .....	4
<b>3. CHAPTER 3 - REGIONAL AND LOCAL GEOLOGY</b> .....	10
<b>4. CHAPTER 4 - PETROGRAPHY</b> .....	16
4.1. Hand specimens .....	16
4.1.1. Disseminated, matrix and breccia assemblages.....	16
4.1.2. Massive sulfides - Fe-rich and Cu-rich .....	18
4.2. Polished section descriptions .....	20
4.2.1. Disseminated sulfide .....	22
4.2.2. Breccia sulfide .....	24
4.2.3. Silicate assemblage and textures .....	27
4.2.4. Matrix and Fe-rich assemblages .....	30
4.2.5. Cu-rich assemblage .....	38
4.3. Platinum-Group Minerals, Precious-Metal Minerals, Tellurides, Bismuthides and Arsenides assemblages.....	42
<b>5. CHAPTER 5 - WHOLE ROCK GEOCHEMISTRY</b> .....	46
5.1. Primitive mantle normalized patterns .....	51
5.2. Comparison with previously published data of Voisey's Bay.....	54
5.3. Comparison with other deposits.....	62
5.3.1. Disseminated sulfide .....	62
5.3.2. Breccia sulfide .....	64
5.3.3. Matrix sulfide .....	66
5.3.4. Massive Fe-rich sulfide .....	68
5.3.5. Massive Cu-rich sulfide.....	70
<b>6. CHAPTER 6 - WHOLE ROCK INTERPRETATION</b> .....	72
6.1. Sulfide segregation.....	72
6.2. Sulfide fractional crystallization model .....	75
<b>7. CHAPTER 7 - LA-ICP-MS RESULTS</b> .....	78
7.1. Spidergrams and binary diagrams.....	82
7.1.1. Pyrrhotite .....	82
7.1.2. Pentlandite .....	84
7.1.3. Palladium in pentlandite .....	86

7.1.4. Chalcopyrite .....	89
7.2. Comparison with other deposits.....	92
7.2.1. Matrix + breccia sulfide.....	92
7.2.2. Fe-rich sulfide.....	95
7.2.3. Cu-rich sulfide .....	98
<b>8. CHAPTER 8 - LA-ICP-MS INTERPRETATION .....</b>	<b>100</b>
8.1. Mass balance .....	100
<b>9. CHAPTER 9 - DISCUSSION .....</b>	<b>109</b>
9.1. Sulfide fractionation.....	109
9.1.1. Sulfide fractionation and chalcophile elements distribution among base-metal sulfide minerals .....	109
9.1.2. Palladium diffusion into pentlandite .....	112
9.2. Evolution of sulfide liquid during the fractional crystallization in the Ovoid ...	115
9.3. Implications of depth emplacement .....	117
9.4. Where are the platinum-group elements? .....	120
9.5. Application to exploration.....	122
<b>10. CHAPTER 10 - CONCLUSION .....</b>	<b>126</b>
<b>11. CHAPTER 11 - REFERENCES.....</b>	<b>129</b>
<b>12. CHAPTER 12 - APPENDIX.....</b>	<b>140</b>
12.1. Correction factors for Ru <sup>101</sup> , Rh <sup>103</sup> and Pd <sup>108</sup> .....	140
12.2. Composition of pyrrhotite by LA-ICP-MS analysis .....	141
12.3. Composition of pentlandite by LA-ICP-MS analysis .....	145
12.4. Composition of chalcopyrite by LA-ICP-MS analysis .....	149
12.5. Composition of cubanite by LA-ICP-MS analysis .....	151
12.6. Reference material for LA-ICP-MS analysis.....	153

## LIST OF TABLES

Table 1: Comparison between certified values for reference materials (WMS-1a, SMR-1 and KPT-1) and values measured in this study. ....	6
Table 2: Sample mineralogy from the Ovoid ore body, Voisey's Bay. ....	21
Table 3: Platinum-group minerals, PMM and As-Bi-Te phases and their textural relationship identified in the Ovoid ore body .....	44
Table 4: Whole rock composition of samples from the Ovoid ore body.....	47
Table 5: Whole rock analysis for massive sulfides, breccia and matrix troctolite recalculated to 100% sulfides. ....	55
Table 6: Hypothetical initial liquid composition for the Ovoid.....	75
Table 7: Composition of each BMS as determined by LA-ICP-MS and weight fraction of each BMS. ....	80
Table 8: Sulfur, Co, Ni and Pd content for different pentlandite.....	87
Table 9: Result of mass balance calculation for Fe-rich, Cu-rich and matrix + breccia assemblages .....	102
Table 10: Partition coefficient from chalcophile elements.....	105

## LIST OF FIGURES

Figure 1: Voisey's Bay geological setting.....	11
Figure 2: A 3D view of the Voisey's Bay ore bodies.....	13
Figure 3: West facing geologic section through the Ovoid ore body.....	15
Figure 4: Ovoid pit, plan view of the samples location.....	15
Figure 5: Representative samples of disseminated sulfide, matrix sulfide and breccia sulfide from the Ovoid ore body.....	17
Figure 6: Representative massive sulfide samples from the Ovoid ore body.....	19
Figure 7: Reflected light photomicrographs of typical disseminated sulfide texture from the Ovoid ore body.....	23
Figure 8: Reflected light photomicrographs of typical breccia sulfide textures from the Ovoid ore body.....	26
Figure 9: Transmitted light photomicrographs of silicate texture in; breccia, matrix and disseminated sulfides.....	29
Figure 10: Reflected light photomicrographs of deformation evidences.....	31
Figure 11: Exsolution lamellae of troilite in pyrrhotite.....	33
Figure 12: Reflected light photomicrographs of typical matrix and Fe-rich sulfide textures from the Ovoid ore body.....	36
Figure 13: Reflected light photomicrographs of typical Cu-rich sulfide textures from the Ovoid ore body.....	40
Figure 14: Backscattered electron images of PGM, PMM and bismuth found in massive sulfides from the Ovoid ore body.....	45
Figure 15: Plots of Ag, As, Au, Bi, Cd, Co, Cu, Fe, Ir, Ni, Os.....	49
Figure 16: Primitive mantle normalized multi-element diagram. Disseminated, breccia, matrix, Fe-rich and Cu-rich assemblages are compared.....	52

Figure 17: Multi-element diagram showing partition coefficients .....	53
Figure 18: Primitive mantle normalized multi-element diagram for massive sulfides from the Ovoid.....	57
Figure 19: Primitive mantle normalized multi-element diagram. Breccia sulfide from this study and from Naldrett et al. (2000a) are compared. ....	59
Figure 20: Primitive mantle normalized multi-element diagram. Matrix sulfide from the Ovoid and matrix from the Mini-Ovoid are compared.....	61
Figure 21: Primitive mantle normalized multi-element diagram for disseminated sulfide assemblage.....	63
Figure 22: Primitive mantle normalized multi-element diagram. Breccia sulfide assemblage.....	65
Figure 23: Primitive mantle normalized multi-element diagram. Matrix sulfide assemblage.....	67
Figure 24: Primitive mantle normalized multi-element diagram. Massive Fe-rich sulfides.....	69
Figure 25: Primitive mantle normalized multi-element diagram. Massive Cu-rich sulfides.....	71
Figure 26: Binary diagrams showing that <b>A:</b> Ni; <b>B:</b> Co; <b>C:</b> Fe; <b>D:</b> Cu; and <b>E:</b> Pd correlate with S.....	74
Figure 27: Sulfide fractional crystallization model .....	77
Figure 28: Plots of time (s) versus counts for the base-metal sulfides minerals .....	79
Figure 29: Primitive mantle normalized multi-element diagram of pyrrhotite .....	83
Figure 30: Primitive mantle normalized multi-element diagram of pentlandite .....	85
Figure 31: Time-signal diagrams (time (s) vs counts) of Pd content in different textures of pentlandite .....	88

Figure 32: Primitive mantle normalized multi-element diagram of chalcopyrite .....	90
Figure 33: Binary diagrams. <b>A:</b> Zn vs Cd shows a strong positive correlation.....	91
Figure 34: Binary diagram, Ni vs Co shows a strong positive correlation.....	91
Figure 35: Primitive mantle normalized multi-element diagram of matrix + breccia assemblage.....	94
Figure 36: Primitive mantle normalized multi-element diagram of Fe-rich assemblage. .....	97
Figure 37: Primitive mantle normalized multi-element diagram of Cu-rich assemblage. .....	99
Figure 38: Mass balance of chalcophile and platinum-group elements for Fe-rich assemblage from the Ovoid. ....	107
Figure 39: Mass balance of chalcophile and platinum-group elements for Cu-rich assemblage from the Ovoid. ....	107
Figure 40: Mass balance of chalcophile and platinum-group elements for matrix + breccia assemblage from the Ovoid.....	108
Figure 41: Schematic model of the crystallization history of the Ovoid ore body .....	114
Figure 42: West facing geologic section through the Ovoid ore body showing (Bi+Te+As+Sb) and Pd / Ir ratio .....	116
Figure 43: Nickel-Cu-PGE deposits settings showing the depth of formation.....	119
Figure 44: <b>A:</b> Plan view of the Ovoid, Mini-Ovoid and Southeast Extension Zone projected to the surface.....	121
Fig. 45: Binary diagram of Rh vs Pd (in pentlandite).....	125

## ACKNOWLEDGMENTS

There are so many people who have helped me on this journey. I sincerely wish to express my gratitude to them.

I have the honor to thank my supervisor Sarah-Jane Barnes for giving me this excellent opportunity. Her confidence, patience, passion for teaching and relentless support pushed me to get the best out of myself. Thank you Sarah!

Thanks to my co-supervisor Philippe Pagé for revising and for the intellectual, personal and scientific support.

This project was fully funded by the Canada Research Chair in Magmatic Metallogeny and Multidisciplinary Applied Geochemistry Network (MAGNET). I want to express my gratitude to them.

Thanks are extended to Marko Prasek and Dany Savard from LabMaTer, without them I could not have done all the geochemical and LA-ICP-MS analysis. Also I want to thank Pierre-Jean who spent his time going with me at SEM lab for analysis.

This thesis has benefited greatly from the revisions of the examiners. I sincerely thank Sarah-Jane Barnes, Philippe Pagé, Michael Higgins and Sarah Dare.

I also have the pleasure of thanking my friend Charley Duran for the intellectual and scientific support and my other friends Ben Cave and Cheyenne Sica for English revisions on my text. They have been there to enlighten me in the obscure moments of my research. Thank you Charley, Ben and Chey!

I would also like to thank the entire staff of the teaching unit in Earth Sciences at UQAC and students from REDIST. At their side, I was able to enjoy an optimal working environment.

I could not forget my friends that were my companions during this time and who became real and good friends. Thank you Gugu, Alexandre, João, Deborah, Silvaninha, Bruna, Renato, Jaíne, Shahriyar, Charley, Ben, Cheyenne, Pierre-Jean and Lucas. Also, I want to thank my good friends from Brazil who are: Iguinho, ET, Biel, Jabu, Migui, Leo, Tuta, Hebert, Eltinho, Fabinho, Dani, Mahyra. Thank you everybody for sharing good moments with me!

I especially want to thank my family who have always supported and encouraged me. I dedicate this work to my parents and my brother, who I know, are proud of me wherever they are. Also I want to thank the rest of my family (my aunts, uncles and cousins) who have always sent me words of encouragement. Special thank for Márcia, Maria, Cláudia, Amid, Cleide, Beto, Zé, Leo, Bruno, Michelle and Marcinho.

Last but not least, I thank God for giving me the health and wisdom to face all the adversities that have arisen during this time.

## CHAPTER 1

### 1. INTRODUCTION

Magmatic sulfide deposits which contain nickel, copper and platinum-group elements (PGE) are generally found at the base of mafic and ultramafic rock assemblages. Typically in magmatic sulfide deposits, Ni and Cu are the main resources, and the PGE are by-products (Barnes and Lightfoot 2005).

Some deposits in the Sudbury (Naldrett et al. 1982; Li et al. 1992; Dare et al. 2014) and Noril'sk mining camps (Distler et al. 1977; Zientek et al. 1994) show a variation and zonation in their Fe and Cu contents (e.g., some of them are Fe-rich ore and some are Cu-rich ore). The Fe-rich ores typically are enriched in IPGE (Os, Ir, Ru), Rh, Ni and Co, whilst the Cu-rich ores are typically enriched in Cu, Zn, As, Ag, Cd, Te, Bi, and Pb. Experimental work (Kullerud et al. 1965; Naldrett 1969; Barnes et al. 1997; Mungall et al. 2005; Liu and Brenan 2015) suggests this zonation likely results from the fractional crystallization of the sulfide liquid, where Fe-rich zones represent cumulates of the first mineral to crystallize, monosulfide solid-solution (MSS), and the Cu-rich zones represents combination of fractionated liquid and intermediate solid-solution (ISS) cumulate. As the sulfides cool, MSS exsolved to form pyrrhotite and pentlandite with minor chalcopyrite, and ISS exsolved to form cubanite and chalcopyrite, together with minor amounts of pentlandite and pyrrhotite.

The Voisey's Bay sulfide deposit is located in Labrador, Canada, and has an estimated resource of 142 million tonnes at 1.59% Ni; 0.85% Cu; 0.09% Co and less than 0.5g/t PGE (Naldrett and Li 2007). The intrusions hosting the Voisey's Bay deposits was emplaced  $1332.7 \pm 1.0$  Ma (U-Pb) (Amelin et al. 1999) within the suture zone between the Archean Nain and Paleoproterozoic Churchill provinces (Barnes and

Lightfoot 2005). The Ovoid ore body that is part of the Voisey's Bay deposits, and consists of up to 110 m thickness of massive sulfide hosted within a bowl-shaped structure (Li and Naldrett 1999). The ore body shows a zonation with a Cu-rich center and Fe-rich margins.

In the last 10 years, laser ablation inductively coupled plasma mass spectrometry (LA-ICP-MS) has become an important and powerful tool for measuring a full suite of trace elements in pyrrhotite, pentlandite, chalcopyrite and cubanite at ppm to ppb-levels. This technique has led to a better understanding of the petrogenesis of the base-metal sulfides (BMS) and has indicated which BMS host the PGE and other chalcophile elements. The chalcophile element contents of BMS from PGE rich deposits have been reported by, Holwell and McDonald 2007; Godel et al. 2007; Godel and Barnes 2008; Barnes et al. 2008; Hutchinson and McDonald 2008; Holwell and McDonald 2010; Djon and Barnes 2012; Osbahr et al. 2013; Duran et al. 2016b; Piña et al. 2016. For Ni – Cu magmatic sulfide deposits results have been reported by Huminicki et al. 2005; Barnes et al. 2006; Dare et al. 2010b, 2011, 2014; Piña et al. 2012, 2014; Godel et al. 2012; Chen et al. 2014. The results for deposits demonstrates that (1) pyrrhotite and pentlandite host the bulk of Os, Ir, Ru, Rh, Re and Co; (2) the bulk of Ni and Pd is in pentlandite, with Pd also found in platinum-group minerals (PGM), Pd minerals; (3) chalcopyrite / cubanite contains the bulk of Cu, Ag, Zn, Cd; and (4) Pt, Au and semi-metals (Bi, Te, As, Sb) are not commonly present in the BMS and form their own minerals, such as Pt-Pd arsenides or bismuth-tellurides and antinomides.

The main purpose of this research is to contribute to the development of the use of the BMS geochemistry as an exploration technique. It is thought that most magmatic Ni-Cu-PGE sulfide deposits that occur at or near the surface have already been discovered. Thus it is important to develop new tools to help exploration to find

deposits at depth and under cover. To help develop an effective exploration tool capable of helping to make new discoveries, a better understanding of the trace element fingerprints in BMS from major deposits is necessary. Data for trace element contents of BMS has already been obtained from the large PGE and Ni-Cu deposits (Bushveld, Great Dyke, Stillwater, Penikat, Noril'sk, Lac des Iles, Sudbury, Jinchuan, and Aguablanca). However, to date the base metals sulfides of Voisey's Bay, one of the world's largest magmatic Ni-Cu sulfide deposits, have not yet been completely investigated. This study is intended to fill this crucial gap. An additional aim of this research is to document the behavior of the elements (Te, As, Bi, Sb and Sn, TABS) that do not partition into MSS or ISS and which are commonly found in platinum-group minerals to establish how they behave during the fractional crystallization of sulfide liquid.

This study provides detailed documentation and description of PGE and other chalcophile elements, and their distribution among the BMS minerals in the Ovoid ore body from Voisey's Bay deposit. Incorporating this, a model is presented to explain the trace element distribution among the BMS. Finally, data gathered during this study is compared to previously published BMS trace element data from important magmatic sulfide deposits (Bushveld, Plat Reef, Great Dyke, Stillwater, Penikat, Noril'sk, Lac des Iles, Jinchuan, Sudbury and Aguablanca) in an attempt to develop and assess previously developed exploration tools.

## CHAPTER 2

### 2. METHODOLOGY

Twenty one samples from the Ovoid ore body were chosen for this study. One of which consists of disseminated sulfide containing <10 % S, one consists of breccia sulfide and two consist of matrix sulfide, containing 10-25 % S. In addition, thirteen samples consisting of Fe-rich massive sulfides and four samples consisting of Cu-rich massive sulfides were studied. Samples were selected to show maximum variation in BMS mineralogy with the aim of tracing the crystallization of the sulfide liquid. About 600 g of each sample was crushed, and approximately 200 g of each sample was pulverized to less than 200 mesh in an alumina ceramic mill at Université du Québec à Chicoutimi (UQAC).

A petrographic study was carried out on the polished sections from each sample. Sulfides, oxides and silicates were described using an optical microscope OLYMPUS DP71 coupled with a digital camera at UQAC. This was undertaken to establish which oxide, silicate and base-metal sulfide minerals are present and characterize their textures. An additional aim was to investigate whether the sulfides represent igneous, metamorphic, or hydrothermal sulfides, or a combination of these.

Platinum-group minerals, precious-metal minerals (PMM), tellurides, bismuthides and arsenides were searched for using a scanning electron microscope (SEM) JEOL JSM-6480LV at Centre universitaire de recherche sur l'Aluminium (CurAl) at UQAC. The backscattered electron images were collected with an accelerating voltage of 20 keV, working distance of 9.0 mm and a beam size of 0.2  $\mu\text{m}$ . Astimex reference material from University of Toronto was used to calibrate and monitor the data. For calibration:  $\text{SnO}_2$  (cassiterite),  $\text{Cu}_2\text{O}$  (cuprite),  $\text{CoAsS}$  (cobaltite),

PbS (galena), FeS<sub>2</sub> (marcasite), MoS<sub>2</sub> (molybdenite), (FeNi)<sub>9</sub>S<sub>8</sub> (pentlandite), ZnS (sphalerite), Sb<sub>2</sub>S<sub>3</sub> (stibnite), Bi<sub>2</sub>Se<sub>3</sub> (bismuth selenide) and Sb<sub>2</sub>Te<sub>3</sub> (antimony telluride) were used.

Sulfur, Fe, As, Ag, Co, Cu, Ni, Se and Zn from the massive sulfides were determined by instrumental neutron activation analysis (INAA) after irradiation at École Polytechnique, Montréal, Slowpoke laboratory, and data reduction at UQAC, according to the method of Bédard et al. (2008). Bismuth, Cd, Sn, Pb, Sb, Re and Te for massive and disseminated sulfides were determined by aqua regia digestion and inductively coupled plasma mass spectrometry (ICP-MS) at Actlabs, Ancaster (Ontario). The same method was used to determine As, Ag, Co, Se and Zn in the disseminated sulfide samples, but at LabMaTer (UQAC). Sulfur, Fe, Ni and Cu from disseminated sulfides were determined by hand held XRF at LabMaTer (UQAC). Platinum-group elements and Au for all samples were determined at LabMaTer by Ni-sulfide fire assay, followed by Te co-precipitation and ICP-MS solution analysis (Savard et al. 2010). Table 1 compares the certified value for the reference materials (WMS-1a, SMR-1 and KPT-1) and the value measured in this study.

Table 1: Comparison between certified values for reference materials (WMS-1a, SMR-1 and KPT-1) and values measured in this study.

Sample	WMS-1a		KPT-1		SMR-1		SMR-1	
	INAA	Working values	INAA	Working values	AR	Working values	HH	Working values
<b>Ag (ppm)</b>	2.00	3.7 ± 1.3	0.91	0.75 ± 0.15	9.72	10.5	n.a.	n.a.
<b>As (ppm)</b>	30.9	30.9 ± 4.8	2.14	2.2 ± 0.53	1.90	3.32	n.a.	n.a.
<b>Au (ppb)</b>	n.a.	300	n.a.	n.a.	n.a.	n.a.	n.a.	n.a.
<b>Bi (ppm)</b>	n.a.	1.20	n.a.	n.a.	0.87	0.8	n.a.	n.a.
<b>Cd (ppm)</b>	1.25	1.40	n.a.	n.a.	3.42	3.3	n.a.	n.a.
<b>Co (ppm)</b>	1380	1450 ± 170	74.10	78.92 ± 5.6	1610	1614	n.a.	n.a.
<b>Cu (%)</b>	1.05	1.39 ± 0.045	0.10	0.111 ± 0.010	n.a.	n.a.	4.46	3.70
<b>Fe (%)</b>	43.9	45.4 ± 1.2	8.38	8.56	n.a.	n.a.	44.09	48.67
<b>Ir (ppb)</b>	n.a.	n.a.	n.a.	n.a.	n.a.	n.a.	n.a.	n.a.
<b>Ni (%)</b>	2.30	3.22 ± 0.15	0.095	0.101 ± 0.007	n.a.	n.a.	7.9	7.18
<b>Os (ppb)</b>	n.a.	n.a.	n.a.	n.a.	n.a.	n.a.	n.a.	n.a.
<b>Pb (ppm)</b>	n.a.	n.a.	n.a.	n.a.	9.90	7.60	n.a.	n.a.
<b>Pd (ppb)</b>	n.a.	1450 ± 110	n.a.	n.a.	n.a.	n.a.	n.a.	n.a.
<b>Pt (ppb)</b>	n.a.	1910 ± 100	n.a.	n.a.	n.a.	n.a.	n.a.	n.a.
<b>Re (ppb)</b>	n.a.	n.a.	n.a.	n.a.	0.16	n.a.	n.a.	n.a.
<b>Rh (ppb)</b>	n.a.	222 ± 52	n.a.	n.a.	n.a.	n.a.	n.a.	n.a.
<b>Ru (ppb)</b>	n.a.	145 ± 0.96	n.a.	n.a.	n.a.	n.a.	n.a.	n.a.
<b>S (%)</b>	26.0	28.1	n.a.	n.a.	n.a.	n.a.	32.47	36.13
<b>Sb (ppm)</b>	6.84	6.92 ± 0.96	8.80	10.01	2.04	2.4	n.a.	n.a.
<b>Se (ppm)</b>	107	87	2.60	2.93	40.9	51.67	n.a.	n.a.
<b>Sn (ppm)</b>	n.a.	2.30	n.a.	n.a.	1.45	0.97	n.a.	n.a.
<b>Te (ppm)</b>	n.a.	n.a.	n.a.	n.a.	5.72	4.49	n.a.	n.a.
<b>Zn (ppm)</b>	172	130 ± 19	143.00	120	230	211.6	n.a.	n.a.

Abbreviations: INAA = instrumental neutron activation analysis; AR = aqua regia; HH = handheld X-ray fluorescence; FA = Fire assay and n.a. = not available.

Table 1 continuation: Comparison between certified value for standards (WMS-1a, SMR-1 and KPT-1) and value measured in this study.

Sample	KPT-1		WMS-1a		SMR-1	
	HH	Working values	FA	Working values	FA	Working values
<b>Ag (ppm)</b>	n.a.	n.a.	n.a.	n.a.	n.a.	n.a.
<b>As (ppm)</b>	n.a.	n.a.	n.a.	n.a.	n.a.	n.a.
<b>Au (ppb)</b>	n.a.	n.a.	293	300 ± 18	41.6	63.5
<b>Bi (ppm)</b>	n.a.	n.a.	n.a.	n.a.	n.a.	n.a.
<b>Cd (ppm)</b>	n.a.	n.a.	n.a.	n.a.	n.a.	n.a.
<b>Co (ppm)</b>	n.a.	n.a.	n.a.	n.a.	n.a.	n.a.
<b>Cu (%)</b>	0.11	0.111 ± 0.010	n.a.	n.a.	n.a.	n.a.
<b>Fe (%)</b>	8.70	8.56 ± 0.34	n.a.	n.a.	n.a.	n.a.
<b>Ir (ppb)</b>	na	na	320	322 ± 19	227	214 ± 12
<b>Ni (%)</b>	0.08	0.101 ± 0.007	n.a.	n.a.	n.a.	n.a.
<b>Os (ppb)</b>	n.a.	n.a.	153	150.00	297	226 ± 95
<b>Pb (ppm)</b>	n.a.	n.a.	n.a.	n.a.	n.a.	n.a.
<b>Pd (ppb)</b>	n.a.	n.a.	1489	1450 ± 50	2218	2360 ± 95
<b>Pt (ppb)</b>	n.a.	n.a.	1786	1910 ± 50	1414	1504 ± 68
<b>Re (ppb)</b>	n.a.	n.a.	n.a.	n.a.	n.a.	n.a.
<b>Rh (ppb)</b>	n.a.	n.a.	245	222 ± 38	520	576 ± 12
<b>Ru (ppb)</b>	n.a.	n.a.	144	145 ± 7	1224	1261 ± 50
<b>S (%)</b>	0.092	1.02 ± 0.3	n.a.	n.a.	n.a.	n.a.
<b>Sb (ppm)</b>	n.a.	n.a.	n.a.	n.a.	n.a.	n.a.
<b>Se (ppm)</b>	n.a.	n.a.	n.a.	n.a.	n.a.	n.a.
<b>Sn (ppm)</b>	n.a.	n.a.	n.a.	n.a.	n.a.	n.a.
<b>Te (ppm)</b>	n.a.	n.a.	n.a.	n.a.	n.a.	n.a.
<b>Zn (ppm)</b>	n.a.	n.a.	n.a.	n.a.	n.a.	n.a.

Abbreviations: INAA = instrumental neutron activation analysis; AR = aqua regia; HH = hand held X-ray fluorescence; and n.a. = not available.

Laser ablation inductively coupled plasma mass spectrometer (LA-ICP-MS) analysis were carried out at LabMaTer using an Excimer 193 nm Resolution M-50 laser ablation system coupled with an Agilent 7700x ICP-MS. Line analysis was used with a beam size of 44  $\mu\text{m}$ , with a speed of 5  $\mu\text{m/s}$  and fluence of 5.9  $\text{J/cm}^2$ . The gas blank (argon-helium mix) was measured for 30 s before turning on the laser. Lines were ablated across the base metal sulfides grains for a period of 30 to 60 s depending on the grain size.  $^{57}\text{Fe}$  was used as the internal standard. Iolite package of Igor Pro software was used to process the data (Paton et al. 2011). The isotopes monitored were:  $^{29}\text{Si}$ ,  $^{34}\text{S}$ ,  $^{57}\text{Fe}$ ,  $^{59}\text{Co}$ ,  $^{60}\text{Ni}$ ,  $^{61}\text{Ni}$ ,  $^{63}\text{Cu}$ ,  $^{65}\text{Cu}$ ,  $^{66}\text{Zn}$ ,  $^{75}\text{As}$ ,  $^{82}\text{Se}$ ,  $^{95}\text{Mo}$ ,  $^{101}\text{Ru}$ ,  $^{103}\text{Rh}$ ,  $^{105}\text{Pd}$ ,  $^{108}\text{Pd}$ ,  $^{109}\text{Ag}$ ,  $^{111}\text{Cd}$ ,  $^{120}\text{Sn}$ ,  $^{121}\text{Sb}$ ,  $^{128}\text{Te}$ ,  $^{185}\text{Re}$ ,  $^{189}\text{Os}$ ,  $^{193}\text{Ir}$ ,  $^{195}\text{Pt}$ ,  $^{197}\text{Au}$ ,  $^{208}\text{Pb}$  and  $^{209}\text{Bi}$ . Po 727 and MASS-1 certified reference materials and JB-MSS5, an in-house reference material, were used for calibration and monitoring. Po 727 is a synthetic FeS from Memorial University of Newfoundland, doped with ~40 ppm PGE and Au and was used to calibrate PGE and Au. MASS-1 is ZnCuFeS pressed powder pellet from United States Geological Survey (USGS), doped with 50-70 ppm Ag, As, Bi, Pb, Re, Sb, Se, Sn and Te, and was used to calibrate Ag, As, Bi, Cd, Co, Cu, Mo, Pb, Sb, Se, Sn and Te. JB-MSS5 is a synthetic FeS sulfide that was provided by Prof. James Brennan, which contain 50-70 ppm of most chalcophile elements. It was used to calibrate  $^{60}\text{Ni}$  and  $^{185}\text{Re}$  and also to monitor the calibrations of Po727 and MASS-1.  $^{101}\text{Ru}$ ,  $^{103}\text{Rh}$ ,  $^{105}\text{Pd}$  and  $^{108}\text{Pd}$  were corrected for interferences.  $^{101}\text{Ru}$  has interference with  $^{61}\text{Ni}^{40}\text{Ar}$  and was corrected using NiS blank.  $^{103}\text{Rh}$  has interference with  $^{63}\text{Cu}^{40}\text{Ar}$  and was corrected using Cu-blank which does not contain  $^{103}\text{Rh}$ . For Cu-rich minerals  $^{103}\text{Rh}$  could not be corrected, because the signal of  $^{63}\text{Cu}$  makes up more than 50% of the  $^{103}\text{Rh}$  signal.  $^{65}\text{Cu}^{40}\text{Ar}$  interferes with  $^{105}\text{Pd}$  and this was corrected using Cu-blank, however in Cu-rich minerals the correction is too large and  $^{108}\text{Pd}$  was used.  $^{108}\text{Cd}$  interferes with  $^{108}\text{Pd}$  and

this was corrected by monitoring  $^{111}\text{Cd}$  and making theoretical correction in proportion to isotope abundances. The potential for  $^{68}\text{Zn}^{40}\text{Ar}$  interference on  $^{108}\text{Pd}$  was monitored but no interference was detected.

## CHAPTER 3

### 3. REGIONAL AND LOCAL GEOLOGY

Located in eastern Labrador, Canada, the Voisey's Bay deposit is hosted by troctolite to gabbroic rocks that were emplaced along the tectonic contact between the Archean Nain and the Paleoproterozoic Churchill provinces and that were intruded into the metasedimentary rocks of the Churchill province (Fig. 1). Collectively these troctolite to gabbroic rocks are referred to as the Voisey's Bay intrusion that has been dated at  $1332.7 \pm 1.0$  Ma (U–Pb) (Amelin et al. 1999).

The Churchill Province comprises reworked Archean rocks, interbanded sulfide-graphite-bearing garnet-sillimanite, quartz-feldspathic paragneisses collectively known as "Tasiuyak gneiss" and minor massive to lineated enderbitic gneiss. The Nain Province comprises interbanded granitic, intermediate and mafic orthogneisses that exhibit retrogressed granulite and amphibolite-facies mineral assemblages (Li and Naldrett 1999).

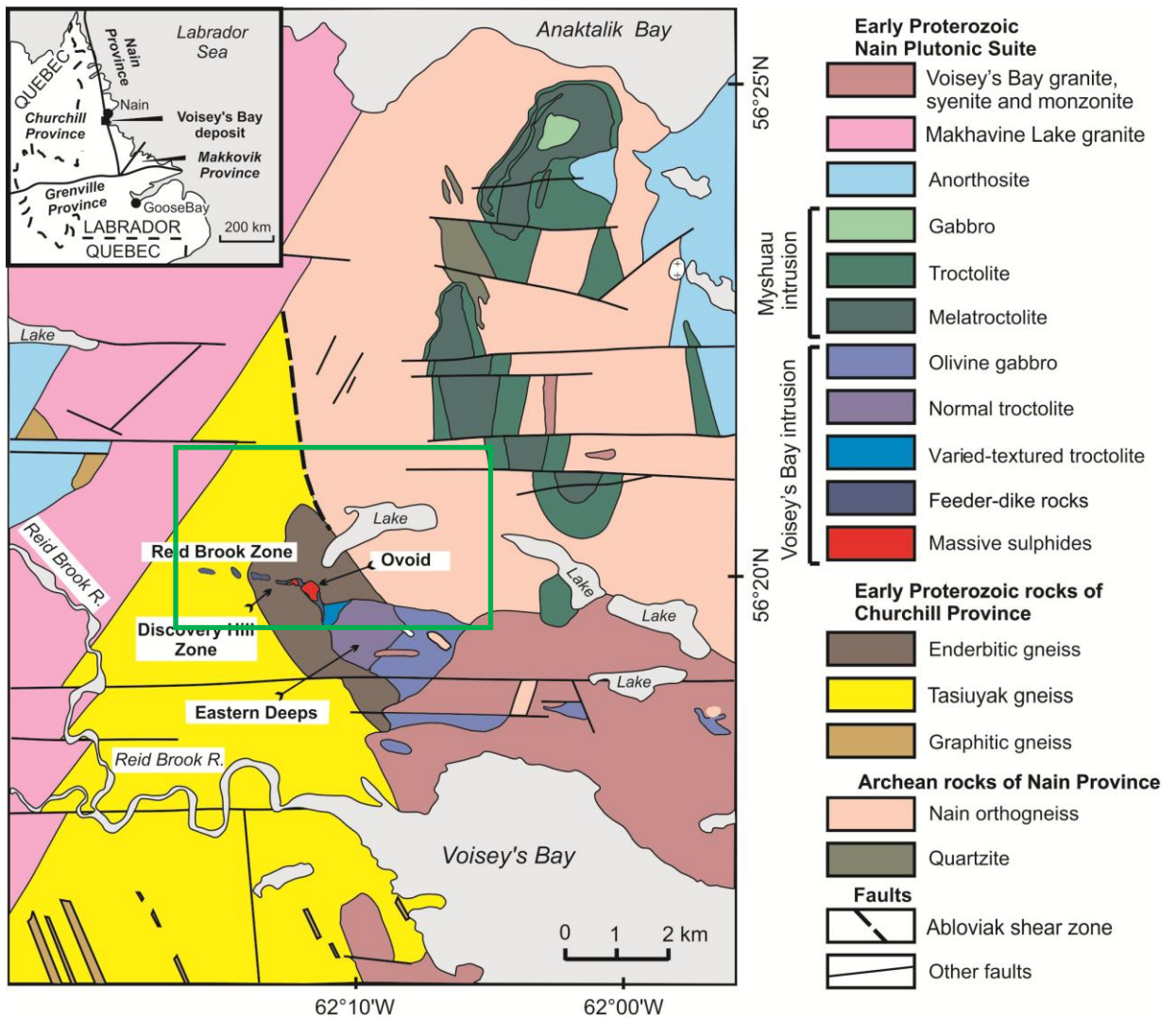


Fig. 1: Voisey's Bay geological setting. The area in green is shown in more detail on figure 2 (modified from Li and Naldrett 1999).

Previous studies have proposed that the Voisey's Bay intrusion represents a conduit-like intrusive system (Li and Naldrett 1999). Connection of troctolite-gabbro dykes to two troctolite magma-chambers, the Reid Brook chamber at depth and the Eastern Deeps chamber at a higher level in the crust is additionally suggested (Ryan 2000) (Fig. 2). Crustal rocks (including the sulfur-rich gneisses and organic carbon-rich sediments) contaminated the parental mafic magma (Ripley et al. 1999) during its ascent and emplacement (~11 km depth) and are thought to be an important ore forming process (Naldrett 2004).

Subdivision of the Voisey's Bay deposit into five distinct ore-bearing zones is suggested by Li and Naldrett (1999) and Li et al. (2007). These five distinct ore-bearing zones are from east (shallowest) to west (deepest): (1) Eastern Deeps (upper chamber); (2) Ovoid, which is situated between the Eastern Deeps and the Discovery Hill zone; (3) Mini-Ovoid lies directly west of the Ovoid but is separate from it; (4) Discovery Hill zone; (5) Reid Brook zone (lower chamber) (Fig. 2-A-B).

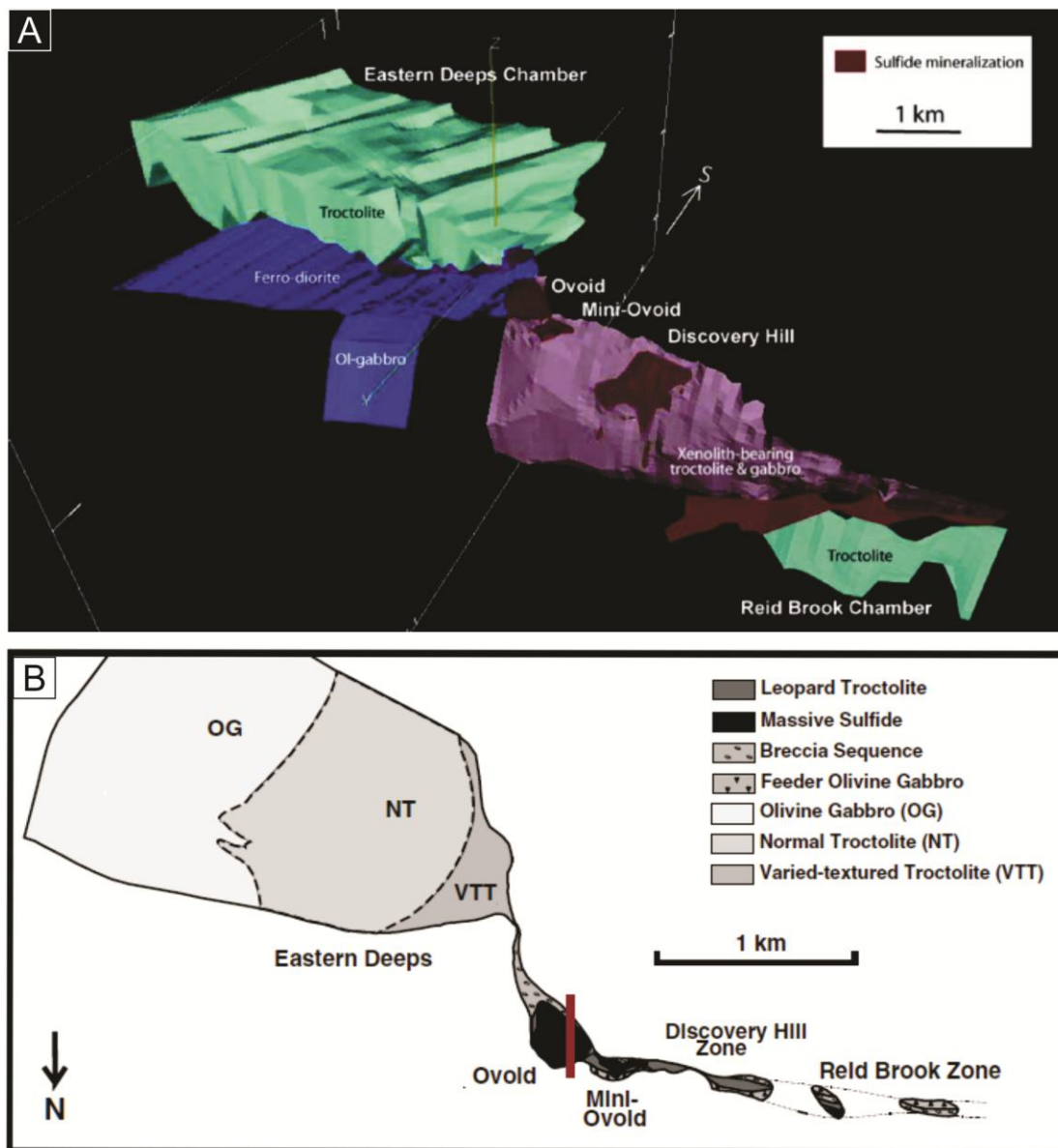


Fig. 2: **A:** A 3D view of the Voisey's Bay ore bodies (Eastern Deeps, Ovoid, Mini-Ovoid, Discovery Hill and Reid Brook) (Li et al. 2007). **B:** Geological map of the Voisey's Bay intrusion. Red line represents the transversal section of the Ovoid (Modified from Li et al. 2000).

The original estimated resource of the massive sulfide ore at the Ovoid ore body indicated that it contained 31.7 million tonnes at 2.83% Ni, 1.68% Cu and 0.12% Co (Lightfoot et al. 2012). The Ovoid ore body consists of up to 110 m thickness of massive sulfide all located within a bowl-shaped structure (Fig. 3), and overlain by 10 – 20 m of gravel. It is underlain by a thin (10 – 20 m) feeder sheet (Li and Naldrett 1999). The Ovoid ore body comprises a dominant Fe-rich margin of pyrrhotite – pentlandite-rich ore, and a small core of cubanite-rich ore (Boutroy et al. 2014). Naldrett et al. (2000a) proposed that the Ovoid ore body formed by the solidification of a sulfide melt in a closed system, with crystallization of sulfides from the margin to the core.

Seventeen samples of massive, one disseminated, one breccia and two matrix sulfides were selected for detailed study. These samples were selected so as to have a range in composition and textural types. Fifteen samples of massive sulfides were the same as those used in the study of Boutroy et al. (2014) and were collected from drillholes at regular intervals (Fig. 3). Two massive Cu-rich sulfides (VB5 and VB6) were collected from the center of Ovoid open pit represented in figure 4. The disseminated sulfide (VB2 – troctolite), the breccia (VB8 – breccia sulfide) and one matrix sulfide (VB7 – matrix troctolite) were collected from the margins of Ovoid open pit (Fig. 4). The other matrix sulfide sample was collected from the drillhole (VB21 – matrix troctolite). Further description of the sampling procedure is provided within chapter 4 (Petrography).

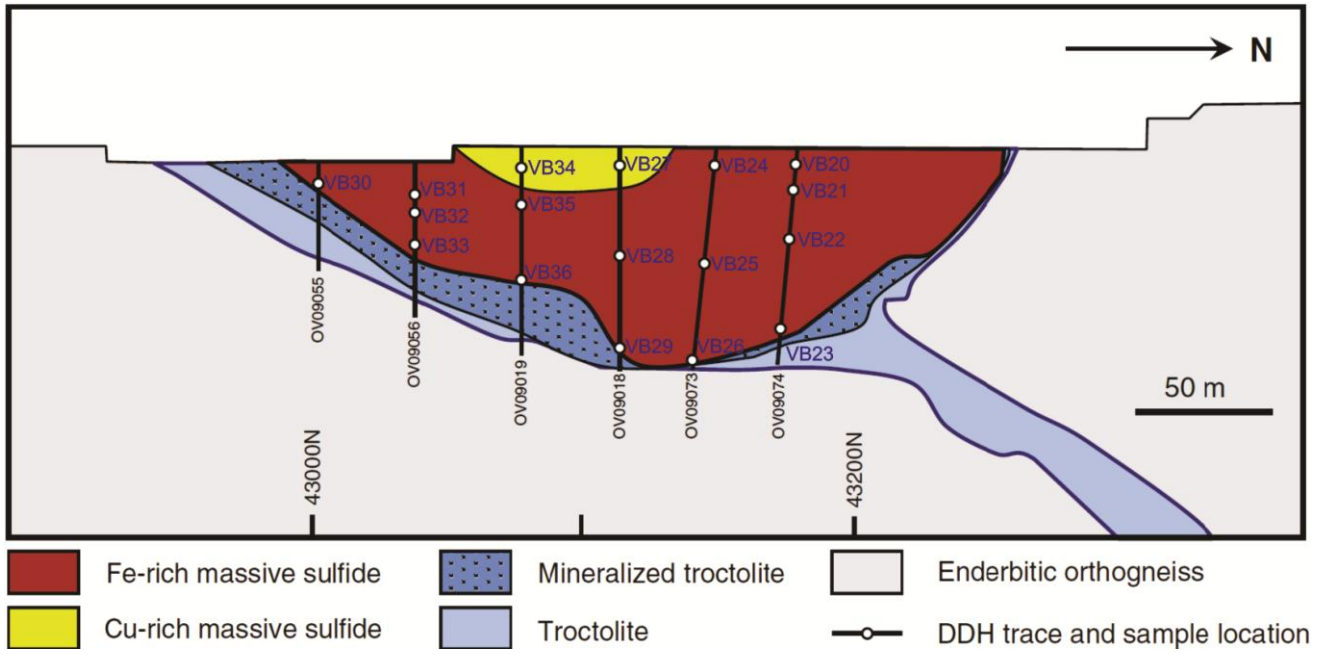


Fig. 3: West facing geologic section through the Ovoid ore body showing location of boreholes available for sampling (Boutroy et al. 2014).

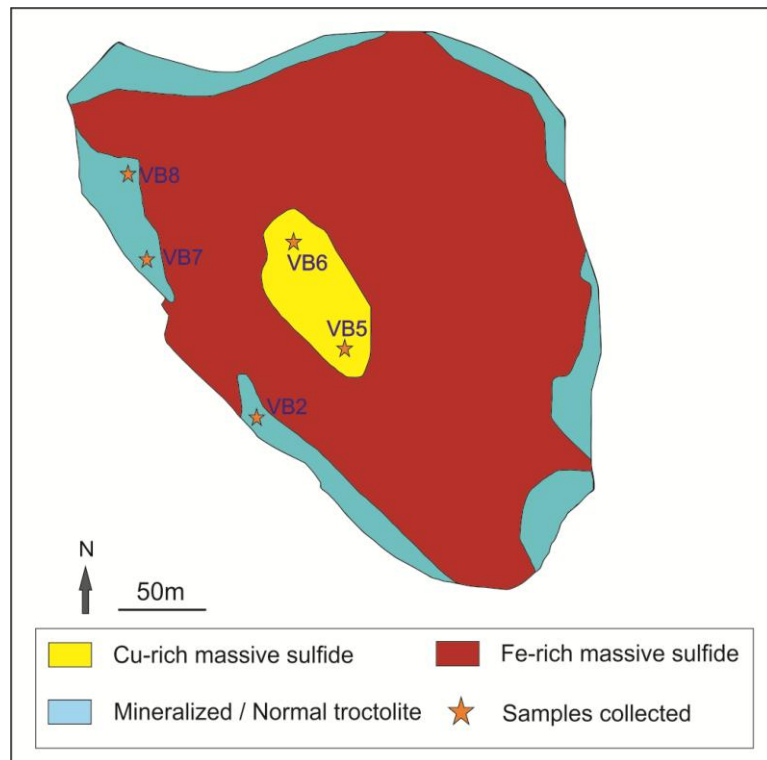


Fig. 4: Ovoid pit, plan view of the samples location.

## CHAPTER 4

### 4. PETROGRAPHY

The samples were grouped into five different assemblages, depending on the sulfide content and the mineralogy of the sample: 1- Disseminated sulfide (VB2 - normal troctolite); 2- Breccia sulfide (VB8 - breccia sulfide); 3- Matrix sulfide (VB7 and VB21 - matrix troctolite); 4- Fe-rich massive sulfide; and 5- Cu-rich massive sulfide.

#### 4.1. Hand specimens

##### *4.1.1. Disseminated, matrix and breccia assemblages*

Disseminated sulfide sample (Fig. 5 A) consist mainly of a troctolite with uniform texture and containing minor fine (0.2 mm) patches of sulfide. About 95 % of the rock consists of troctolite and 5 % consist of sulfides. In the matrix sulfide (Fig. 5 B), sulfides form the matrix to troctolite patches (2-5 mm). The breccia sulfide contains patches (3-4 cm) of sulfides (Fig. 5 C) and the matrix of the rock is a troctolite. For matrix and breccia samples, the sulfide abundance correspond of ~ 45 %, the silicate consists of ~ 45 % and magnetite ~ 10 % of the sample.

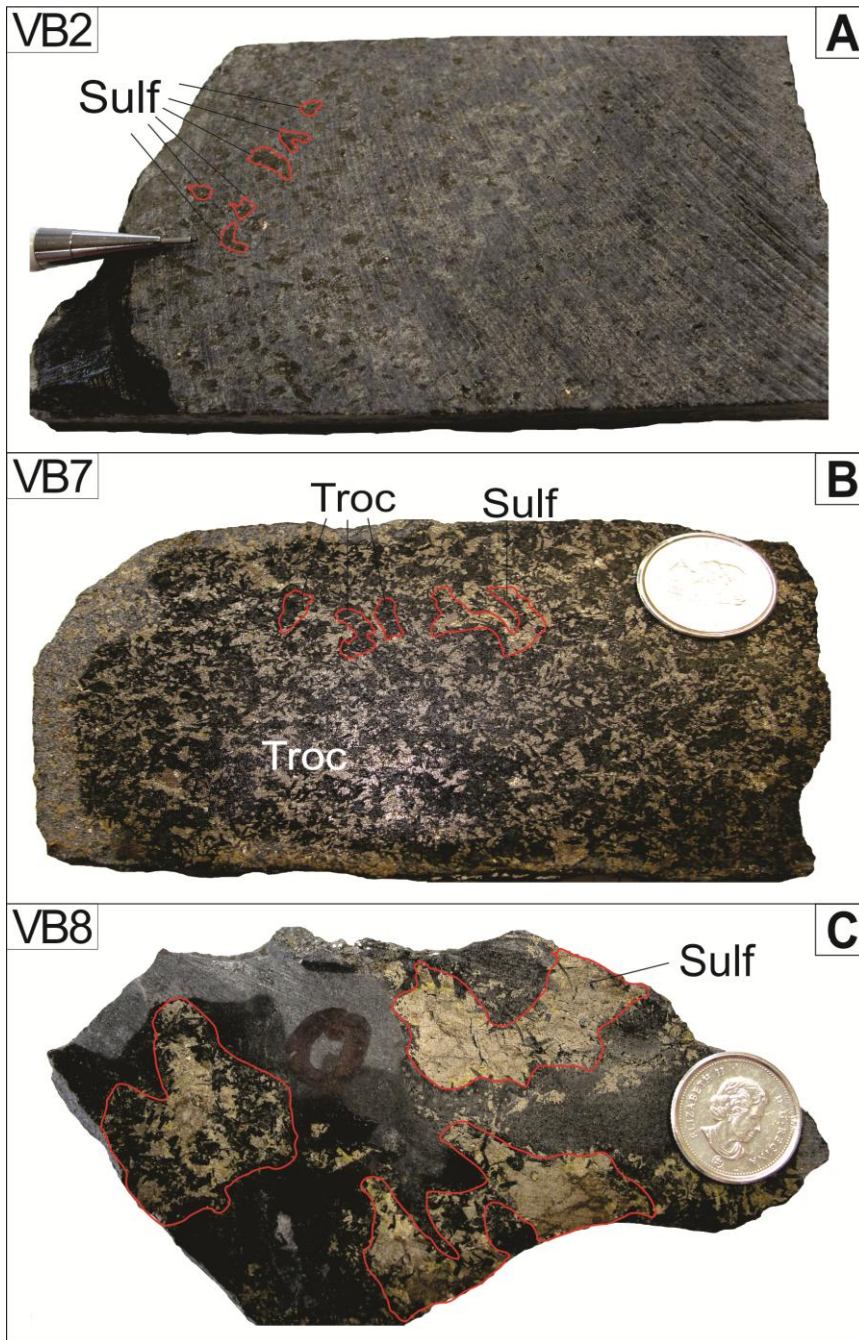


Fig. 5: Representative samples of disseminated sulfide, matrix sulfide and breccia sulfide from the Ovoid ore body. **A:** Disseminated sulfides (0.2 mm) in a matrix of troctolite. **B:** Matrix sulfides, interconnected sulfides with troctolite interstitial to the sulfides. **C:** Breccia sulfide with patches (3-4 cm) of sulfides and troctolite. Abbreviations: Sulf = sulfide, Troc = troctolite, VB = sample name. Coin diameter = 1.7 cm.

#### 4.1.2. Massive sulfides - Fe-rich and Cu-rich

The massive sulfides samples can be divided into Fe-rich and Cu-rich assemblages. Pyrrhotite is the main sulfide mineral in the Fe-rich assemblage and forms the matrix to the other minerals. Coarse grains of pentlandite (2-3 cm) and chalcopyrite (1-1.5 cm) occur in association with pyrrhotite (Fig. 6 A). Magnetite grains are generally 0.2 to 0.3 mm, but can be larger (0.7 mm - 1cm) in some Fe-rich massive sulfide samples (Fig. 6 B). For Fe-rich samples ~ 60 % of the rock consists of pyrrhotite, ~ 20 % of pentlandite, ~ 10 % chalcopyrite and ~ 10 % magnetite.

Chalcopyrite and Cubanite represent the main sulfide minerals in the Cu-rich assemblage, and occur as the matrix in Cu-rich samples. Coarse grains of pentlandite (1 - 2.5 cm) and pyrrhotite (1 - 3 cm) are also present. Medium grains of magnetite (0.5 cm) occur as inclusions in the chalcopyrite / cubanite matrix (Fig. 6 C), but can be associated with pyrrhotite, or in contact with pentlandite. Figure 6 D shows a Cu-rich sample, where cubanite / chalcopyrite represent the matrix, containing few fine grains of magnetite (0.1 cm) and medium grains of pentlandite and pyrrhotite (0.5 - 1 cm). For VB6, ~ 50 % consists of cubanite / chalcopyrite, ~ 25 % of magnetite, ~ 15 % of pentlandite and ~ 10 % of pyrrhotite. For VB34 the mineral abundance consists of ~ 70 % of cubanite / chalcopyrite, ~ 15 % of pentlandite, ~ 10 % pyrrhotite and ~ 5 % of magnetite.

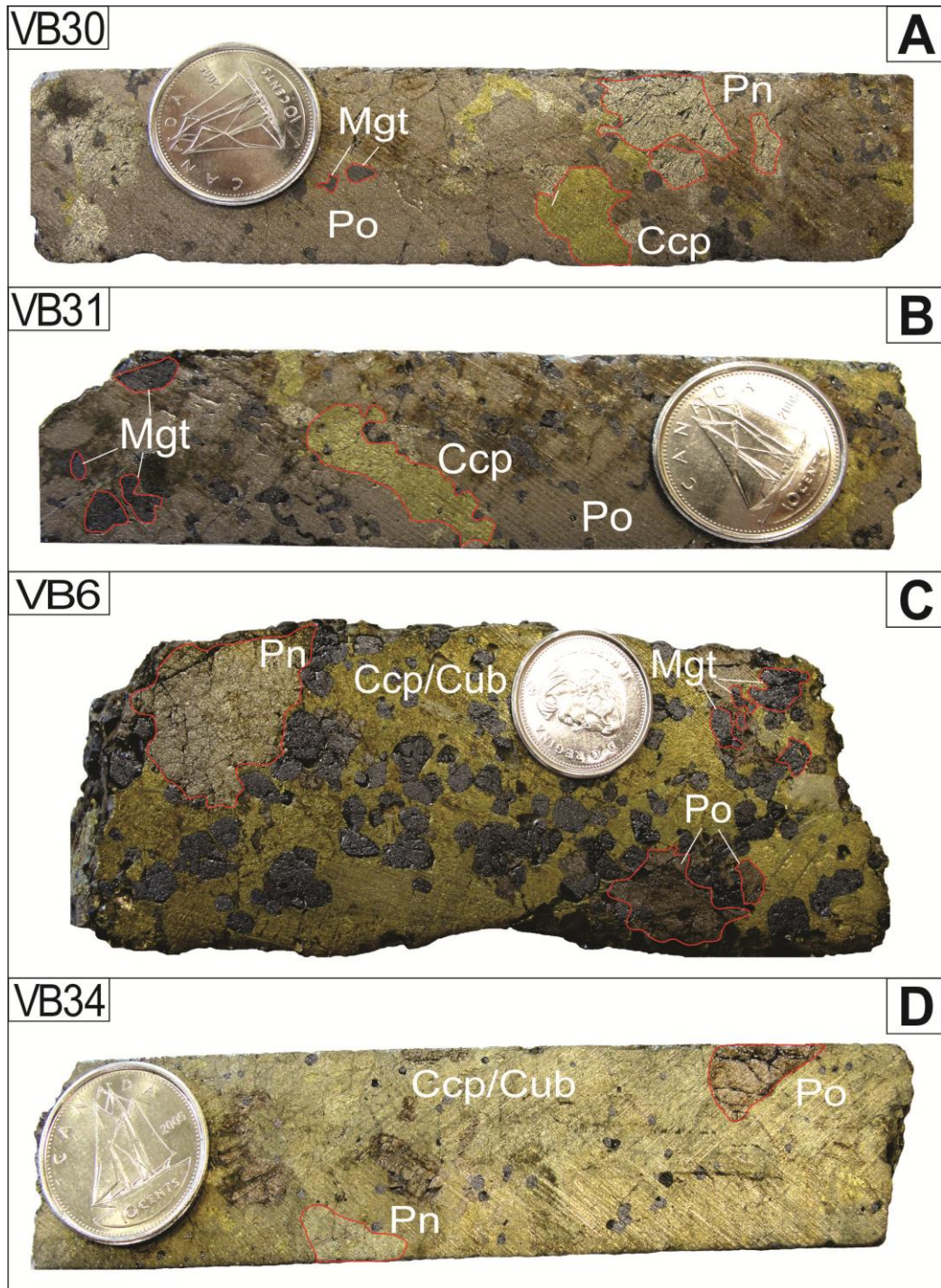


Fig. 6: Representative massive sulfide samples from the Ovoid ore body. **A:** Fe-rich massive sulfide showing the common assemblage (pyrrhotite, pentlandite, chalcopyrite and magnetite) and coarse grained texture. **B:** Fe-rich massive sulfide showing coarse grained magnetite. **C:** Cu-rich massive sulfide showing coarse grained texture and common assemblage (chalcopyrite / cubanite, pentlandite, pyrrhotite and magnetite). **D:** Cu-rich sulfide showing coarse grained magnetite. Abbreviations: Po = pyrrhotite, Pn = pentlandite, Ccp = chalcopyrite, Cub = cubanite, Mgt = magnetite and VB = sample name. Coin diameter = 1.7 cm.

## **4.2. Polished section descriptions**

Naldrett et al. (2000b) and Huminicki (2007) have previously described the mineralogy and textures of sulfide minerals at the Ovoid ore body, and Li and Naldrett (1999) and Naldrett and Li (2007) have previously described in detail all rock types that comprise the Voisey's Bay intrusion. Table 2 provides a summary of the mineralogy of each sample presented in this study.

Table 2: Sample mineralogy from the Ovoid ore body, Voisey's Bay.

Sample name	VB2	VB7	VB21	VB8	VB5	VB6	VB27
Drillcore n° / depth	Field sample	Field sample	VX92132 / 14m	Field sample	Field sample	Field sample	VX88239 / 4.8m
Rock	Normal troctolite	Matrix troctolite	Matrix troctolite	Breccia sulfide	Cu-rich	Cu-rich	Cu-rich
Sulfide texture	Disseminated	Matrix	Matrix	Breccia	Massive	Massive	Massive
Pyrrhotite	abundant	abundant	abundant	abundant	abundant	abundant	abundant
Troilite		abundant	minor		abundant	minor	minor
Pentlandite	trace	abundant	abundant	trace	trace	abundant	minor
Chalcopyrite	minor	minor	minor	minor	abundant	abundant	abundant
Cubanite					abundant	abundant	abundant
Magnetite		abundant	abundant		abundant	abundant	abundant
Ilmenite		trace	minor				
Galena							trace
Sphalerite					trace	trace	minor
Sample name	VB34	VB22	VB23	VB24	VB25	VB26	VB28
Drillcore n° / depth	VX88333 / 5.7m	VX92153 / 32.6m	VX92183 / 66.7m	VX92034 / 4.9m	VX92074 / 42m	VX92117 / 81.8m	VX88276 / 39m
Rock	Cu-rich	Fe-rich	Fe-rich	Fe-rich	Fe-rich	Fe-rich	Fe-rich
Sulfide texture	Massive	Massive	Massive	Massive	Massive	Massive	Massive
Pyrrhotite	abundant	abundant	abundant	abundant	abundant	abundant	abundant
Troilite	minor	abundant	abundant	abundant	abundant	abundant	abundant
Pentlandite	trace	abundant	abundant	abundant	abundant	abundant	abundant
Chalcopyrite	abundant	minor	trace	minor	minor	minor	minor
Cubanite	abundant						
Magnetite	abundant	abundant		abundant	abundant	abundant	abundant
Ilmenite		trace				trace	
Galena	trace					trace	
Sphalerite	minor						
Sample name	VB29	VB30	VB31	VB32	VB33	VB35	VB36
Drillcore n° / depth	VX88318 / 74m	VX90843 / 6.2m	VX90884 / 7.8m	VX90891 / 14.8m	VX90904 / 27.2m	VX88348 / 19.6m	VX88379 / 47.6m
Rock	Fe-rich	Fe-rich	Fe-rich	Fe-rich	Fe-rich	Fe-rich	Fe-rich
Sulfide texture	Massive	Massive	Massive	Massive	Massive	Massive	Massive
Pyrrhotite	abundant	abundant	abundant	abundant	abundant	abundant	abundant
Troilite	abundant	minor	abundant	abundant	abundant	abundant	abundant
Pentlandite	abundant	abundant	minor	minor	abundant	minor	abundant
Chalcopyrite	minor	minor	abundant	abundant	trace	trace	abundant
Cubanite			minor	minor			
Magnetite	abundant	abundant	abundant	abundant	abundant	abundant	abundant
Ilmenite							
Galena							
Sphalerite			trace				

#### *4.2.1. Disseminated sulfide*

In VB2, pyrrhotite is the most common sulfide mineral, it has an anhedral form and the grains range from 0.05 – 0.8 mm. Pyrrhotite is in contact with pentlandite, chalcopyrite and silicates (Fig. 7 A). Rare granular pentlandite and few chalcopyrite grains occur and their grains size range from 0.040 – 0.100 mm, they also have an anhedral and subhedral form. They are observed in contact with pyrrhotite and silicate minerals (Fig. 7 B). Mineral abundance corresponds of ~ 95 % silicates and ~ 5 % of sulfides (predominantly pyrrhotite)

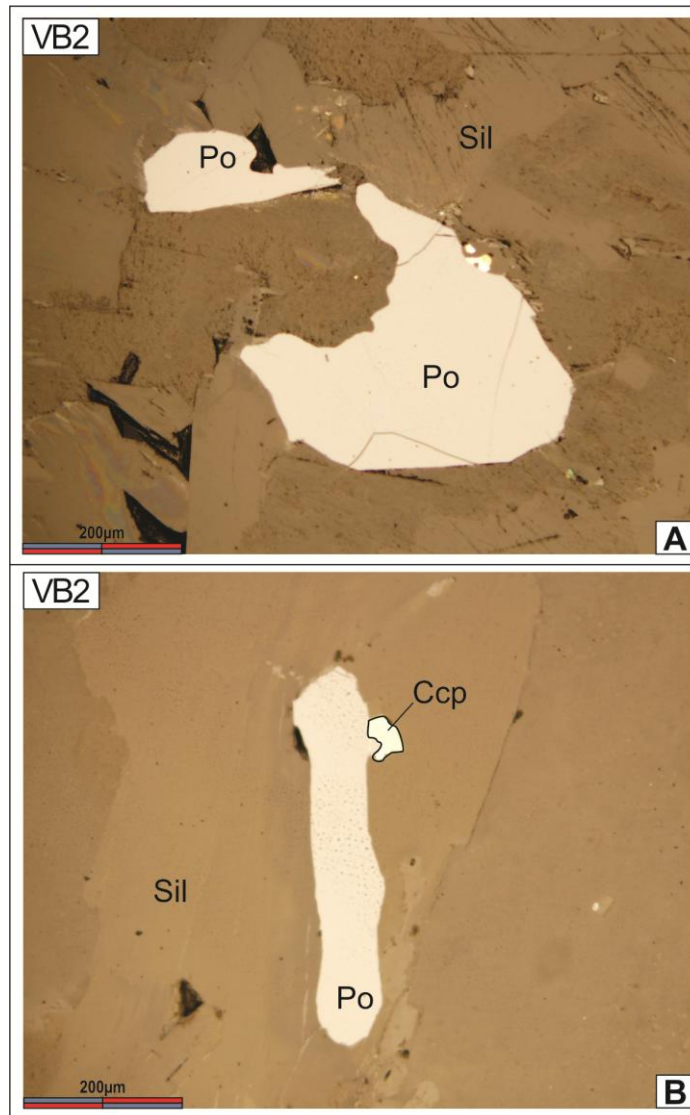


Fig. 7: Reflected light photomicrographs of typical disseminated sulfide texture from the Ovoid ore body. **A:** Pyrrhotite grains in contact with silicate mineral. **B:** Pyrrhotite in contact with tiny chalcopyrite and silicate minerals. Abbreviations: Po = pyrrhotite, Ccp = chalcopyrite, Sil = silicate and VB = sample name.

#### 4.2.2. *Breccia sulfide*

- Pyrrhotite and troilite

In VB 8, pyrrhotite is the predominant sulfide and it represents the matrix to the other sulfides. It has a grain size up to 1 cm and is anhedral in form. Pyrrhotite is observed in contact with pentlandite, chalcopyrite, magnetite and ilmenite. It contains exsolutions lamellae of troilite (Fig. 8 A, B, C). Troilite exsolution has previously been reported by Naldrett et al. (2000b) and Huminicki (2007).

- Pentlandite

Granular pentlandite occurs as anhedral and subhedral forms, ranging from 0.1 – 0.9 mm. Pentlandite is observed mainly in contact with pyrrhotite, chalcopyrite, silicate minerals and in rare cases with magnetite / ilmenite (Fig. 8 A, B, C). Chalcopyrite, silicate minerals and minor magnetite occurs as inclusions and cracks are filled with silicate minerals.

- Chalcopyrite

Chalcopyrite has an anhedral form and ranges from 0.1 – 1.4 mm. It contains silicate mineral inclusions. Chalcopyrite is in contact mainly with pyrrhotite, pentlandite and in some cases with magnetite (Fig. 8 A, B, C).

- Magnetite and ilmenite

Magnetite has an anhedral (rounded or elongate shape) to subhedral form with grain size ranging from 0.05 – 1.4 mm. Magnetite occurs in textural equilibrium with ilmenite, pyrrhotite, chalcopyrite and pentlandite (Fig. 8 A, B). Ilmenite has a similar shape and size to magnetite and is usually associated with the magnetite. In many cases

ilmenite occurs in contact with magnetite and in some cases wraps around the edges of magnetite (Fig. 8 A).

In the breccia sample, the sulfide and oxide abundances correspond of 60 % pyrrhotite, 20 % magnetite, 10 % chalcopyrite and 10 % pentlandite.

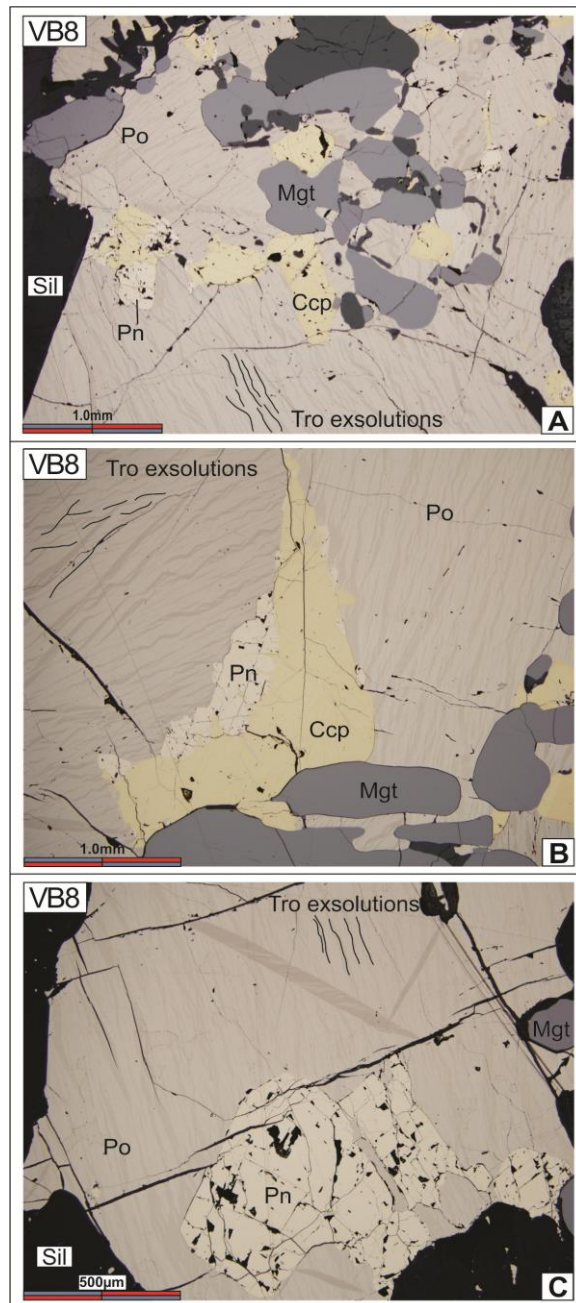


Fig. 8: Reflected light photomicrographs of typical breccia sulfide textures from the Ovoid ore body. **A:** Pyrrhotite and troilite exsolutions in contact with magnetite, pentlandite, chalcopyrite and silicate minerals. **B:** Chalcopyrite in contact with pentlandite, pyrrhotite and magnetite. Also, troilite exsolutions are very clearly evident in pyrrhotite. **C:** Pentlandite with silicate inclusions in contact with pyrrhotite and silicate minerals. Abbreviations: Po = pyrrhotite, Tro = troilite, Pn = pentlandite, Ccp = chalcopyrite, Mgt = magnetite, and VB = sample name.

#### 4.2.3. Silicate assemblage and textures

The silicate and oxide minerals present in the breccia, disseminated and matrix ores is similar and consists of plagioclase, olivine, amphibole, biotite and minor spinel (hercynite).

The mineral assemblage of VB8 (breccia sulfide) is composed of olivine, plagioclase, biotite, coronas of amphibole + spinel. Olivine is the principal mineral, fine (0.1 mm) to coarse (12 mm) grains, anhedral and rounded forms (Fig. 9 A). Plagioclase is fine (0.08 mm) to coarse (12 mm) grained, anhedral to subhedral and in some cases with spindle twinning and undulose extinction. Plagioclase has experienced a little sericitization. Biotite occurs as fine (0.07 mm) to medium (0.6 mm) grains, subhedral and euhedral forms and locally shows undulose extinction. Green or black spinel (hercynite), anhedral and subhedral forms, ranging from 0.3 to 1 mm (Fig. 9 B, F). Coronas (0.1 mm wide) of amphibole and hercynite occur around the olivine (Fig. 9 A, B). The mineral abundance for VB8 consists of ~ 40 % olivine + amphibole, ~ 40 % plagioclase, ~ 15 % biotite and ~ 5 % hercynite.

The mineralogy of VB2 (troctolite) and VB7, VB21 (matrix troctolite) is composed of amphibole (principal mafic mineral), ranging from fine (0.1 mm) to coarse (12 mm) grains, anhedral and subhedral forms. Figures 9 C, D show the amphibole agglomerate in a shape similar to olivine which is interpreted as olivine pseudomorphs. Biotite also occurs as fine (0.08 mm) to medium (0.5 mm) grains, which wrap around the amphibole agglomerates. Plagioclase with spindle twin (Fig. 9 E) and biotite have the same characteristics as in VB8. The mineral abundances for VB2, VB7 and VB21 are similar and corresponds of ~ 45 % amphibole + olivine, ~ 40 % plagioclase and ~ 15 % biotite. In silicates minerals, evidence for some deformation is recorded by spindle

twinning in plagioclase, slightly kinked biotite grains and undulose extension in plagioclase and biotite.

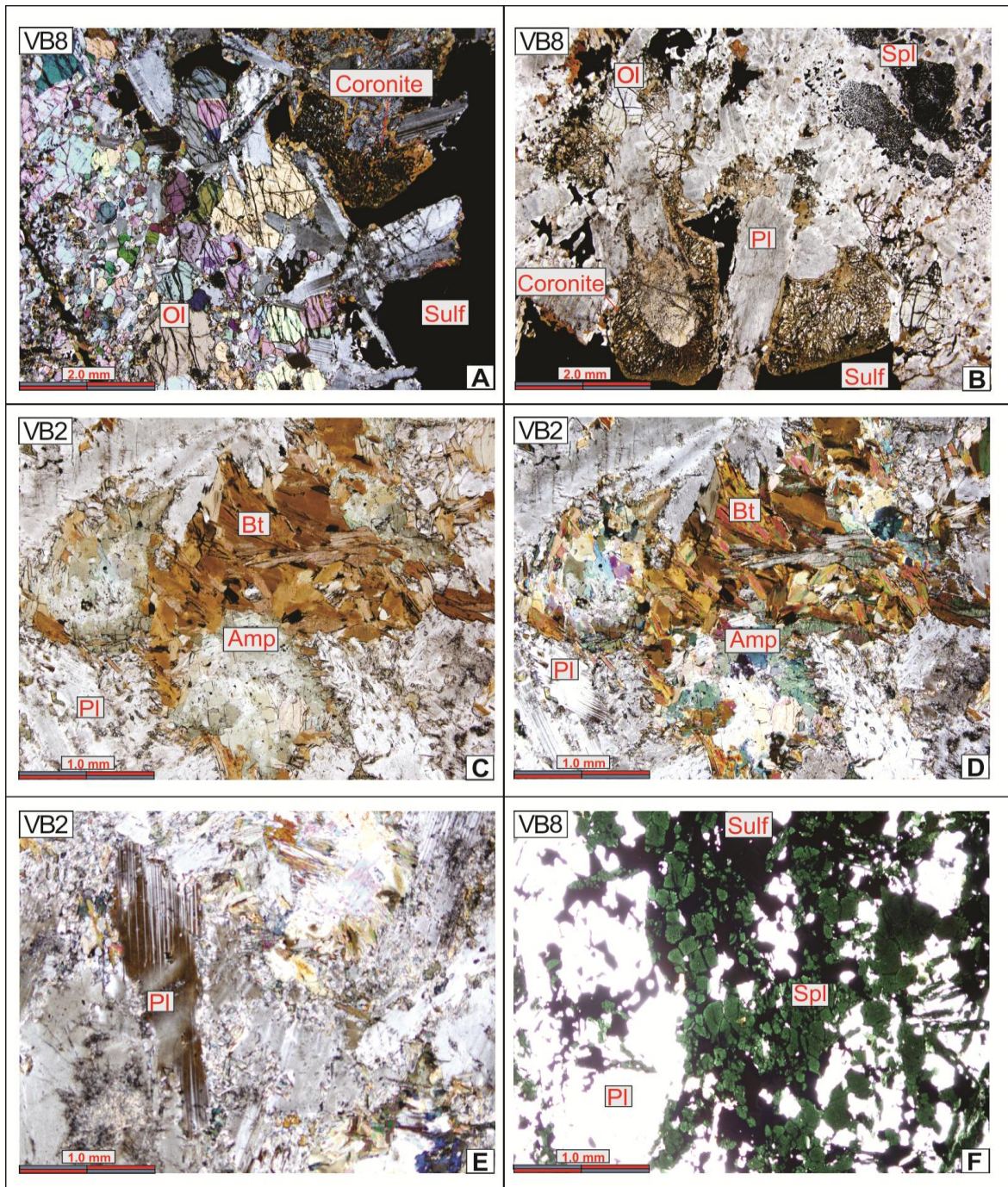


Fig. 9: Transmitted light photomicrographs of silicate texture in; breccia, matrix and disseminated sulfides. **A:** Breccia ore showing olivine ranging from fine to coarse grains in contact with plagioclase and coronite texture. Crossed nicols. **B:** Breccia sulfide showing coarse grains of plagioclase and olivine, medium grain of spinel and coronite texture. **C and D:** Disseminated sulfide showing olivine pseudomorph replaced by amphibole and biotite. In **D** crossed nicols. **E:** Disseminated sulfide showing spindle twins in plagioclase. Crossed Nicols. **F:** Breccia ore sulfide showing green spinel (hercynite) associated with plagioclase and sulfide. Abbreviations: Pl = plagioclase, Ol = olivine, Bt = biotite, Amp = amphibole, Spl = spinel, Sulf = sulfide, VB = sample name.

#### 4.2.4. Matrix and Fe-rich assemblages

Matrix sulfide and Fe-rich massive sulfide assemblages are described together because they are showing similar morphologies and mineral associations.

In the matrix and Fe-rich assemblages, evidences of minor deformation were observed. The most common type of deformation is the wave shape of troilite exsolutions that are hosted in pyrrhotite (Fig. 10 A, B, C). These exsolutions can also form along two structural directions as shown in figure 10 D and in Naldrett et al. (2000b). In addition, the minor troilite exsolutions can be slightly kinked. In some instances, grains of pentlandite (flames too), chalcopyrite and magnetite are oriented in the same direction as the troilite exsolutions (Fig. 10 A, B, C), providing an additional piece of evidence that minor deformation event(s) have occurred. Similar evidences of minor of deformation also occur in Cu-rich assemblage.

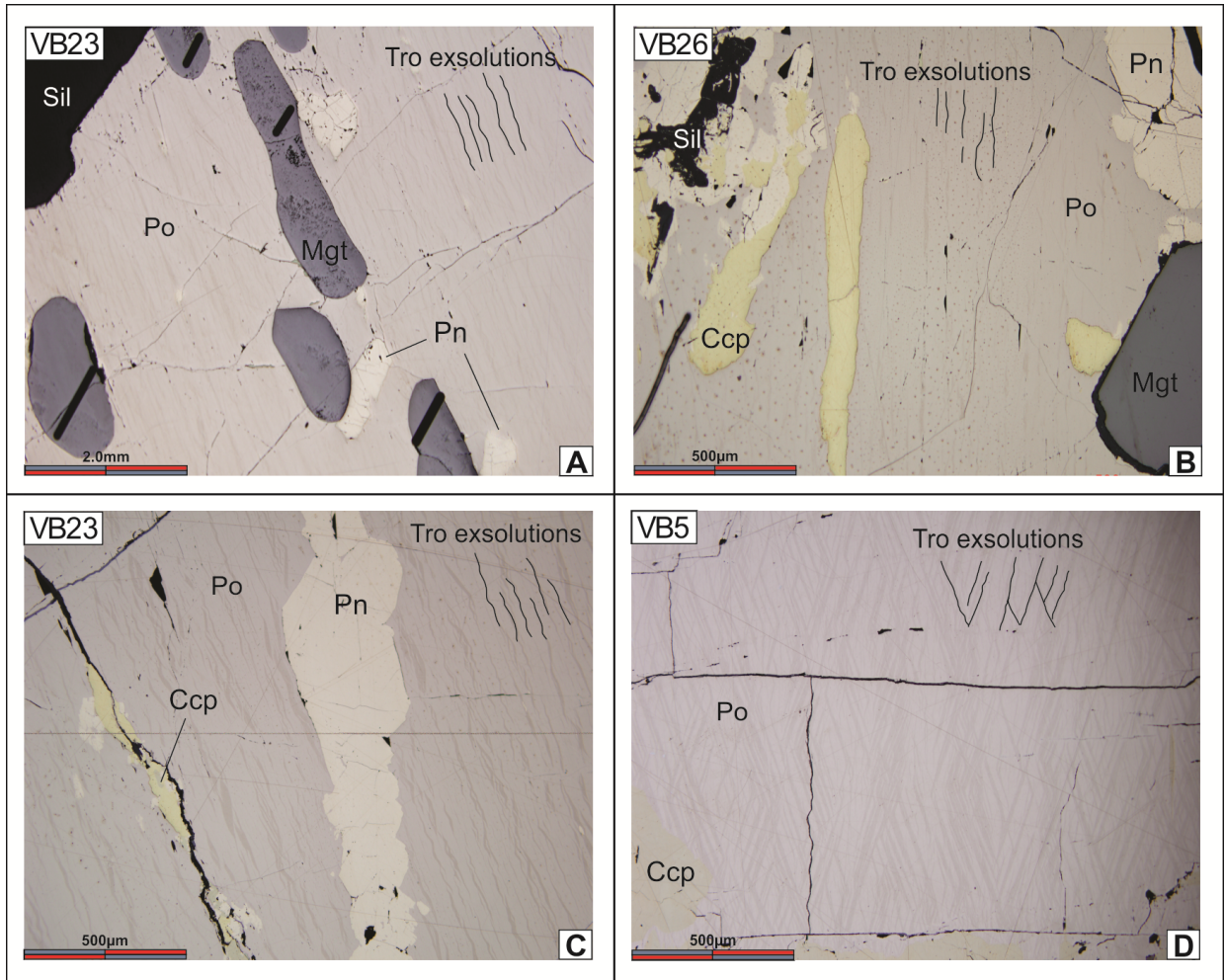


Fig. 10: Reflected light photomicrographs of deformation evidences. **A**, **B** and **C**: Troilite exsolutions in wave shape, also magnetite, chalcopyrite and pentlandite are oriented in the same direction as troilite exsolutions. **D**: Troilite exsolutions along two structural directions. Abbreviations: Po = pyrrhotite, Tro = troilite, Pn = pentlandite, Ccp = chalcopyrite, Mgt = magnetite, VB = sample name. Black lines within the magnetite represent the LA-ICP-MS work of Boutroy et al. (2014).

- Pyrrhotite and troilite exsolution lamellae

Hexagonal pyrrhotite with troilite exsolution lamellae (Fig. 11 A, B) is the predominant sulfide mineral in the matrix and Fe-rich massive samples of the Ovoid and forms the matrix for the rest of ore minerals (Fig. 12 A, B, C, D, E). It has an anhedral form and a grain size of up to 2 cm. Magnetite, pentlandite, chalcopyrite, cubanite and silicate mineral are present as inclusions (Fig. 12 A, B, C, D, E). Cracks are filled with silicate minerals, magnetite, pentlandite and chalcopyrite. The exsolution lamellae of troilite occur in the pyrrhotite (Fig. 11 A, B). These observations are in agreement with Naldrett et al. (2000b), who found that the troilite is devoid of Ni and the hexagonal pyrrhotite / troilite ratio for the Ovoid massive sulfides is 0.7 / 0.3.

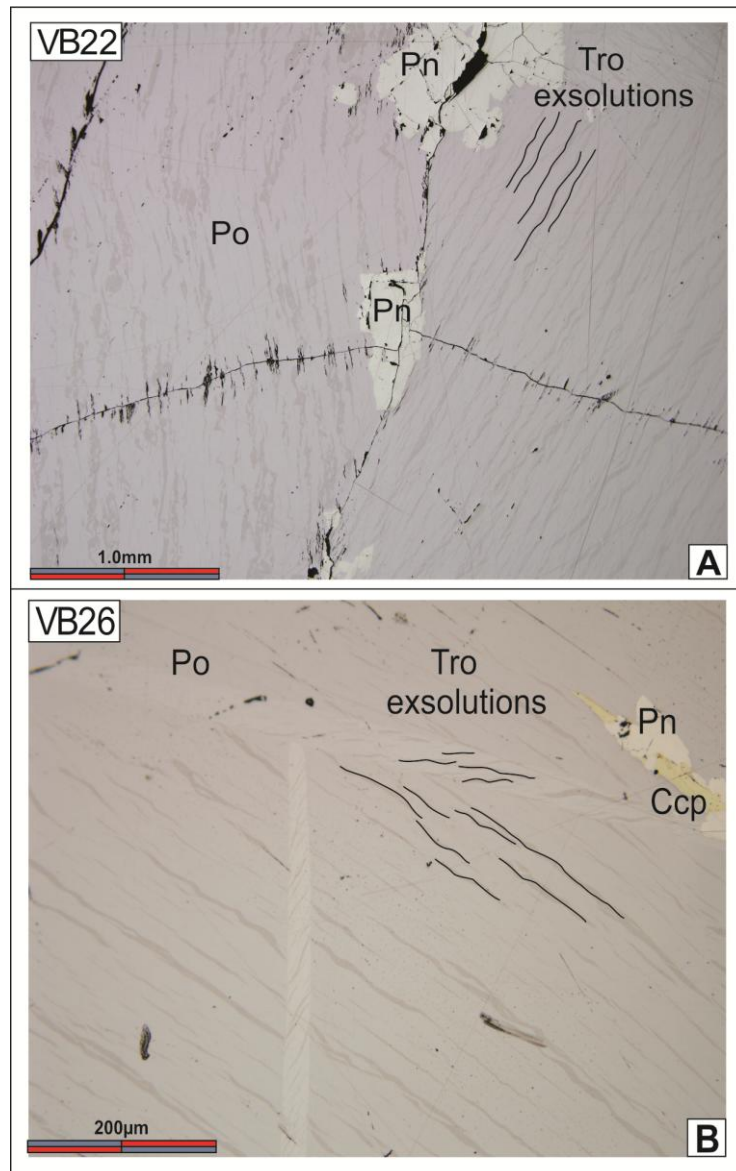


Fig. 11: **A** and **B**: Exsolution lamellae of troilite in pyrrhotite. Abbreviations: Po = pyrrhotite, Pn = pentlandite, Ccp = chalcopyrite, Tro = troilite, Mgt = magnetite and VB = sample name.

- Pentlandite

Pentlandite has anhedral to subhedral forms, ranging from fine grained (0.2 mm) to coarse grained (up to 10 – 15 mm). Pentlandite is observed with three different textures: Coarse granular (Fig. 12 A), medium grains (sometimes veinlets) which wrap around the grain boundaries of chalcopyrite and magnetite (Fig. 12 B), and pentlandite flames both in pyrrhotite and in chalcopyrite. The pentlandite flames in pyrrhotite are oriented parallel to troilite exsolutions (Fig. 12 C). The coarse grained pentlandite texture is the dominant pentlandite texture observed in all of the Fe-rich samples and matrix assemblages contain more coarse grained pentlandite texture than the disseminated, breccia and Cu-rich massive assemblages. Pentlandite is observed in contact with all sulfide minerals and magnetite. Granular magnetite, chalcopyrite, silicate minerals and minor cubanite occurs as inclusions. Cracks in the pentlandite are filled with silicate minerals. Naldrett et al. (2000b) report similar grain size, texture and relationship to other minerals for pentlandite; however they describe a euhedral pentlandite form which was not observed in our matrix and Fe-rich samples.

- *Chalcopyrite*

Chalcopyrite has an anhedral form, and grain size ranging from 0.4 mm, up to 10 – 12 mm. Chalcopyrite is observed in contact with pyrrhotite, pentlandite and magnetite. Inclusions of magnetite and pentlandite are common in chalcopyrite. Cracks observed in chalcopyrite are filled with magnetite and silicate minerals. Cubanite and sphalerite exsolutions occur within chalcopyrite as shown in (Fig. 12 F), these exsolutions are more common in Fe-rich assemblage than in matrix assemblage. Naldrett et al. (2000b) report similar characteristics for chalcopyrite.

- Galena and sphalerite

Galena and sphalerite occur as accessory minerals typically associated with chalcopyrite. Galena occurs as fine grains (0.2 mm), anhedral (rounded) shapes (Fig. 12 D) and sometimes the cleavage is evident. Sphalerite occurs as small skeletal star-shaped or as lath-shaped exsolutions in chalcopyrite and / or cubanite (Fig. 12 F), but can occur as laths. Naldrett et al. (2000b) reported similar textures.

- Magnetite and ilmenite

Magnetite grains range from 0.1 to 2.3 mm in size and have an anhedral (rounded or elongate shape), subhedral, tetrahedral and octahedral forms (Fig. 12 A B E and Fig. 10 A). Magnetite occurs in textural equilibrium with pyrrhotite, chalcopyrite, pentlandite and / or silicate minerals (Fig. 12-E) and can contain ilmenite exsolutions. In addition, magnetite can be surrounded by pentlandite and chalcopyrite veinlets and / or stringers.

Ilmenite is associated with the magnetite as tiny (0.1 mm) grains or exsolutions lamellae. Naldrett et al. (2000b) and Boutroy et al. (2014) describe very similar characteristics for magnetite and Dare et al. (2012) reports the distribution of Fe-oxides at Sudbury that is similar to that observed at the Ovoid ore body.

The mineral abundances, for sulfides and oxides, for matrix and Fe-rich assemblages are similar and consists of ~ 50 % pyrrhotite + troilite, ~ 20 % pentlandite, ~ 15 % magnetite, ~ 10 % chalcopyrite and ~ 5 % galena, sphalerite and silicates.

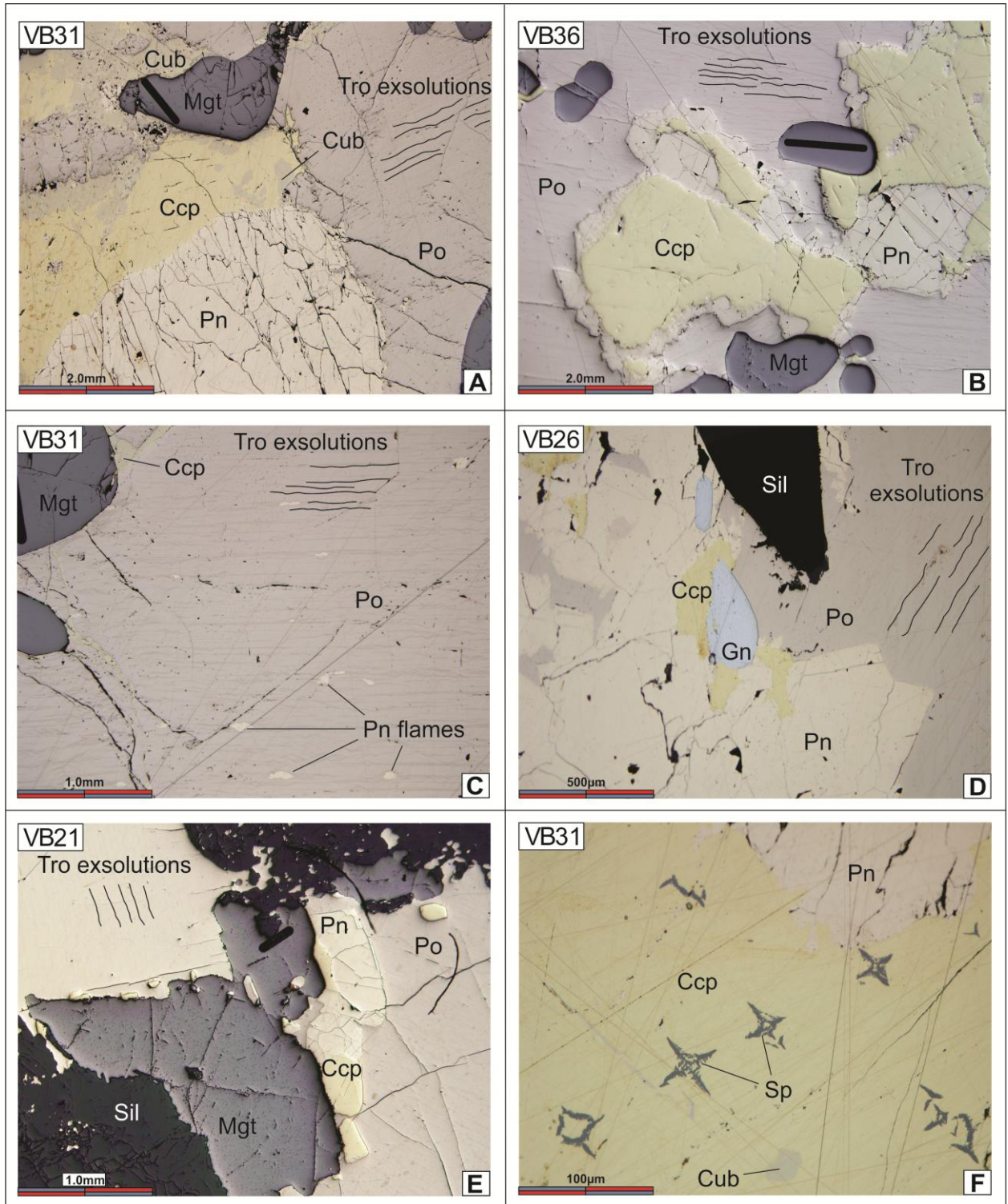


Fig. 12: Reflected light photomicrographs of typical matrix and Fe-rich sulfide textures from the Ovoid ore body. **A:** Massive sulfide showing coarse grains of pentlandite, chalcopyrite with cubanite exsolutions, surrounded by pyrrhotite matrix with troilite exsolutions and magnetite in rounded shapes. **B:** Massive sulfide showing pyrrhotite with troilite exsolutions and pentlandite which wrap around chalcopyrite grains. Magnetite grains in rounded shape. **C:** Massive sulfide showing pentlandite flames parallel to troilite

exsolutions. **D:** Massive sulfide showing pyrrhotite matrix with troilite exsolution, coarse grains of pentlandite and galena associated with pentlandite and chalcopyrite. **E:** Matrix sulfide showing pyrrhotite matrix with coarse grained magnetite and silicate mineral, also occur medium grained of pentlandite and chalcopyrite. **F:** Massive sulfide showing skeletal star-shaped sphalerite exsolutions within chalcopyrite. Abbreviations: Po = pyrrhotite, Tro = troilite, Pn = pentlandite, Ccp = chalcopyrite, Cub = cubanite, Mgt = magnetite, Gn = galena, Sp = sphalerite and VB = sample name. Black line within the magnetite represents the LA-ICP-MS work of Boutroy et al. (2014).

#### 4.2.5. *Cu-rich assemblage*

- Pyrrhotite and troilite exsolution lamellae

Pyrrhotite with exsolution lamellae of troilite in Cu-rich assemblage has the same characteristics (size, form and inclusions) as those described in matrix and Fe-rich assemblages (Fig. 13 A). Pyrrhotite is observed in contact with sulfide minerals (pentlandite, chalcopyrite and cubanite).

- Pentlandite

Pentlandite in Cu-rich assemblage has the same characteristics (grain size, form, inclusions and textures) as those described in matrix and Fe-rich assemblage, however pentlandite flames are not as common in Cu-rich assemblage. In addition, VB6 is the richest sample in pentlandite among all studied samples, and about 40-50 % of the thin section corresponds to coarse grained pentlandite (Fig. 13 B).

- Cubanite and chalcopyrite

Cubanite and chalcopyrite are the dominant sulfide minerals in all Cu-rich samples of the Ovoid ore body and form the matrix for the rest of ore minerals. Typically, cubanite is the most common copper sulfide mineral in Cu-rich assemblage, followed by chalcopyrite. There are cubanite exsolution within chalcopyrite (Fig. 13 C, D) and chalcopyrite exsolution within cubanite (Fig. 13 B).

Cubanite has an anhedral form, and grain size range from 0.4 mm up to 20 mm. Cubanite is observed in contact with chalcopyrite, pyrrhotite, pentlandite and magnetite. Minor chalcopyrite, pyrrhotite, pentlandite and magnetite inclusions are observed within the cubanite. Cracks in the cubanite are filled by magnetite and minor silicate minerals.

Chalcopyrite has similar characteristics as the matrix and Fe-rich assemblages. In both skeletal star-shaped exsolutions of sphalerite are observed.

- Galena and sphalerite

Sphalerite and galena occur as accessory minerals usually associated with cubanite / chalcopyrite. Galena (Fig. 13 D) and sphalerite (Fig. 13 E, F) have similar characteristics to the matrix and Fe-rich assemblages. Naldrett et al. (2000b) reported similar textures.

- Magnetite and ilmenite

Magnetite and ilmenite have similar characteristics (grain size, form, texture and inclusions) as those described for the matrix and Fe-rich assemblages (Fig. 13 D).

The mineral abundances, for sulfides and oxides, for Cu-rich assemblage (except for VB6) consists of ~ 60 % cubanite, ~ 10 % pyrrhotite + troilite, ~ 10 % pentlandite, ~ 10 % magnetite, ~ 7 % chalcopyrite and ~ 3 % galena, sphalerite and silicates.

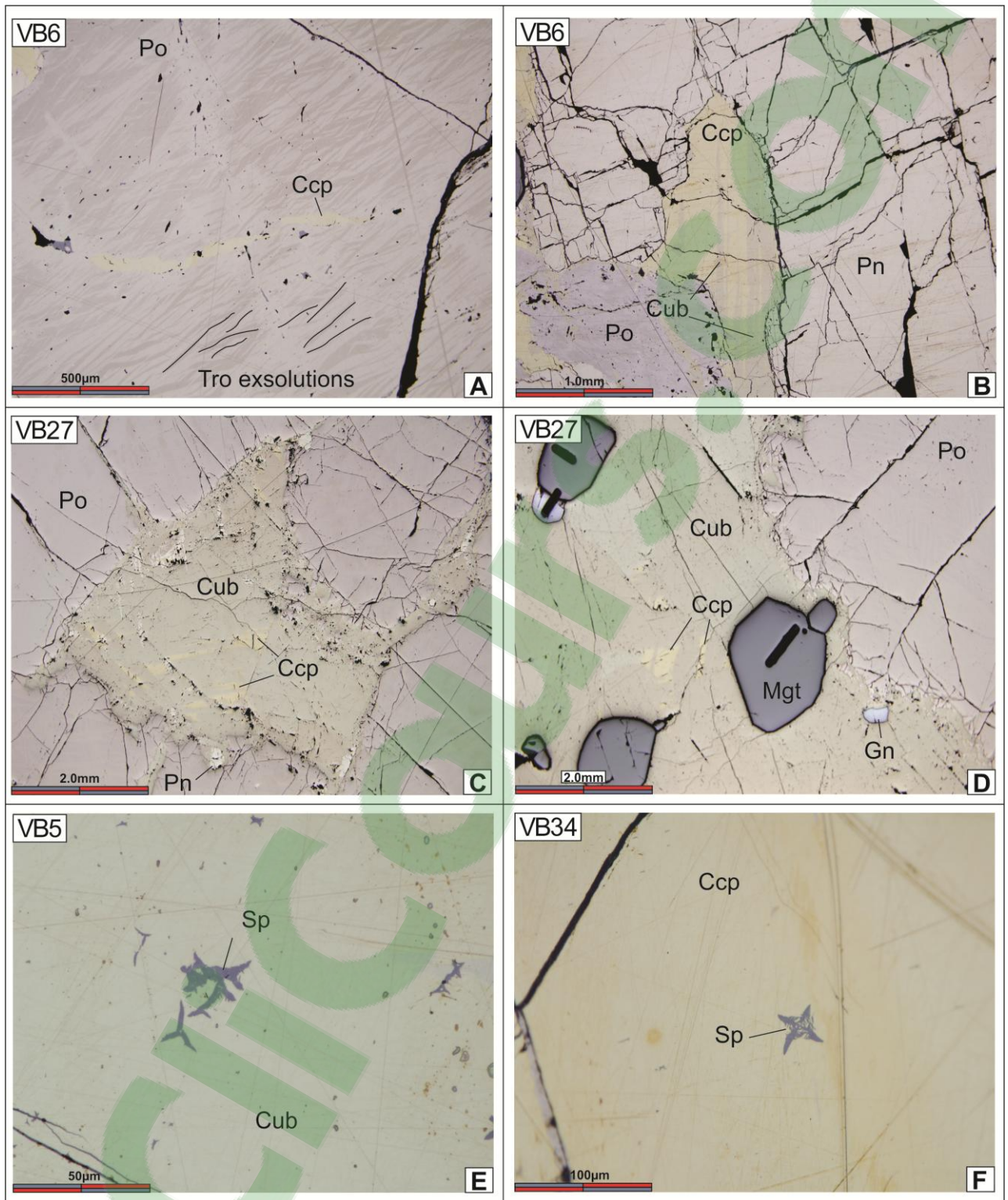


Fig. 13: Reflected light photomicrographs of typical Cu-rich sulfide textures from the Ovoid ore body. **A:** Massive sulfide showing troilite exsolutions in wave shape, also chalcopyrite oriented in the same direction. **B:** Massive sulfide showing coarse grained pentlandite and chalcopyrite with cubanite exsolutions. **C:** Massive sulfide showing cubanite with exsolutions of chalcopyrite. Also note the presence of pyrrhotite and few grains of pentlandite. **D:** Cubanite with chalcopyrite exsolutions and presence of galena and

magnetite. **E:** Massive sulfide showing exsolutions of sphalerite laths within cubanite. **F:** Massive sulfide showing skeletal star-shaped sphalerite exsolution within chalcopyrite. Abbreviations: Po = pyrrhotite, Tro = troilite, Pn = pentlandite, Ccp = chalcopyrite, Cub = cubanite, Mgt = magnetite, Gn = galena, Sp = sphalerite, VB = sample name. Black lines within the magnetite represent the LA-ICP-MS work of Boutroy et al. (2014).

### **4.3. Platinum-Group Minerals, Precious-Metal Minerals, Tellurides, Bismuthides and Arsenides assemblages**

Based on the whole rock concentrations of PGE and on the variations in Cu content, the main target to choose the samples is the highest PGE content, followed by highest Te, Bi, As and Sb content of the samples, which allows a greater chance of finding platinum-group minerals and precious-metal minerals. Six polished sections (Matrix: VB21; Fe-rich: VB30 and VB36; and Cu-rich: VB5, VB27 and VB34), were selected for a minor phase study. The occurrence of PGM, PMM, tellurides, bismuthides, and arsenides in each polish section is summarized in Table 3.

Platinum-group minerals, PMM, tellurides, bismuthides and arsenides were observed among the base metal sulfides minerals (cubanite is the principal host), although some occur as inclusions in magnetite, sphalerite and galena. In most cases they occur as single grain with anhedral to euhedral forms, ranging from 3 to 35  $\mu\text{m}$ . However, they can form composite grains in association with galena and sphalerite. The main PGM is froodite ( $\text{PdBi}_2$ ) (Fig. 14 A), but sobolevskite ( $\text{PdBi}$ ) is also present (Fig. 14 B, C). Hessite ( $\text{Ag}_2\text{Te}$ ) corresponds to the most common PMM followed by electrum ( $\text{Ag,Au}$ ). Bismuth-As-Te phases are well represented by native bismuth (Bi) which occurs as fine grains (3 – 7  $\mu\text{m}$ ) associated with electrum (Fig. 14 D) or as single grains, or as exsolution lamellae associated with galena (Fig. 14 E). Altaite ( $\text{PbTe}$ ) ranging from (5 – 12  $\mu\text{m}$ ) is associated with hessite (Fig. 14 F), or as single grains (Fig. 14 G) and nickeline ( $\text{NiAs}$ ) occurs as single grains ranging from (3 – 11  $\mu\text{m}$ ). The Ovoid samples are poor in PGE so the PGM and PMM were not common (Table 3).

Kelvin et al. (2011) reported some platinum-group mineral and precious metal minerals in the Ovoid which is in agreement with this study. The most common PGM

they reported is froodite ( $\text{PdBi}_2$ ) and the most abundant PGM in volume is sperrylite ( $\text{PtAs}_2$ ). They also report some PMM containing As, Bi, Te and small amount of Sb were also found and native Bi exsolutions within galena.

Table 3: Platinum-group minerals, PMM and As-Bi-Te phases and their textural relationship identified in the Ovoid ore body, Voisey's Bay.

Sample	Host mineral	PGM		PMM		As-Bi-Te phases		
		Froodite (PdBi <sub>2</sub> )	Sobolevskite (PdBi)	Electrum (Ag,Au)	Hessite (Ag <sub>2</sub> Te)	Native Bi	Nickeline (NiAs)	Altaite (PbTe)
		N° of grains	N° of grains	N° of grains	N° of grains	N° of grains	N° of grains	N° of grains
<b>Matrix sulfide</b>								
VB21	Po							1
	Pn						1	
<b>Fe-rich</b>								
VB30	Po							
	Pn		1					1
	Ccp		2				1	
VB36	Po							1
<b>Cu-rich</b>								
VB5	Po			1		1		1
	Cub/Ccp				1	1	1	
	Sp/Cub							1
VB27	Po				2			
	Pn					1		1
	Ccp		1					
	Cub				2	2		2
	Cub/Ccp			1	3	1		1
	Sp/Cub				2			
	Gn/Cub				2	1	2	
VB34	Po				1			1
	Pn						1	
	Cub	2			1	1		
	Cub/Ccp				3			1
	Sp/Cub		1					1
Size range of grains (µm):		6x3 to 8x4	2x1 to 5x3	2x1 to 2x2	5x4 to 10x6	3x1 to 7x3	3x1 to 11x2	5x3 to 12x5

Abbreviations: Po = pyrrhotite, Pn = pentlandite, Ccp = chalcopyrite, Cub = cubanite, Gn = galena, Sp = sphalerite.

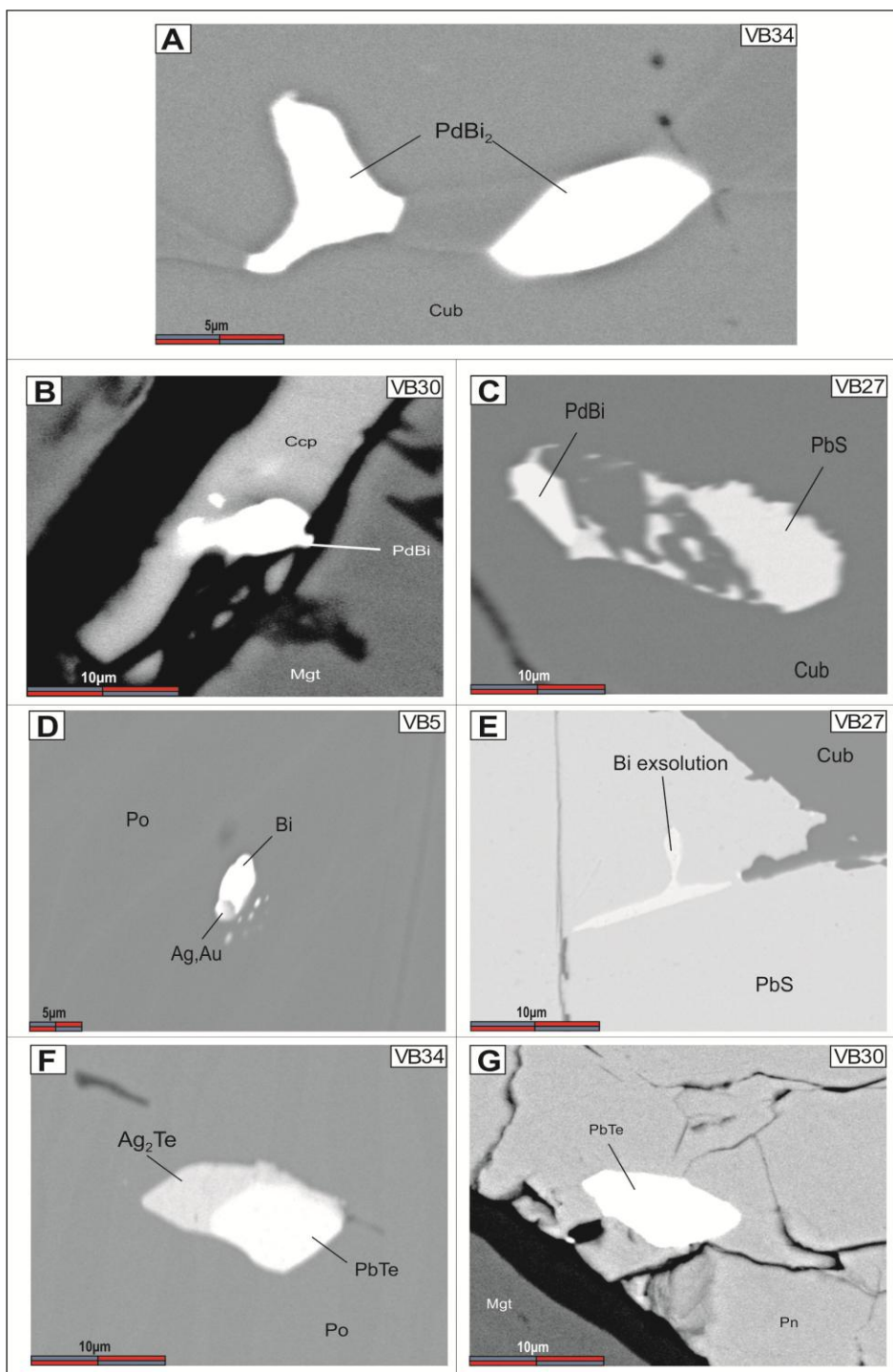


Fig. 14: Backscattered electron images of PGM, PMM and bismuth found in massive sulfides from the Ovoid ore body. **A:** Subhedral-euhedral froodite ( $\text{PdBi}_2$ ) hosted in cubanite. **B:** Anhedral sobolevskite ( $\text{PdBi}$ ) hosted in chalcopyrite. **C:** Anhedral sobolevskite ( $\text{PdBi}$ ), associated with galena and hosted in cubanite. **D:** Electrum ( $\text{Ag,Au}$ ) associated with native Bi hosted in pyrrhotite. **E:** Native Bi exsolution associated with galena and hosted in cubanite. **F:** Subhedral altaite ( $\text{PbTe}$ ), associated with anhedral hessite ( $\text{Ag}_2\text{Te}$ ), hosted in pyrrhotite. **G:** Subhedral altaite ( $\text{PbTe}$ ) hosted in pentlandite. Abbreviations: Po = pyrrhotite, Pn = pentlandite, Ccp = chalcopyrite, Cub = cubanite, VB = sample name.

## **CHAPTER 5**

### **5. WHOLE ROCK GEOCHEMISTRY**

Results for the whole rock analyses are presented in Table 4. Figure 15 shows the range of composition for each element for Fe-rich, Cu-rich, matrix, disseminated and breccia assemblages. Some elements are below the detection limit, in these cases the detection limit was considered to be the maximum value for data interpretations.

Table 4: Whole rock composition of samples from the Ovoid ore body, Voisey's Bay.

Sample	D.L.	VB2	VB7	VB21	VB8	VB5	VB6	VB27	VB34	VB22	VB23
Rock		Normal troctolite	Matrix troctolite	Matrix troctolite	Breccia sulfide	Cu-rich	Cu-rich	Cu-rich	Cu-rich	Fe-rich	Fe-rich
S (wt %)	0.35	0.47	22.6	10.3	10.5	26.6	19.2	31.3	26.7	30.4	36.8
Fe (wt %)	0.01	8.53	35.0	54.0	21.3	46.2	54.4	46.7	41.5	60.2	55.4
Ni (wt %)	0.01	0.07	2.06	0.93	0.90	1.38	3.07	2.46	1.99	1.42	2.58
Cu (wt %)	0.01	0.02	1.16	0.50	0.54	8.94	4.80	11.1	11.5	0.14	0.59
Os (ppb)	0.17	0.26	6.91	<i>bdl</i>	2.04	0.17	0.17	0.29	0.17	6.34	9.69
Ir (ppb)	0.05	<i>bdl</i>	3.40	0.58	1.38	0.83	0.27	0.30	0.19	3.29	4.30
Ru (ppb)	0.67	<i>bdl</i>	10.5	<i>bdl</i>	2.93	0.89	<i>bdl</i>	1.05	0.76	6.32	7.78
Rh (ppb)	0.08	0.20	6.22	1.86	3.72	2.38	1.35	0.32	<i>bdl</i>	8.02	8.57
Pt (ppb)	0.25	43.2	4.70	119	38.1	0.72	1.13	0.56	0.37	0.25	0.53
Pd (ppb)	0.47	10.6	106	41.0	44.8	475	254	539	751	78	181
Au (ppb)	0.48	94.47	49.88	6.73	22.04	667	68	2338	975	3.84	17.7
Re (ppb)	1.00	<i>bdl</i>	151.0	21.00	44.00	13.0	9.00	12.0	10.00	116	170
Ag (ppm)	0.30	<i>bdl</i>	0.76	<i>bdl</i>	<i>bdl</i>	32.0	7.78	24.81	33.57	<i>bdl</i>	<i>bdl</i>
As (ppm)	0.20	0.30	0.80	0.78	0.50	9.67	1.69	4.63	4.47	1.40	0.20
Bi (ppm)	0.02	0.41	0.63	0.11	0.30	9.14	0.71	6.51	16.2	0.18	0.54
Cd (ppm)	0.10	0.64	2.89	0.74	1.06	280	49.2	296	389	0.24	1.56
Co (ppm)	0.10	60.0	885	536	390	773	1476	1370	1136	803	1522
Pb (ppm)	0.01	37.7	32.5	5.46	37.3	280	26.4	99.2	637	4.81	9.11
Sb (ppm)	0.02	0.10	0.08	0.09	0.13	1.14	0.14	0.24	0.48	0.07	0.08
Se (ppm)	2.00	<i>bdl</i>	25.0	14.8	11.2	89.8	36.8	91.2	91.9	34.4	34.5
Sn (ppm)	0.05	2.72	2.54	10.5	2.02	21.8	26.0	24.5	32.9	2.42	1.57
Te (ppm)	0.02	0.75	1.63	0.63	1.16	80.8	8.75	75.4	84.0	1.65	2.73
Zn (ppm)	2.00	70.3	90.5	837	92.4	1058	451	1148	1588	58.1	86.8
Ni/Cu		3.50	1.78	1.87	1.67	0.15	0.64	0.22	0.17	9.83	4.36
Pd/Ir		-	31.2	70.7	32.5	572	933	1772	4058	23.7	42.1

Abbreviations: *bdl* = below detection limit and *n.a.* not available.

Table 4 continuation: Whole rock composition of samples from the Ovoid ore body, Voisey's Bay.

Sample name	D.L.	VB24	VB25	VB26	VB28	VB29	VB30	VB31	VB32	VB33	VB35	VB36
Rock		Fe-rich	Fe-rich	Fe-rich	Fe-rich	Fe-rich	Fe-rich	Fe-rich	Fe-rich	Fe-rich	Fe-rich	Fe-rich
S (wt %)	0.35	33	31.1	31.3	27.7	31.4	35.8	25.5	33.5	37.4	27.5	31.1
Fe (wt %)	0.01	56.8	52.5	54.0	47.7	55.0	51.8	53.1	55.3	51.7	57.2	57.1
Ni (wt %)	0.01	1.62	3.26	2.28	1.65	2.78	3.80	3.58	2.49	2.29	2.52	3.5
Cu (wt %)	0.01	0.40	0.70	0.58	1.34	0.70	1.58	2.57	0.57	4.57	0.69	0.91
Os (ppb)	0.17	0.17	4.87	8.33	3.16	6.66	7.14	2.55	9.45	4.53	0.44	8.4
Ir (ppb)	0.05	0.59	3.31	3.67	2.06	3.23	3.90	2.25	4.92	2.25	0.52	4.42
Ru (ppb)	0.67	<i>bdl</i>	4.76	6.70	2.27	5.80	6.08	2.68	10.3	3.45	<i>bdl</i>	7.36
Rh (ppb)	0.08	2.49	7.58	7.50	5.71	9.52	10.34	6.24	11.8	5.16	2.77	10.4
Pt (ppb)	0.25	33.40	4.69	27.43	0.25	2.80	1.05	1.04	47	82.02	0.40	1.90
Pd (ppb)	0.47	70.87	158	127	245	290	436	372	141	126	155	334
Au (ppb)	0.48	67.0	16.48	13.78	6398	23.0	140	177	6.82	40.01	264	19.3
Re (ppb)	1.00	n.a.	126	125	n.a.	141	139	84.0	n.a.	154.0	10.0	172
Ag (ppm)	0.30	2.31	0.85	0.48	1.65	1.12	0.99	1.56	1.74	1.81	3.62	1.75
As (ppm)	0.20	2.43	1.39	0.20	0.73	<i>bdl</i>	<i>bdl</i>	1.02	0.76	<i>bdl</i>	3.20	<i>bdl</i>
Bi (ppm)	0.02	n.a.	0.25	0.53	n.a.	0.73	0.57	0.81	n.a.	0.61	2.03	0.59
Cd (ppm)	0.10	n.a.	1.27	0.12	n.a.	1.19	2.82	7.57	n.a.	10.3	5.73	1.62
Co (ppm)	0.10	728	1631	1251	954	1532	1774	1656	1253	1123	1149	1736
Pb (ppm)	0.01	n.a.	21.4	14.5	n.a.	174	15.4	28.9	n.a.	16.0	38.7	16.1
Sb (ppm)	0.02	0.03	0.09	0.07	0.41	0.26	0.06	0.10	<i>bdl</i>	0.18	0.11	0.06
Se (ppm)	2.00	43.1	30.8	31.0	28.9	35.7	36.0	33.5	32.8	33.1	39.0	32.7
Sn (ppm)	0.05	n.a.	1.72	2.64	n.a.	3.06	2.40	3.15	n.a.	4.21	11.7	1.85
Te (ppm)	0.02	n.a.	1.95	2.33	n.a.	2.92	2.27	2.77	n.a.	3.57	9.32	2.45
Zn (ppm)	2.00	46.8	85.8	56.4	103.7	82.1	108	237	55.1	243	92.2	110
Ni/Cu		4.10	4.62	3.9	1.2	4.0	2.4	1.4	4.4	0.50	3.7	3.8
Pd/Ir		119	47.7	34.5	119	90	112	165	28.6	55.9	298	76

Abbreviations: *bdl* = below detection limit and *n.a.* not available.

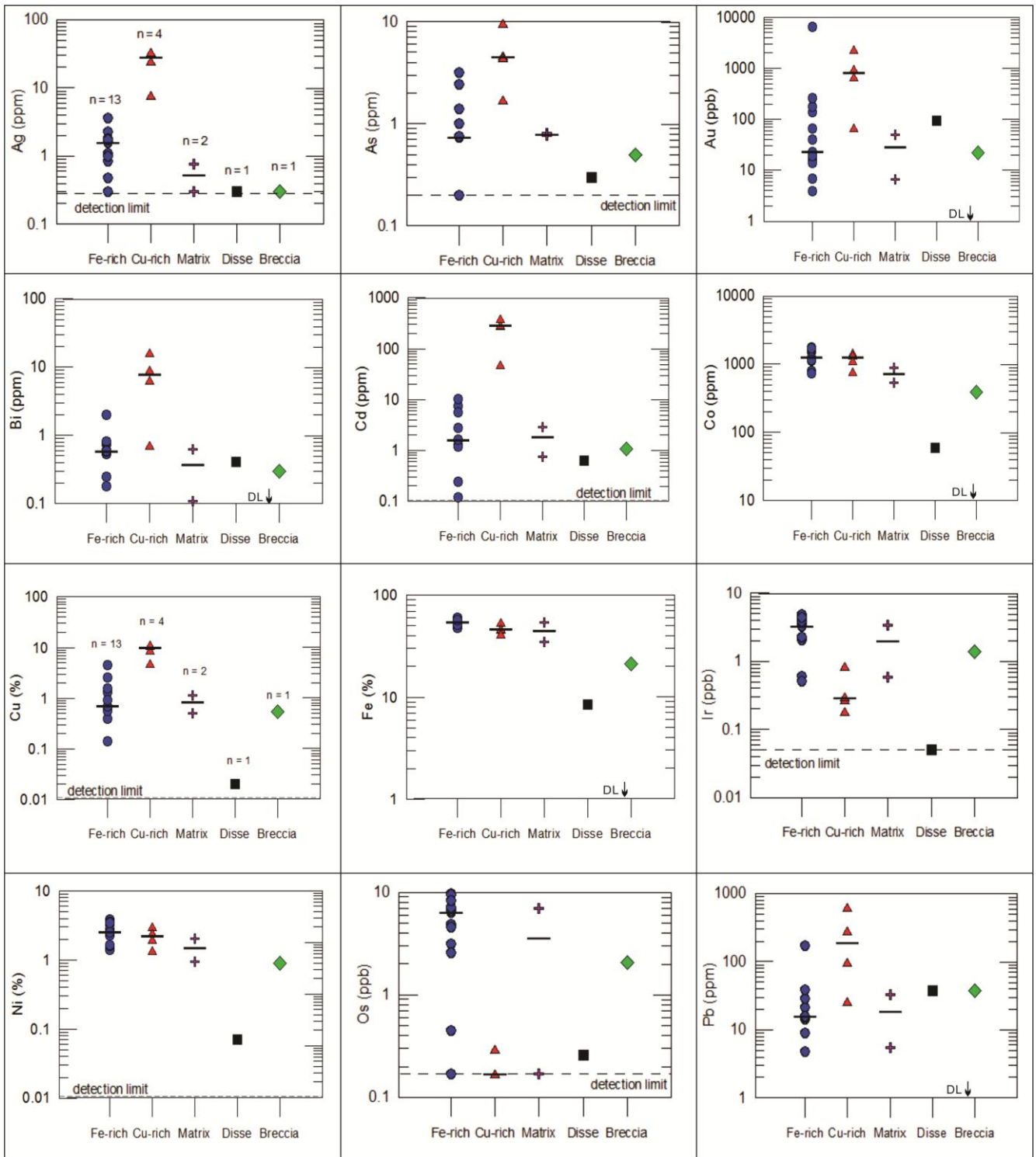


Fig. 15: Plots of Ag, As, Au, Bi, Cd, Co, Cu, Fe, Ir, Ni, Os, Pb, Pd, Pt, Re, Rh, Ru, S, Sb, Se, Sn, Te, and Zn for each assemblage according to whole rock results. Median values are shown by black lines on each assemblage. Detection limits are represented by the dashed lines. Abbreviation: DL = detection limit.

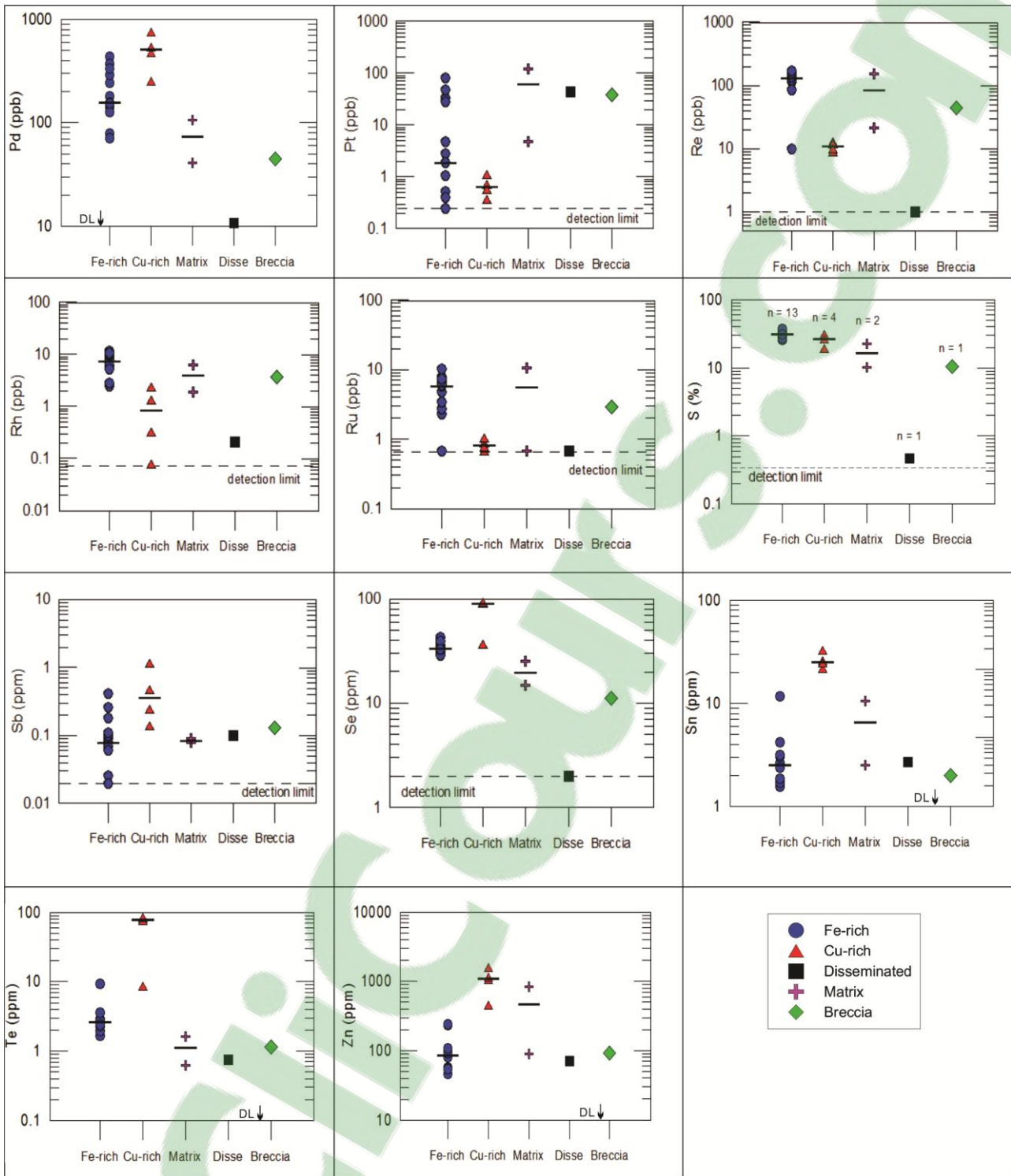


Fig. 15 continuation: Plots of Ag, As, Au, Bi, Cd, Co, Cu, Fe, Ir, Ni, Os, Pb, Pd, Pt, Re, Rh, Ru, S, Sb, Se, Sn, Te, and Zn for each assemblage according to whole rock results. Median values are shown by black lines on each assemblage. Detection limits are represented by the dashed lines. Abbreviation: DL = detection limit.

## 5.1. Primitive mantle normalized patterns

The composition of all samples have been recalculated to 100% sulfides according to the equation proposed in Barnes and Lightfoot (2005):

$$C_{(100\% \text{ sul})} = C_{\text{wr}} * 100 / (2.527 * S + 0.3408 * \text{Cu} + 0.4715 * \text{Ni}) \quad (1)$$

where  $C_{(100\% \text{ sul})}$  = concentration of an element in 100% sulfides;  $C_{\text{wr}}$  = concentration of the element in the whole rock; S, Cu and Ni = concentration in the whole rock, in wt %.

In figure 16, the five assemblages are compared on a multi-element diagram. The elements on the multi-element diagram are plotted in order of increasing compatibility (from left to right) during partial melting of the mantle to produce a picrite (Barnes, 2016). The disseminated sulfide and Cu-rich sulfide assemblages are richest in the incompatible elements (Sn through to Pd, except for Re). In contrast the Cu-rich assemblage is poorest in IPGE (Os, Ir, Ru) and Rh whereas the disseminated sulfide assemblage is richest in these elements. Matrix, breccia and Fe-rich assemblages have patterns that are similar to each other except for slightly variations for some elements (As, Ag, Cu) and a negative Pt anomaly in the Fe-rich assemblage. These assemblages are poorer in the incompatible elements but richer in Re, Pt, Rh, Ru, Ir and Os than the Cu-rich assemblage resulting in flatter patterns overall. Matrix and breccia assemblages are slightly richer in almost all elements compared to Fe-rich assemblage. Disseminated and Cu-rich assemblages show a marked positive Bi anomaly.

All of the patterns from all of the assemblages are depleted in PGE relative to Ni and Cu. This type of depletion is generally attributed to an earlier segregation of sulfide liquid because the PGE have much higher partition coefficients into sulfide liquid than the other chalcophile elements (Fig. 17).

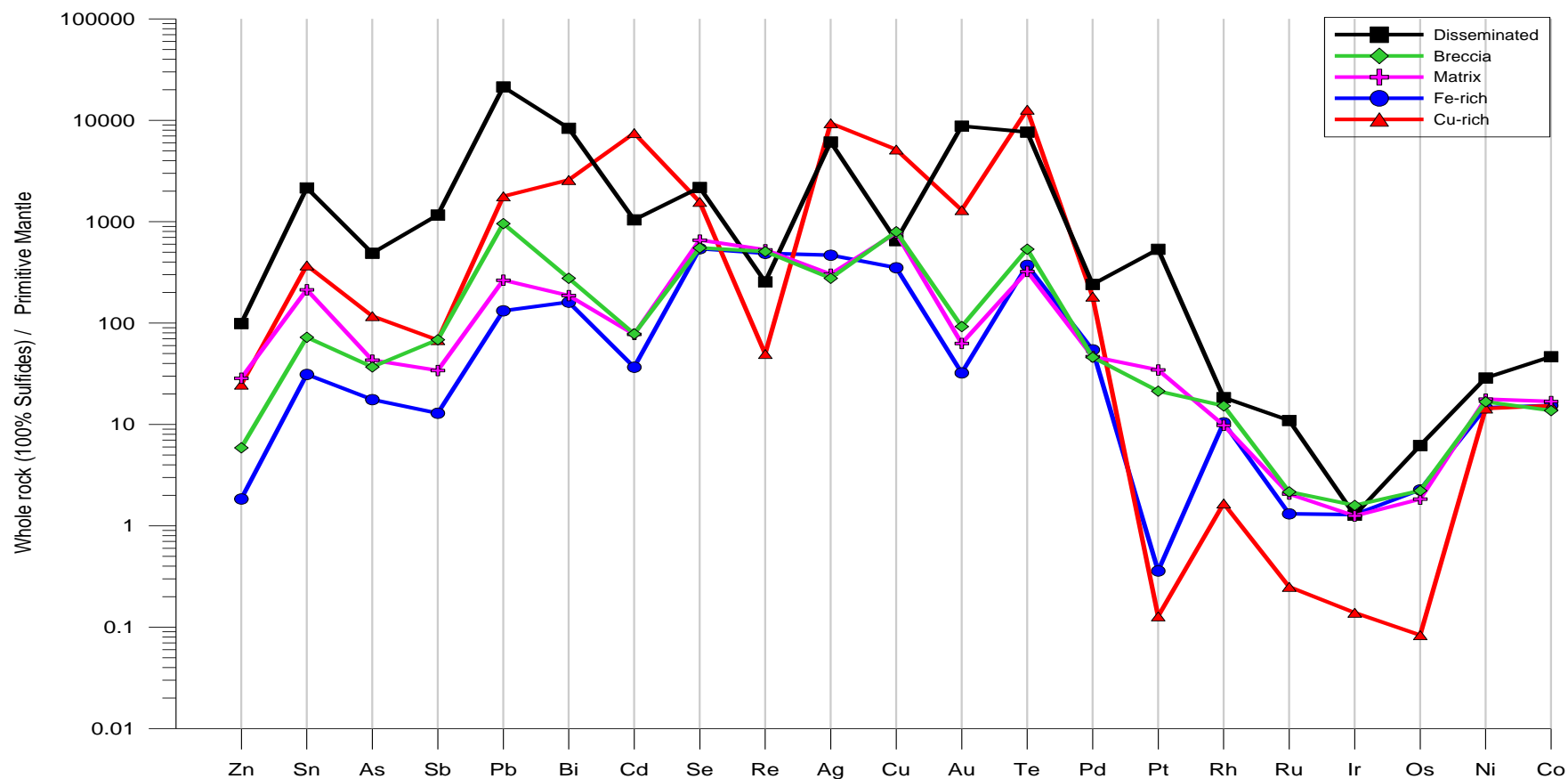


Fig. 16: Primitive mantle normalized multi-element diagram. The elements are ordered relative to their compatibility during partial melting of the mantle, from the most incompatible to the left to the most compatible to the right. Disseminated (n=1), breccia (n=1), matrix (n=2), Fe-rich (n=13) and Cu-rich (n=4) assemblages are compared. Disseminated, breccia, matrix and Fe-rich are richer in IPGE. Disseminated sulfide and Cu-rich are richer in Pd, trace and incompatible elements. Data were recalculated to 100% sulfides and primitive mantle values from Lyubetskaya and Korenaga (2007).

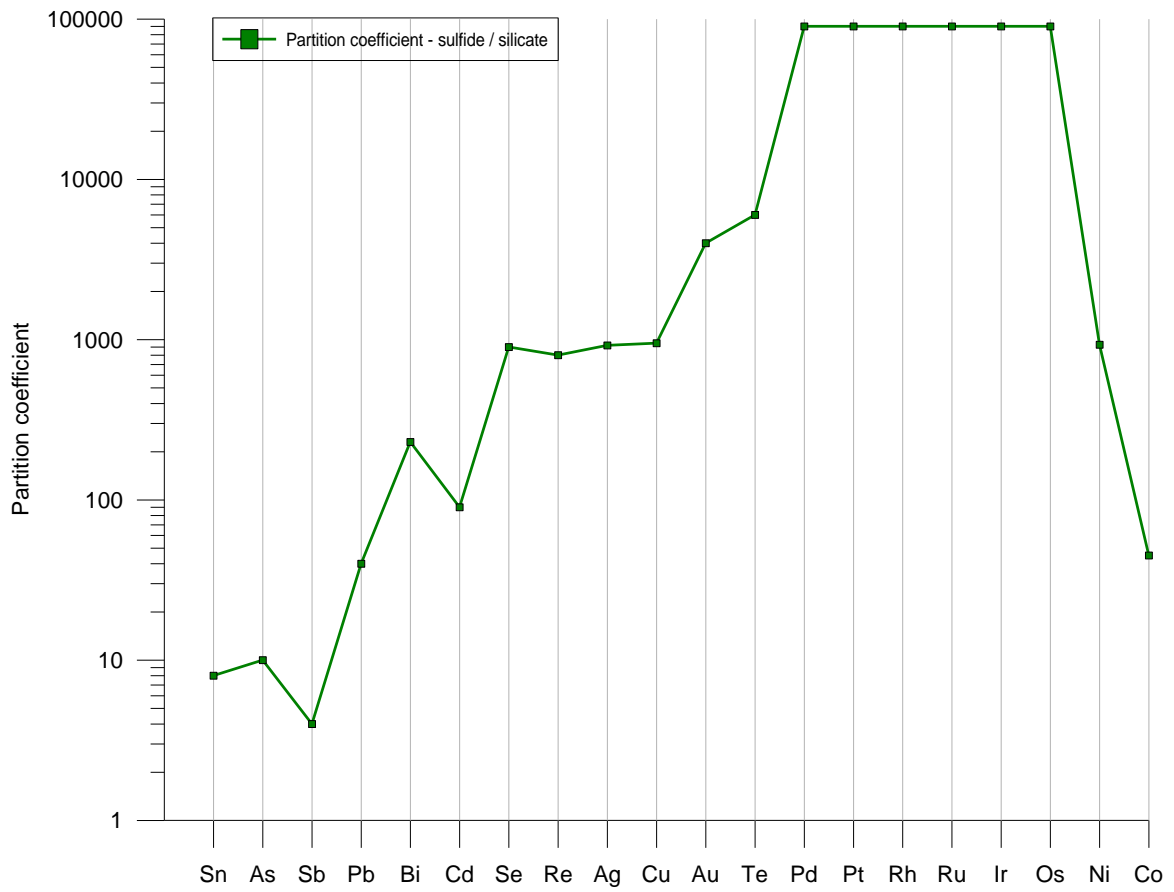


Fig. 17: Multi-element diagram showing partition coefficients (sulfide / silicate liquid) based on Barnes and Ripley (2016).

## **5.2. Comparison with previously published data of Voisey's Bay**

Naldrett et al. (2000a) and Kelvin et al. (2011) have published whole rock results for some elements recalculated to 100% sulfides (Table 5). Massive sulfides data for the Ovoid from all studies are compared in figure 18 and the breccia sulfide in figure 19. The matrix troctolite of the Ovoid was compared with the same rock-type from the Mini-Ovoid in figure 20, because this is the only information available in Naldrett et al. (2000a). All studies have similar concentrations, however, the samples for this study are depleted in PGE compared to Naldrett et al. (2000a) and Kelvin et al. (2011).

Table 5: Whole rock analysis for massive sulfides, breccia and matrix troctolite recalculated to 100% sulfides. Results of this present work compared to Naldrett et al. (2000a) and Kelvin et al. (2011).

<b>This study</b>													
<b>Assemblage</b>	<b>Ni %</b>	<b>Cu %</b>	<b>Co %</b>	<b>Os ppb</b>	<b>Ir ppb</b>	<b>Ru ppb</b>	<b>Rh ppb</b>	<b>Pd ppb</b>	<b>Pt ppb</b>	<b>Au ppb</b>	<b>Pb ppm</b>	<b>Zn ppm</b>	<b>Ag ppm</b>
<b>Breccia sulfide</b>	3.32	1.99	0.14	7.54	5.09	10.81	13.72	165.27	140.59	81.29	137.59	340.83	1.11
<b>Matrix troctolite</b>	3.52 (0.14)	1.94 (0.07)	0.17 (0.04)	6.24 (7.92)	4.01 (2.57)	10.3 (11.6)	8.83 (2.58)	168 (19)	227 (310)	55.39 (42.48)	38.1 (24.8)	1747 (1989)	1.12 (0.016)
<b>Fe-rich</b>	2.89 (1.05)	1.43 (1.35)	0.17 (0.05)	6.61 (3.66)	4.11 (1.58)	6.54 (3.42)	9.01 (3.28)	196 (151)	2.36 (27.16)	85 (118)	19 (62.3)	106 (83.86)	1.79 (1.27)
<b>Cu-rich</b>	2.84 (1.75)	12.74 (2.64)	0.18 (0.08)	0.29 (0.06)	0.44 (0.41)	1.24 (0.54)	1.49 (1.38)	655 (232)	0.84 (0.76)	1143 (1110)	256 (377)	1481 (546)	37 (14.7)
<b>Naldrett et al. (2000)</b>													
<b>Massive sulfide - Ovoid</b>	4.61 (1.06)	2.84 (1.4)	0.18	4 (1.5)	2 (1.1)	17 (10)	8 (3)	252 (115)	123 (111)	93 (130)	-	-	-
<b>Breccia sulfide - Ovoid</b>	4.14 (1.10)	3.44 (1.31)	0.19	13 (4)	9.1 (1.9)	70 (16)	23 (5)	521 (136)	430 (159)	469 (178)	-	-	-
<b>Leopard troctolite - Mini Ovoid</b>	3.94 (0.85)	2.77 (0.94)	0.19	7 (2)	2.9 (0.91)	25 (16)	12 (6)	288 (60)	145 (71)	224 (80)	-	-	-
<b>Kelvin et al. 2011</b>													
<b>Massive sulfide - Ovoid Pd+Pt+Pb rich</b>	4.4	2.45	0.145	-	bdl	bdl	4	483	469.5	146.5	1010	398	27

Abbreviation: bdl = below detection limit and n.d. = not determined. Leopard troctolite corresponds to the matrix troctolite in this study. Values in the brackets: (1 standard deviation).

The average massive sulfide from Naldrett et al. (2000a) and Kelvin et al. (2011) of the Ovoid plot between our Fe-rich massive sulfide and our Cu-rich sulfide (except for Pb, Pt, Ru and Ni). The intermediate position for the massive sulfides is reasonable considering that Naldrett et al. (2000a) data represents an average which included both Fe-rich and Cu-rich rocks. The high Pb reported by Kelvin et al. (2011) is also reasonable because these samples were investigated because they are exceptionally galena-rich. Kelvin's samples are also richer in Ag, Au, Pd and Pt compared to Naldrett et al. (2000a) and Fe-rich assemblage, but not as rich as our Cu-rich assemblage (Fig. 18).

The Pt concentrations found in our study are much lower than those reported by either Naldrett et al. (2000a) or Kelvin et al. (2011). This does not appear to be an analytical error because results for the international reference materials analyzed at the same time as the Voisey's Bay samples give normal results for Pt (Table 1 – Methodology). Also despite being analyzed in the same batch of samples some samples are not Pt depleted (e.g. VB33, VB21, VB26, VB8). It should be noted that Pt results from Naldrett et al. (2000a) and this study have a very high standard deviation (Table 5), ~100 %. Therefore the reason for the low Pt values in the massive sulfides compared with previous results could be a sampling problem, with the samples with low Pt being over represented in the current sample set.

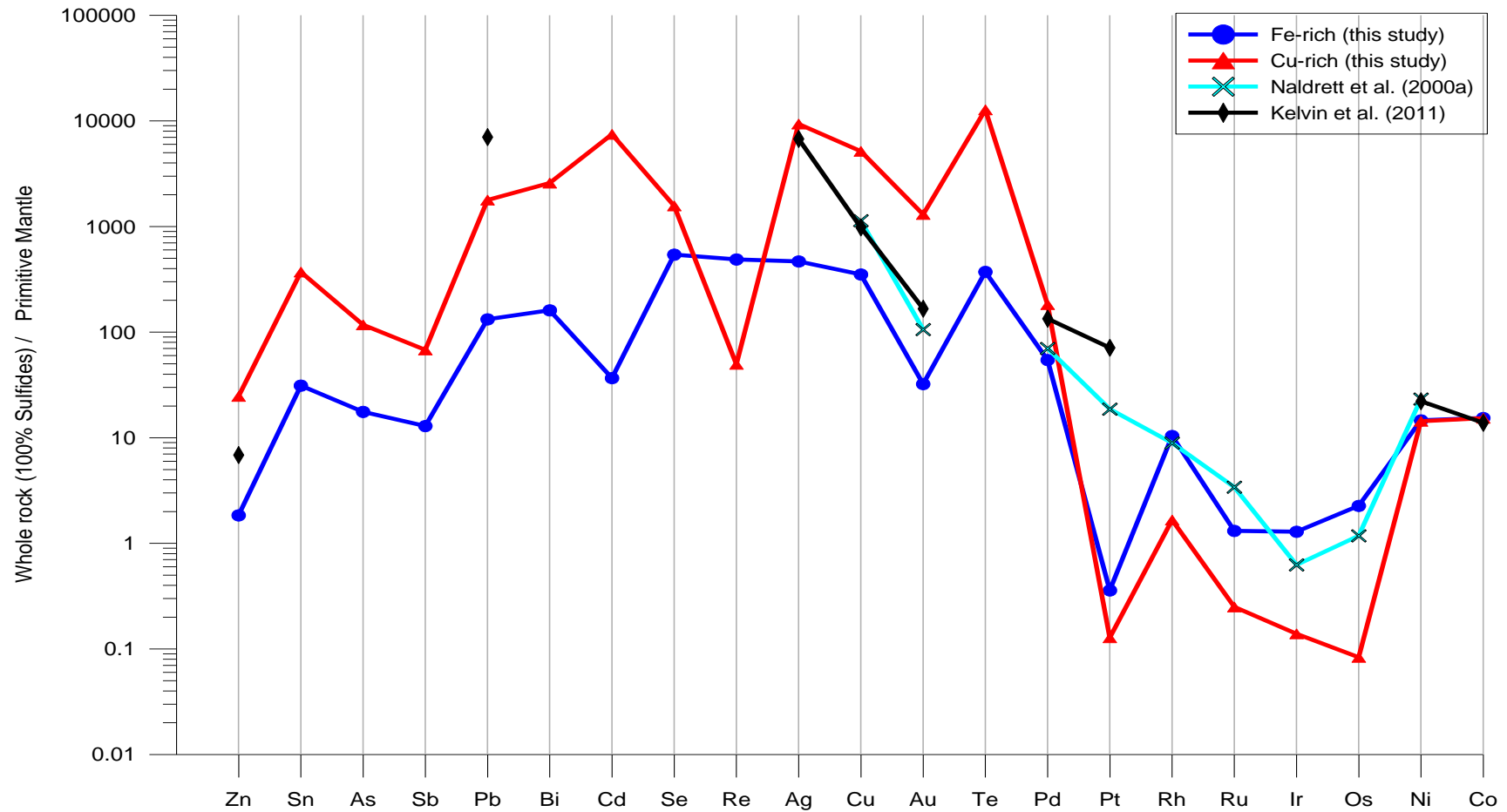


Fig. 18: Primitive mantle normalized multi-element diagram for massive sulfides from the Ovoid. The elements are ordered relative to their compatibility during partial melting of the mantle, from the most incompatible to the left to the most compatible to the right. Data were recalculated to 100% sulfides and primitive mantle values from Lyubetskaya and Korenaga (2007).

In figure 19, breccias samples from Naldrett et al. (2000a) and from this study are compared. The shapes of the patterns are similar. The averages reported by Naldrett et al. (2000a) are higher, however given that in both studies the number of samples analyzed was small (4 and 1 respectively) the difference is not considered to be significant and many elements were not analyzed by Naldrett et al. (2000a).

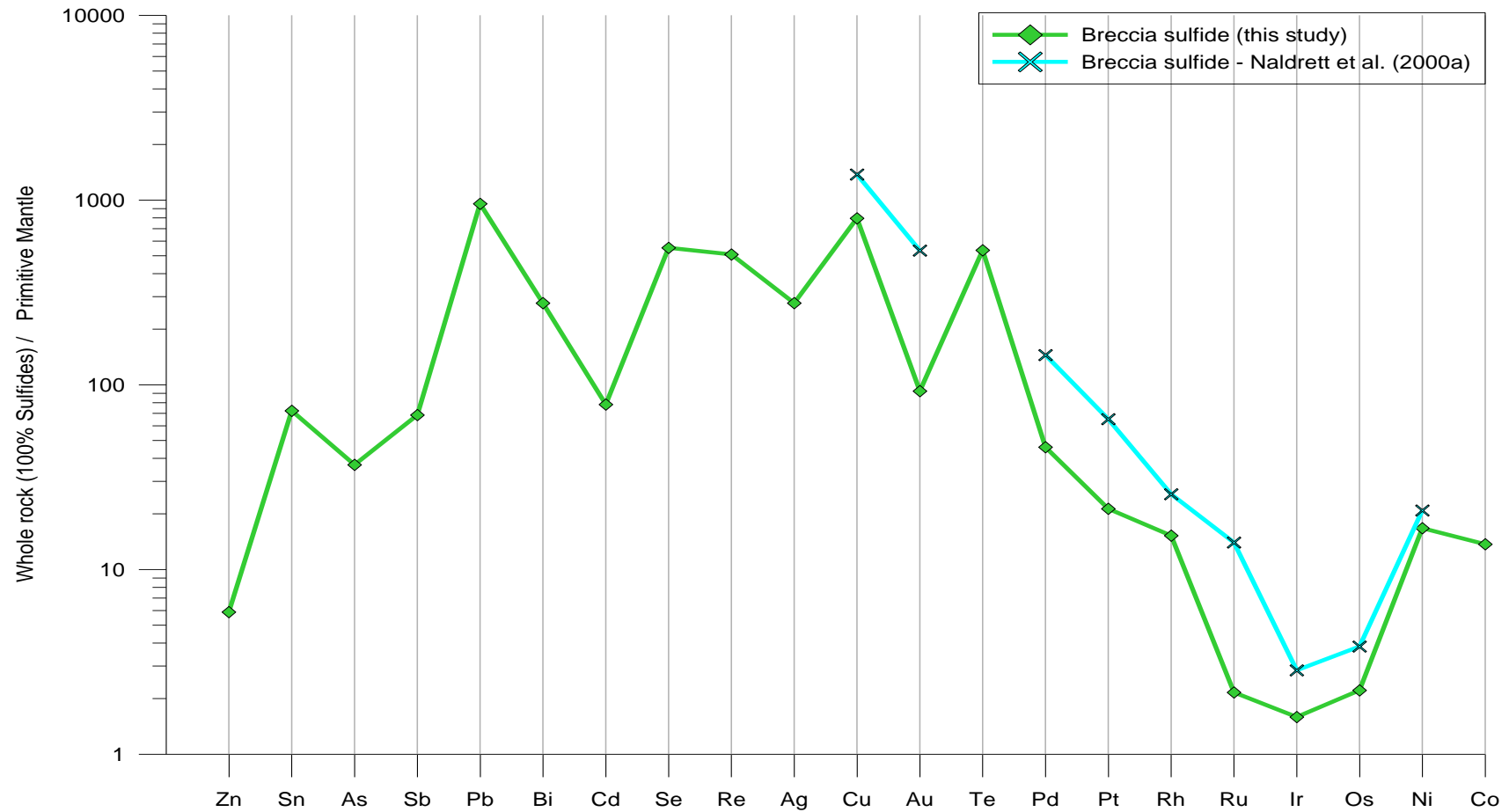


Fig. 19: Primitive mantle normalized multi-element diagram. Breccia sulfide from this study and from Naldrett et al. (2000a) are compared. Naldrett et al. (2000a) samples is richer in all elements. Data were recalculated to 100% sulfides and primitive mantle values from Lyubetskaya and Korenaga (2007).

Figure 20 compares Naldrett et al. (2000a) matrix troctolite from Mini-Ovoid and matrix troctolite from the Ovoid of this study. They have similar mantle normalized patterns and concentrations except for Cu and Au which are higher in the Mini-Ovoid.

Clicours.com

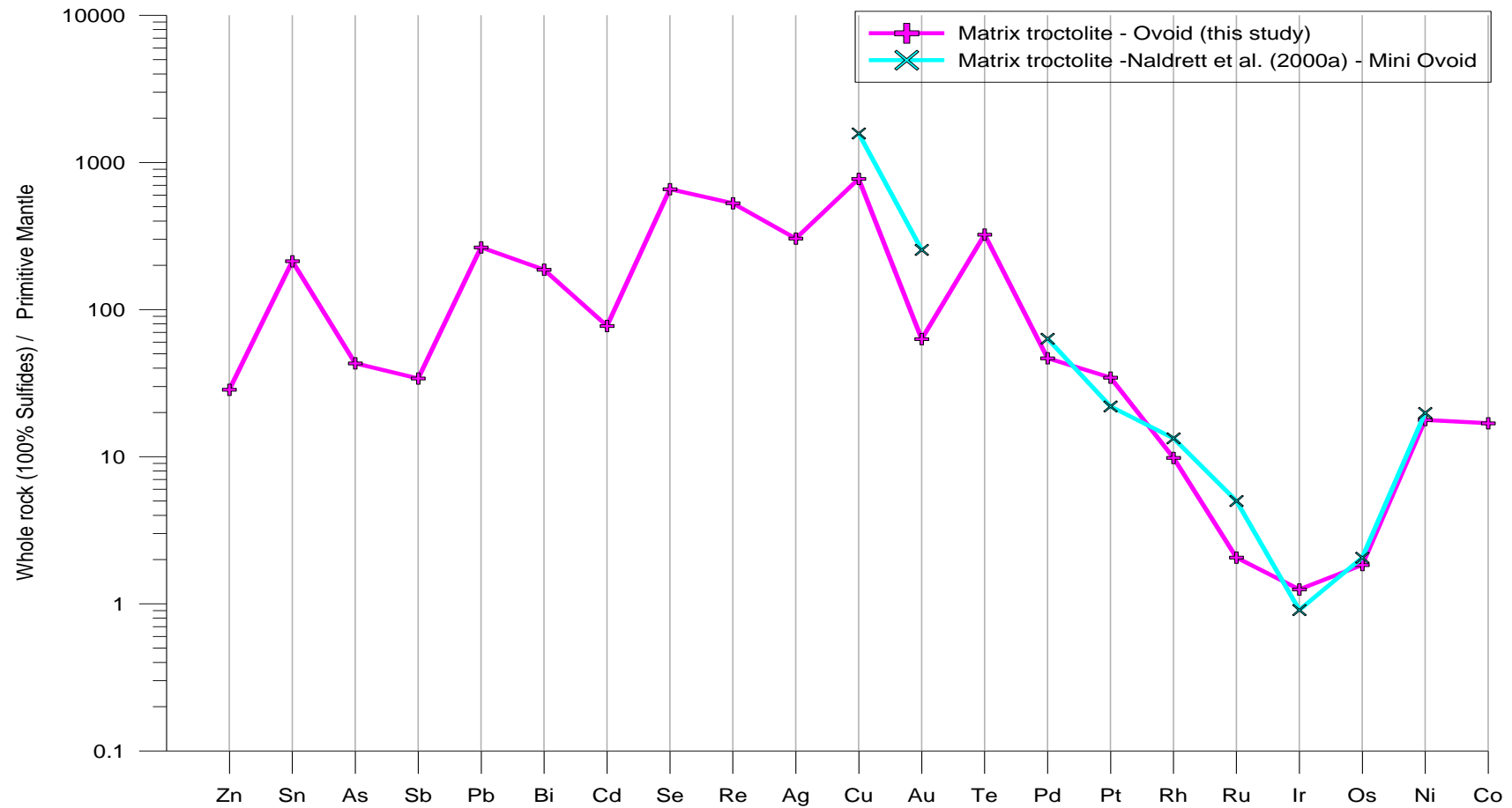


Fig. 20: Primitive mantle normalized multi-element diagram. Matrix sulfide from the Ovoid and matrix from the Mini-Ovoid in Naldrett et al. (2000a) are compared and both have a similar pattern. Data were recalculated to 100% sulfides and primitive mantle values from Lyubetskaya and Korenaga (2007).

### 5.3. Comparison with other deposits

The whole rock analysis from the Ovoid are compared with various deposits including Sudbury, Jinchuan, Lac des Îles and Aguablanca. The disseminated, breccia, matrix, Fe-rich and Cu-rich assemblages were compared separately to make this comparison clearer.

#### 5.3.1. *Disseminated sulfide*

The disseminated assemblage of Voisey's Bay is compared with disseminated assemblages of Aguablanca (Piña et al. 2012) and Jinchuan (Song et al. 2009) (Fig. 21). All deposits have similar concentrations of Pd, Rh and Ni. Voisey's Bay is the richest in Bi, Se, Au, Te, Pt, Os and Co, Jinchuan is the richest in Ru and Ir and Aguablanca is the richest in Cu. From Pd to Ni in figure 21, Aguablanca and Voisey's Bay have similar pattern except for Os that has a negative anomaly in Aguablanca. Comparing Voisey's Bay with Jinchuan, both have similar concentrations of Cu, and Jinchuan is depleted in Pt and richer in Ru and Ir.

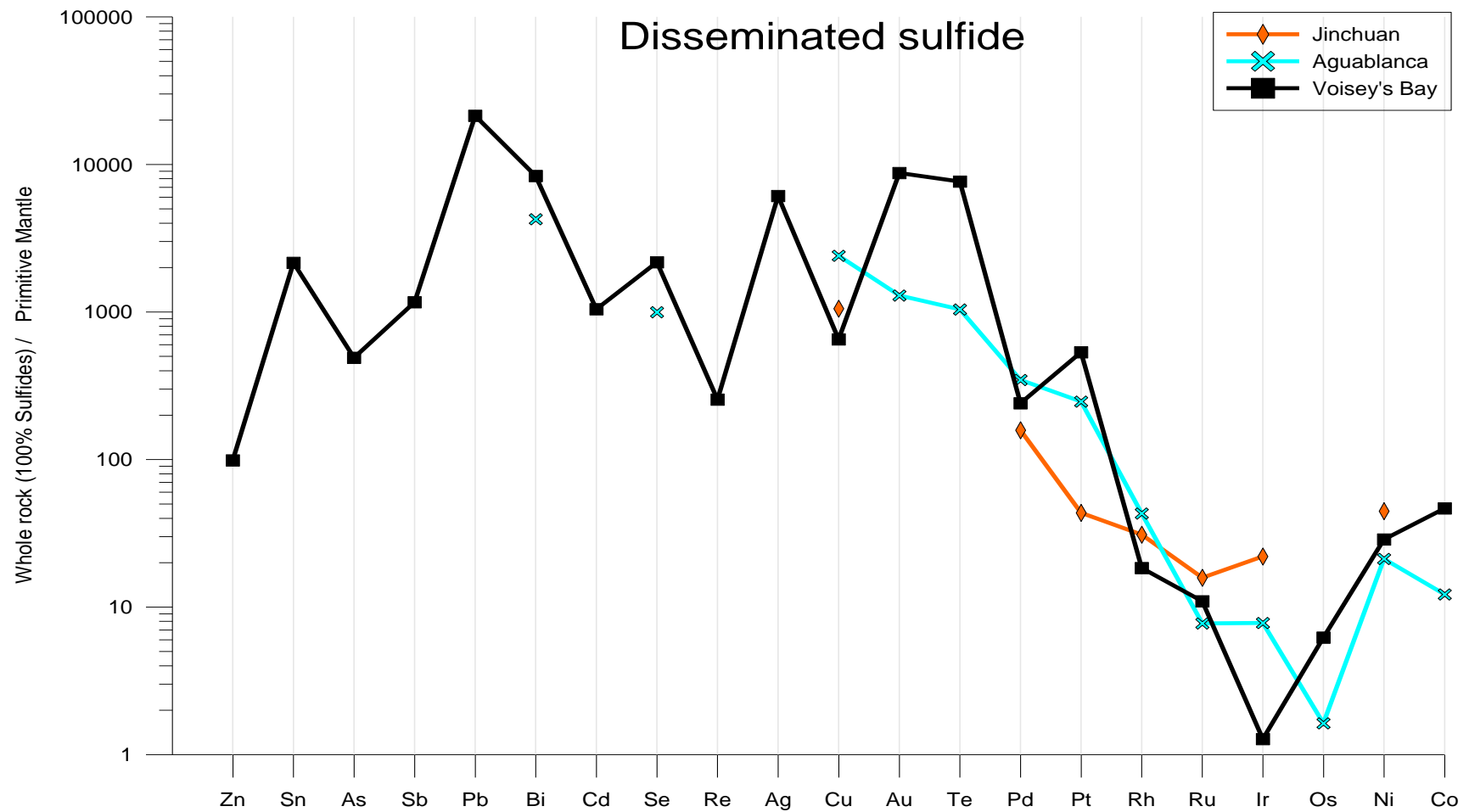


Fig. 21: Primitive mantle normalized multi-element diagram for disseminated assemblage from Voisey's Bay, Aguablanca (Piña et al. 2012) and Jinchuan (Song et al. 2009). Data were recalculated to 100% sulfides and primitive mantle values from Lyubetskaya and Korenaga (2007).

### 5.3.2. Breccia sulfide

Breccia assemblage of the Ovoid was compared with breccia assemblage of Aguablanca (Piña et al. 2012) (Fig. 22). Both deposits have similar concentrations of Cu, Te and Co. Aguablanca is the richest Se, Au, PGE and Ni, and the Ovoid is the richest in Bi. From Cu to Co, both breccias have steep patterns in PGE direction and Aguablanca has positive anomaly in Ir.

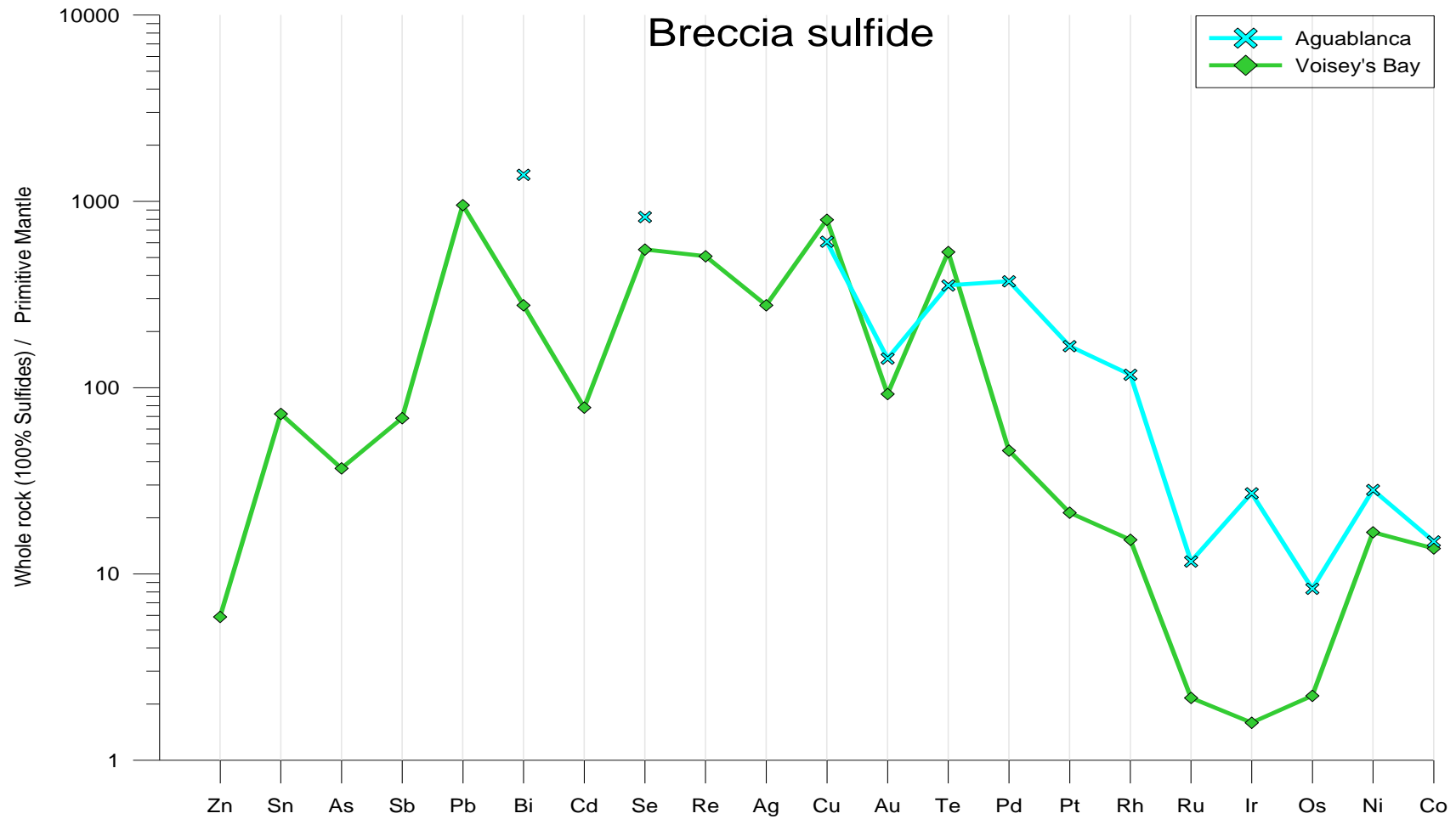


Fig. 22: Primitive mantle normalized multi-element diagram. Breccia sulfide assemblage from Voisey's Bay and Aguablanca (Piña et al. 2012) are compared. Data were recalculated to 100% sulfides and primitive mantle values from Lyubetskaya and Korenaga (2007).

### 5.3.3. *Matrix sulfide*

In figure 23, the matrix sulfide assemblages from Voisey's Bay, Aguablanca (Piña et al. 2012), Jinchuan (Song et al. 2009) and Lac des Îles (Duran et al. 2016a) are compared. Compared to Voisey's Bay, all other deposits are richer in PGE. Lac des Îles is the richest in most elements such as As, Sb, Se, Ag, Cu, Au, Te, Pd, Pt, Rh, Ru, Os, Ni and Co. Voisey's Bay is the most depleted in PGE, but on the other hand is the richest in Zn and Sn, and has similar amount of Pb, Bi and Cd compared to Lac des Îles. Aguablanca has a similar concentration of Se, Au, Te and Co compared to Voisey's Bay. Jinchuan is the richest in Ir and has a significant amount of Cu and Pd. It has similar pattern for PGE compared to Aguablanca, but it is richer in those elements. Lac des Iles shows marked Bi positive anomaly.

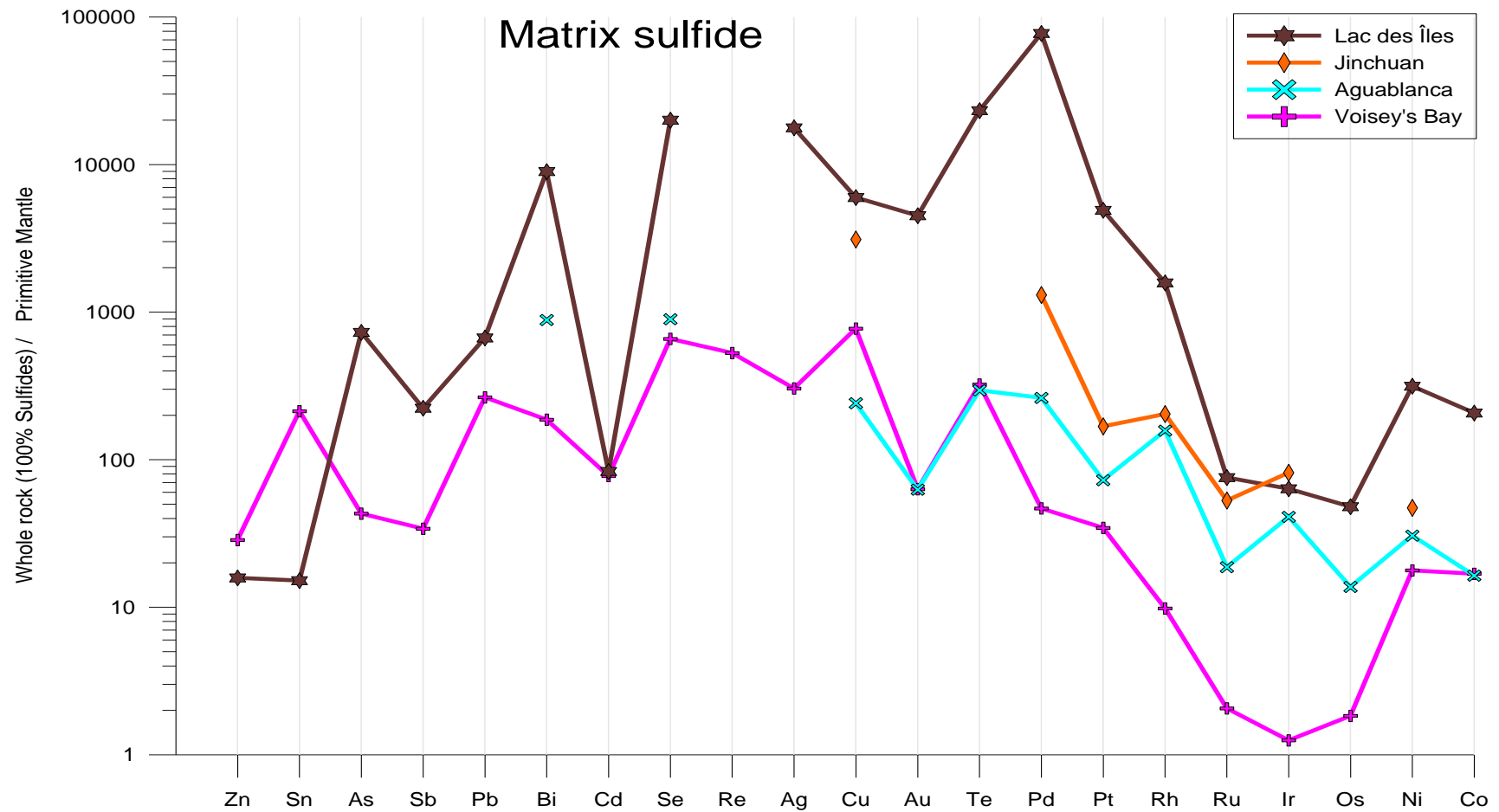


Fig. 23: Primitive mantle normalized multi-element diagram. Matrix sulfide assemblage from Voisey's Bay, Aguablanca (Piña et al. 2012), Lac des Îles (Duran et al. 2016a) and Jinchuan (Song et al. 2009) are compared. Data were recalculated to 100% sulfides and primitive mantle values from Lyubetskaya and Korenaga (2007).

#### 5.3.4. Massive Fe-rich sulfide

Figure 24 compares Voisey's Bay with Jinchuan (Song et al. 2009), Sudbury (McCreedy mine – Dare et al. 2011), Sudbury (Creighton mine – Dare et al. 2010a) and Lac des Îles (Duran et al. 2016a) deposits. All deposits have a similar concentration in Sb, also they have negative anomalies in Zn, Cd and Au. Lac des Îles is the richest deposit in Te and Pd, Creighton is the richest in Bi, Re, IPGE and Rh, and Voisey's Bay is the richest in Pb. Part of the Rh and Ir budget from Creighton are hosted in IPGE-sulfarsenides Dare et al. (2010a). However Voisey's Bay is the most depleted in Ir, Ru, Rh and Pt. McCreedy is the richest deposit for Pt. McCreedy has similar concentrations in Rh and Ni compared to Lac des Îles, and also has similar concentration in Os compared to Voisey's Bay. Jinchuan, Creighton and Voisey's Bay have a similar pattern including the steeply negative anomaly of Pt, however Jinchuan is richer in Cu, IPGE, Rh, Pt and Ni.

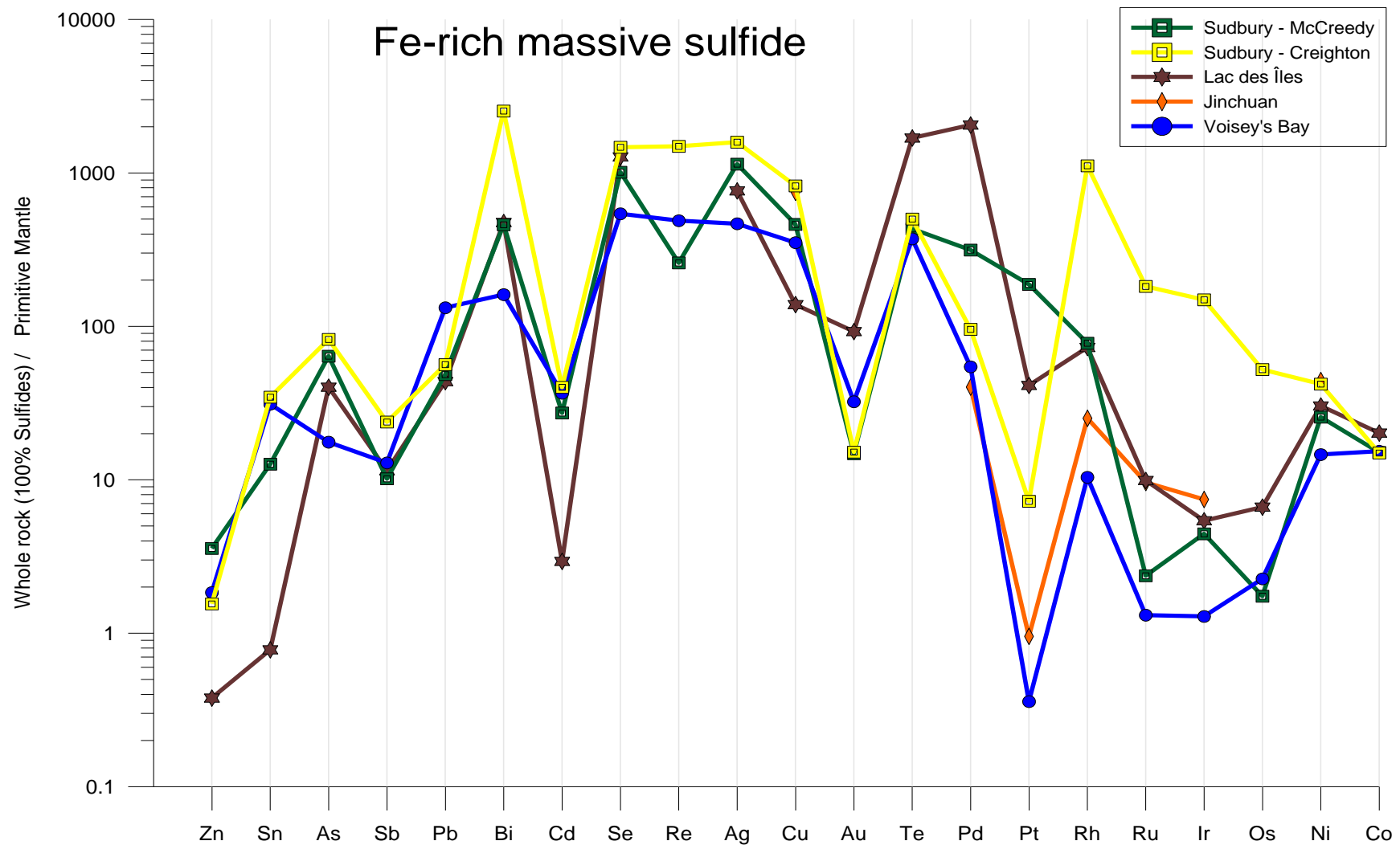


Fig. 24: Primitive mantle normalized multi-element diagram. Massive Fe-rich sulfides from Voisey's Bay, Sudbury – McCreedy mine (Dare et al. 2011), Sudbury – Creighton mine (Dare et al. 2010a) Lac des Îles (Duran et al. 2016a) and Jinchuan (Song et al. 2009) are compared. Data were recalculated to 100% sulfides and primitive mantle values from Lyubetskaya and Korenaga (2007).

### 5.3.5. Massive Cu-rich sulfide

In figure 25 Cu-rich assemblage from Voisey's Bay, Sudbury (McCreedy mine) (Dare et al. 2014) and Lac des Îles (Duran et al. 2016a) are compared. All deposits have negative anomalies for Re and Au. Lac des Îles is the richest in PGE and Voisey's Bay is the richest in Cd, Re, Au and Co, however it has a steeply negative Pt anomaly. Voisey's Bay and Sudbury Bay are depleted in IPGE and enriched in incompatible elements from Sn to Cd compared to Lac des Îles. Sudbury and Voisey's Bay have similar patterns from Zn to Pd. These deposits have a steeply pattern in the direction of PGE.

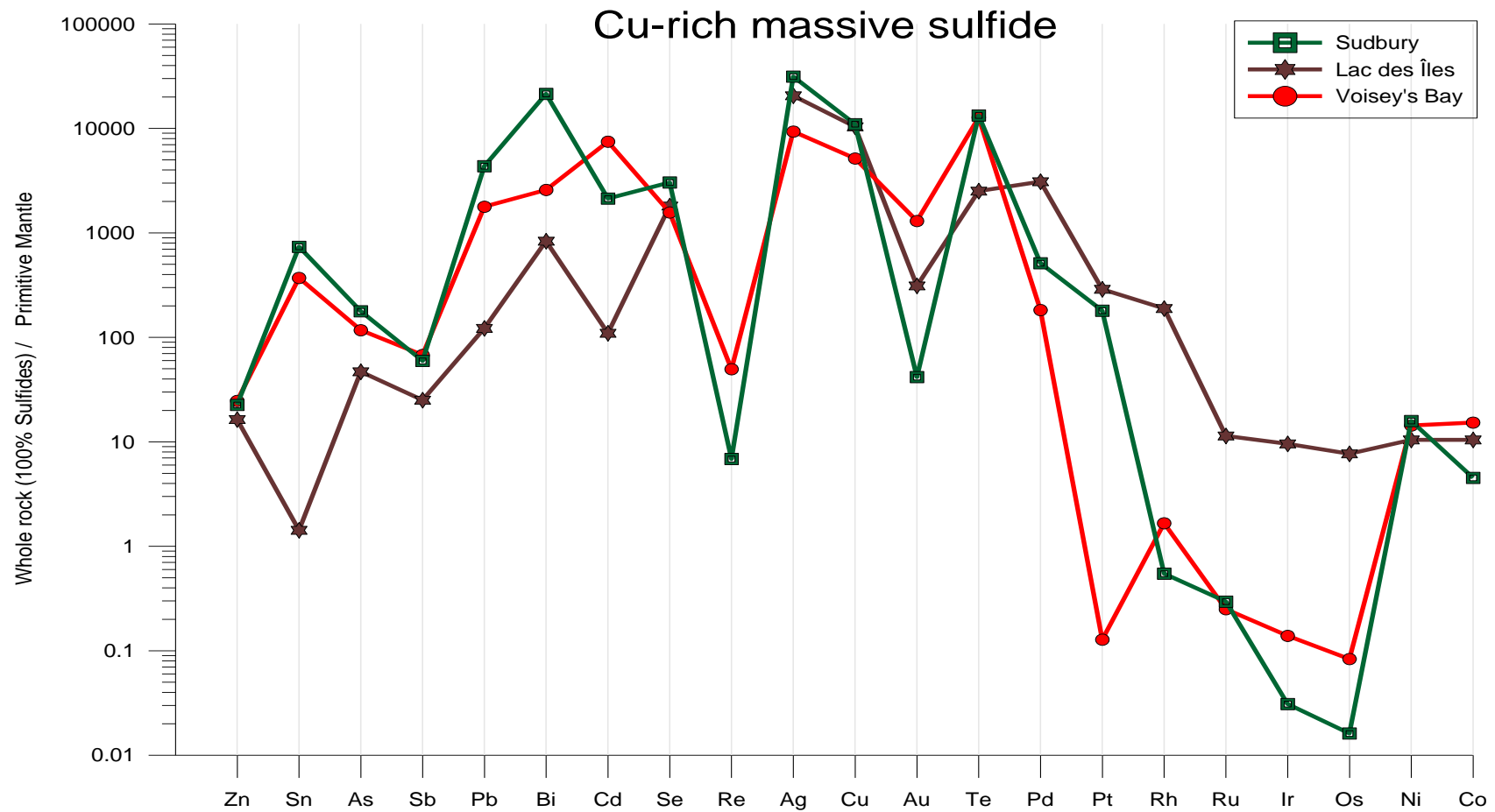


Fig. 25: Primitive mantle normalized multi-element diagram. Massive Cu-rich sulfides from Voisey's Bay, Lac des Îles (Duran et al. 2016a) and Sudbury (Dare et al. 2014) are compared. Data were recalculated to 100% sulfides and primitive mantle values from Lyubetskaya and Korenaga (2007).

## CHAPTER 6

### 6. WHOLE ROCK INTERPRETATION

Based on the whole rock data from the Ovoid it is possible to make some interpretations about sulfide segregation and crystallization of the sulfide liquid.

#### 6.1. Sulfide segregation

In the initial stages of the formation of a magmatic Ni-Cu-PGE sulfide deposit, immiscible sulfide liquid separates from the silicate magma (Naldrett 1980) in a process called sulfide segregation. The sulfides droplets are denser than the silicate magma and tend to settle at the base of the magma chamber (Barnes and Lightfoot, 2005).

The chalcophile metals will partition strongly into the sulfide liquid rather than the silicate melt and figure 26 shows that Ni, Co, Fe, Cu and Pd (representing the PGE) correlate with S and thus are controlled by sulfides. Nickel, Fe and Co (Fig. 26 A, B, C) from all assemblages plot on a single trend representing a tie line between troctolite and average of all sulfide assemblages at 100 % sulfides, but Cu and Pd (Fig. 26 D, E) concentrations in the massive sulfides are variable with some samples plotting above or below the trend defined by the tie line.

It has been proposed by many authors (e.g. Naldrett et al. 1982; Li et al. 1993; Barnes et al. 1997; Dare et al. 2010a) that when Ni-Cu-PGE sulfide deposits form from a sulfide liquid, monosulfide solid-solution (MSS) crystallizes from 1190 °C followed by the crystallization of intermediate solid-solution (ISS) from 900 °C. The Fe-rich sulfide assemblage represents the MSS cumulate and Cu-rich assemblage the ISS

cumulate and fractionated liquid. An extremely fractionated residual liquid enriched in incompatible elements with MSS and ISS (Au, Pd, Pt, Bi, Te, As, Sb, Pb, Liu and Brenan 2015) crystallizes among the ISS grains or may migrate into the surrounding rocks (Dare et al. 2014).

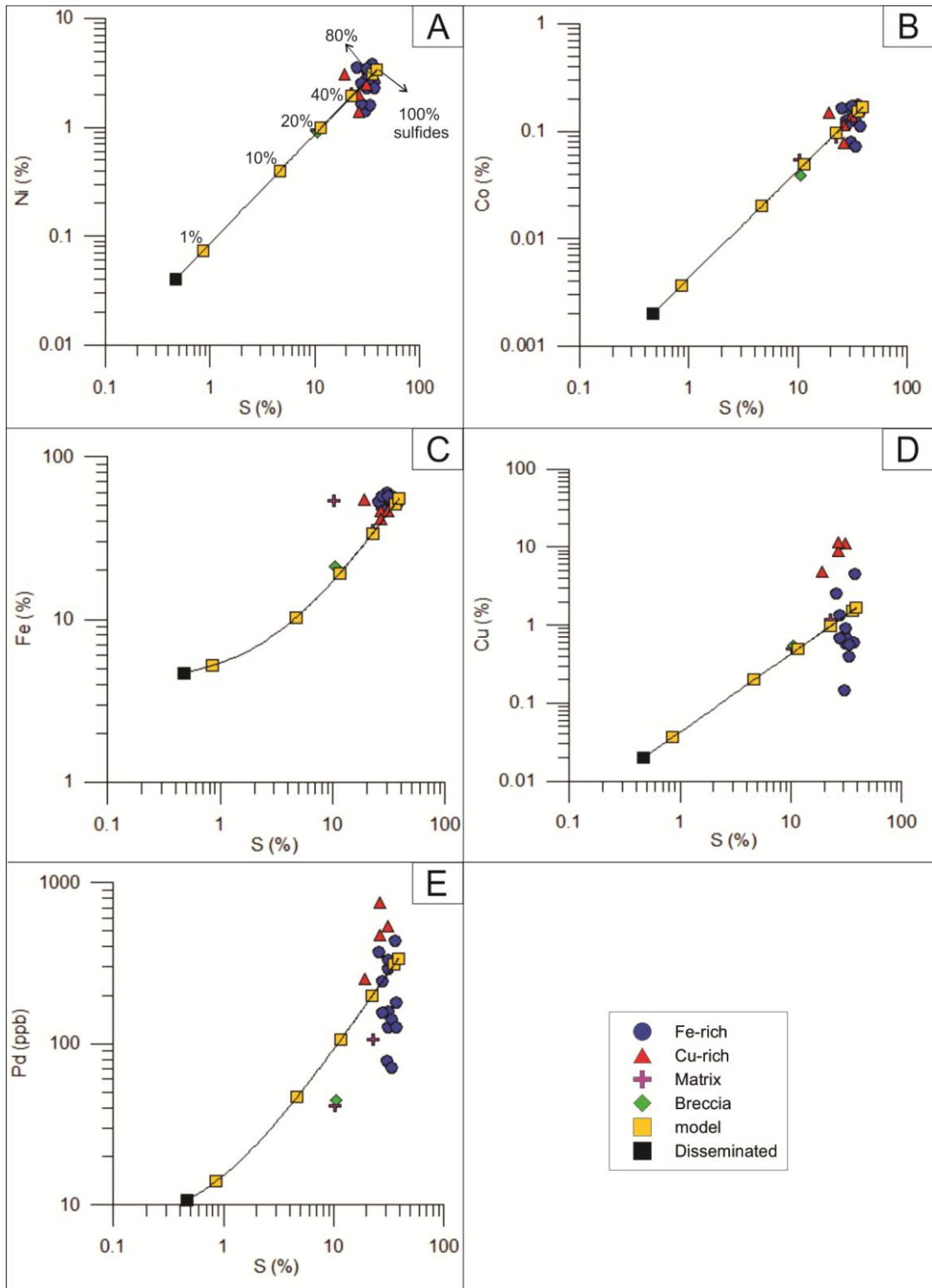


Fig. 26: Binary diagrams showing that **A**: Ni; **B**: Co; **C**: Fe; **D**: Cu; and **E**: Pd correlate with S and thus are controlled by sulfides. The yellow boxes represent the % of sulfides calculated in the model (1%, 10%, 20%, 40%, 80% and 100%).

## 6.2. Sulfide fractional crystallization model

Fractional crystallization is commonly used to model sulfide crystallization and it will be applied in this present work. *Raleigh fractionation* is an end-member process that can be expressed by the equations (2) and (3) below. The fractional crystallization phases are continuously and completely removed from the magma, which results in a depletion of compatible elements, enrichment of incompatible elements and continuously zoned cumulus phases Allegre and Minister (1978).

$$C_L = C_o F^{(D-1)} \quad (2)$$

$$C_{MSS \text{ or } ISS} = C_o D F^{(D-1)} \quad (3)$$

where:  $C_L$  = Concentration of the element in the fractionated liquid;  $C_o$  = Concentration of the element in the initial liquid;  $D$  = partition coefficient;  $F$  = weight fraction liquid remaining;  $C_{MSS \text{ or } ISS}$  = Concentration of the element in the instantaneous cumulate.

The graphs shown in figure 27 represent the model that was applied to the Ovoid ore body. The parallelograms were built based on the equations above, where the orange line represents the evolution of the liquid and the pink line represents the evolution of MSS. After establishing the right proportion of the parallelogram (using  $C_o = 1$ ), an estimate of the hypothetical initial liquid composition for the Ovoid (Table 6) was made by fitting the parallelogram to the data.

Table 6: Hypothetical initial liquid composition for the Ovoid.

<b>Initial liquid</b>	Cu (%)	Pd (ppb)	Bi (ppm)	Te (ppm)
	0.7	250	1.5	4

Figure 27A-B-C, Cu vs Pd, Cu vs Bi and Te vs Bi show most samples falling within the parallelogram (except for the disseminated sulfide and Cu-rich samples) where MSS cumulate has crystallized with some trapped liquid. The Cu-rich samples on Cu vs Pd fall below the fractionated liquid line and therefore cannot represent fractionated liquid. They might represent trapped liquid plus cumulate ISS (Fig. 27 A), however plots of Cu vs Bi and Te versus Bi suggest that this is not the case. On the Cu vs Bi (Fig. 27 B) and Te vs Bi (Fig. 27 C) plots the Cu-rich samples plot above the fractionated liquid line. If the Cu-rich samples represented ISS cumulate the samples should have plotted below the line. The disseminated sulfide is the richest in PGE, because it has a high R-factor.

Based on the model presented, three important considerations can be made about fractional crystallization of the Ovoid: (1) one liquid during fractional crystallization cannot explain the full story of sulfide liquid fractionation for all assemblages for the Ovoid. At least two different liquids are required to form the MSS and ISS. This second liquid that formed ISS appears to be enriched in Bi and Te; (2) if fractional crystallization at the Ovoid ore body results from a single liquid, another event(s) is necessary to explain the enrichment of Te and Bi in the ISS. One such event could have been the collapse of the roof of the chamber with the country rocks that collapsed in being enriched in incompatible elements and mixing with ISS; (3) it is not possible to know the original initial liquid composition when the sulfide liquid started fractionation; however it is possible to estimate and assume an initial liquid composition.

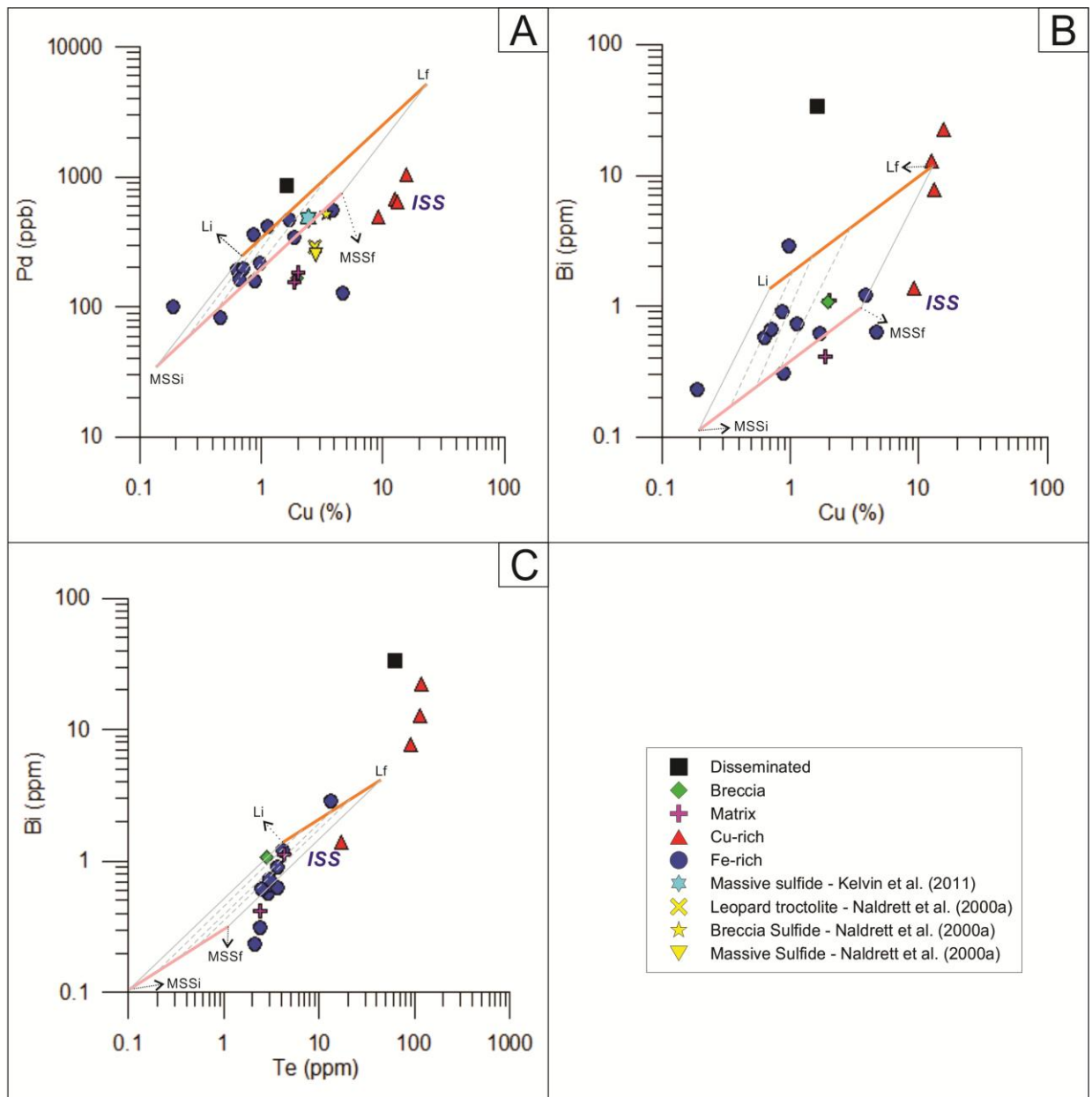


Fig. 27: Sulfide fractional crystallization model: **A:** Cu vs Pd; **B:** Cu vs Bi; **C:** Cu vs Bi; and **D:** Te vs Bi, showing different behavior of assemblages for different elements.

## CHAPTER 7

### 7. LA-ICP-MS RESULTS

The base-metal sulfide minerals (pyrrhotite, pentlandite, chalcopyrite and cubanite) were analyzed by LA-ICP-MS. Figure 28 A, B, C, D show typical spectra's for each mineral. Flat signals are observed for major elements for these minerals and some trace elements. In contrast, peaks of Re and Mo spectra in chalcopyrite (Fig. 28 E) and Pd and Ag in cubanite (Fig. 28 F) suggest the presence of small inclusions of Re-Mo, Pd-Ag and Cd-Zn minerals. It is important to observe that these inclusions were not considered and were excluded in data reduction.

The median and average compositions and standard deviation of each BMS mineral in all 3 assemblages (matrix + breccia, Fe-rich and Cu-rich), the limit of detection and weight fraction values are shown in table 7. Some elements are below the detection limit, in these cases the detection limit was considered to be the maximum value for data interpretation. These elements are outlined in orange in the table 7. Disseminated sulfides were not analysed because they are too small.

Median whole rock compositions of each assemblage are plotted in spidergram plots together with pyrrhotite, pentlandite and chalcopyrite compositions as determined by LA-ICP-MS technique (Figs 29, 30 and 32 respectively). This is done to show which elements are predominately hosted within BMS minerals and which are not.

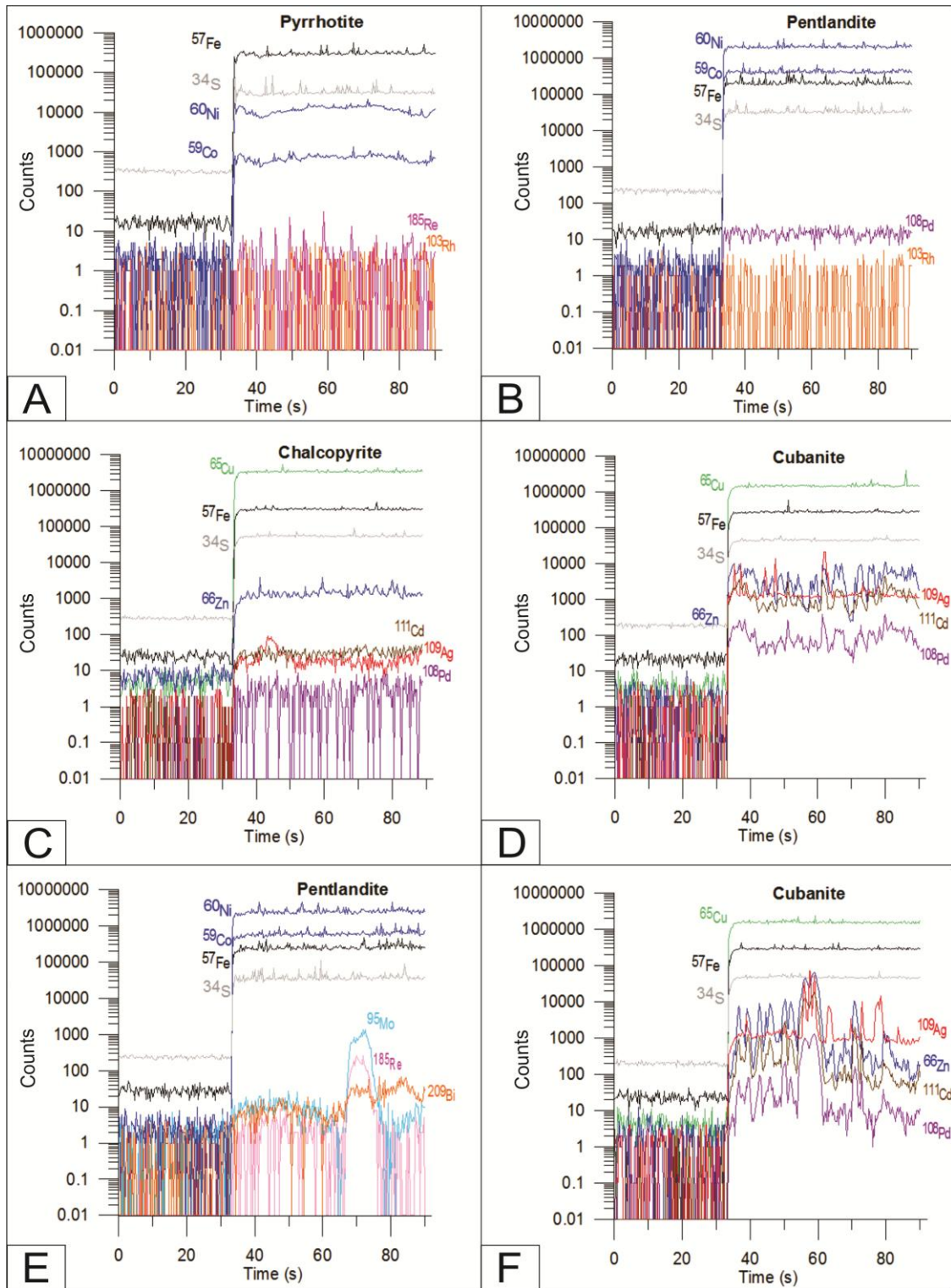


Fig. 28: Plots of time (s) versus counts for the base-metal sulfides minerals; **A**: Pyrrhotite; **B**: Pentlandite; **C**: Chalcopyrite; **D**: Cubanite; **E**: Pentlandite showing Re-Mo-bearing inclusion and **F**: Cubanite showing Pd, Cd, Zn and Ag inclusions.

Table 7: Composition of each BMS as determined by LA-ICP-MS and weight fraction of each BMS.

	Mineral	Weight Fraction	Element	Co	Ni	Cu	Zn	As	Se	Ru	Rh	Pd	Ag	Cd
			Isotope	59	61	65	66	85	82	101	103	108	109	111
<b>Matrix + Breccia</b>	Po	0.83	median	30.4	2260	3.54	0.42	0.289	49.5	<0.031	0.009	<0.012	0.238	<0.056
	n=18		average	33.97	2343	5.95	0.419	0.312	49.9	<0.031	0.009	<0.012	0.229	<0.056
			std. dev.	15.5	472	8.04	8.51	0.120	1.94	0.013	0.005	0.002	0.053	0.068
	Pn	0.11	median	12410	319500	1.24	0.355	0.435	45.1	0.567	<0.006	0.620	1.51	<0.056
	n=19		average	12410	320000	2.16	0.330	0.435	45.4	0.572	<0.006	0.630	1.52	<0.056
			std. dev.	355	12593	3.586	0.323	0.078	2.05	0.039	0.011	0.347	0.983	0.059
	Ccp	0.06	median	0.115	6.25	252600	419	0.1615	52	n.d.	n.d.	<0.012	1.49	12.6
n=7		average	1.49	33.2	134080	492	0.1935	57.7	n.d.	n.d.	<0.012	2.685	21.07	
		std. dev.	0.846	17.200	634	139	0.078	6.20	n.d.	n.d.	0.055	1.10	7.22	
<b>Fe-rich</b>	Po	0.85	median	26.5	2287	2.19	0.435	0.2535	52.2	<0.031	0.010	<0.012	0.215	<0.056
	n=24		average	27.9	2167	5.30	0.598	0.290	53.1	<0.031	0.009	<0.012	0.241	<0.056
			std. dev.	9.61	374.553	5.34	0.320	0.098	2.42	0.014	0.003	0.009	0.053	0.022
	Pn	0.12	median	12497	279625	1.86	0.52	1.005	44.7	0.094	0.007	0.534	0.941	<0.056
	n=20		average	12158	282099	2.97	1.01	0.963	45.9	0.085	0.007	0.613	1.28	<0.056
			std. dev.	438	4837	2.52	1.05	0.125	2.78	0.021	0.004	0.095	0.653	0.025
	Ccp	0.03	median	0.13	39.9	303650	716	<0.116	50.2	n.d.	n.d.	<0.012	1.32	21.8
n=16		average	0.9274	68.6	302565	603	<0.116	54.5	n.d.	n.d.	<0.012	1.58	20.5	
		std. dev.	1.23	39.8	2477	254	0.037	2.76	n.d.	n.d.	0.078	0.762	7.35	
<b>Cu-rich</b>	Po	0.36	median	41.3	1083	2.12	0.760	0.335	117	<0.031	<0.006	<0.012	1.35	0.101
	n=16		average	42.4	1227	2.59	0.706	0.341	118	<0.031	<0.006	<0.012	1.31	0.098
			std. dev.	6.16	299	1.24	0.294	0.146	5.17	0.008	0.002	0.006	0.652	0.027
	Pn	0.13	median	9360	285000	3.19	0.770	0.868	59.9	<0.031	<0.006	1.590	11.2	<0.056
	n=5		average	9434	283520	4.36	0.762	4.19	62.8	<0.031	<0.006	1.387	11.1	<0.056
			std. dev.	582	4442	2.42	0.325	7.33	7.94	0.024	0.003	0.378	6.84	0.022
	Cub	0.51	median	0.121	25.9	200350	1150	<0.116	147	n.d.	n.d.	<0.012	26.3	164
n=18		average	0.516	32.4	200880	1194	<0.116	147	n.d.	n.d.	<0.012	28.5	157	
		std. dev.	0.614	13.5	2342	507	0.022	4.03	n.d.	n.d.	0.931	7.46	65.1	
Detection limit				0.014	1.080	0.159	0.334	0.116	0.744	0.031	0.006	0.012	0.013	0.056

Abbreviation: n.d. = not determined and std. dev. = standard deviation.

Table 7 continuation: Composition of each BMS as determined by LA-ICP-MS and weight fraction of each BMS.

	Mineral	Weight Fraction	Element	Sn	Sb	Te	Re	Os	Ir	Pt	Au	Pb	Bi
			Isotope	120	121	128	185	190	193	195	197	208	209
<b>Matrix + Breccia</b>	Po	0.83	median	0.059	<0.026	0.56	0.077	<0.010	0.004	<0.010	<0.006	0.536	0.066
	n=18		average	0.077	<0.026	0.595	0.066	<0.010	0.006	<0.010	<0.006	0.617	0.076
			std. dev.	0.029	0.010	0.248	0.039	0.005	0.006	0.002	0.002	0.457	0.052
	Pn	0.11	median	0.113	0.043	0.660	0.039	<0.010	0.004	<0.010	<0.006	3.39	0.127
	n=19		average	0.099	0.043	0.660	0.039	<0.010	0.005	<0.010	<0.006	5.68	0.169
			std. dev.	0.062	0.005	0.184	0.018	0.004	0.003	0.003	0.003	1.34	0.094
	Ccp	0.06	median	3.05	<0.026	12.3	<0.004	<0.010	<0.003	<0.010	0.00545	4.60	0.045
	n=7		average	4.71	<0.026	14.5	<0.004	<0.010	<0.003	<0.010	0.00765	4.09	0.110
			std. dev.	1.25	0.007	6.34	0.001	0.001	0.013	0.001	0.005	0.654	0.051
<b>Fe-rich</b>	Po	0.85	median	0.040	0.027	0.922	0.149	<0.010	0.005	<0.010	<0.006	0.477	0.077
	n=24		average	0.044	0.036	0.778	0.152	<0.010	0.004	<0.010	<0.006	1.16	0.148
			std. dev.	0.013	0.021	0.219	0.049	0.007	0.002	0.004	0.003	1.50	0.137
	Pn	0.12	median	0.046	0.030	0.753	0.109	<0.010	<0.003	<0.010	<0.006	8.13	0.184
	n=20		average	0.050	0.072	1.60	0.102	<0.010	<0.003	<0.010	<0.006	8.92	0.714
			std. dev.	0.026	0.078	1.39	0.035	0.005	0.003	0.002	0.003	7.34	0.773
	Ccp	0.03	median	4.37	<0.026	4.34	<0.004	<0.010	<0.003	<0.010	0.008	8.56	0.083
	n=16		average	5.02	<0.026	5.10	<0.004	<0.010	<0.003	<0.010	0.012	15.2	0.111
		std. dev.	0.962	0.070	2.20	0.027	0.003	0.002	0.003	0.005	4.61	0.041	
<b>Cu-rich</b>	Po	0.36	median	0.034	<0.026	1.39	0.034	<0.010	<0.003	<0.010	0.011	0.267	0.066
	n=16		average	0.033	<0.026	1.42	0.035	<0.010	<0.003	<0.010	0.005	0.324	0.074
			std. dev.	0.011	0.025	0.704	0.007	0.004	0.003	0.004	0.004	0.289	0.050
	Pn	0.13	median	0.052	0.050	0.401	0.016	<0.010	<0.003	<0.010	<0.006	4.05	0.186
	n=5		average	0.067	0.056	2.22	0.016	<0.010	<0.003	<0.010	<0.006	10.2	0.248
			std. dev.	0.044	0.031	2.69	0.010	0.004	0.002	0.004	0.005	13.7	0.098
	Cub	0.51	median	12.1	<0.026	29.8	<0.004	<0.010	<0.003	<0.010	0.014	23.9	0.233
	n=18		average	21.9	<0.026	29.5	<0.004	<0.010	<0.003	<0.010	0.017	24.5	0.245
		std. dev.	7.99	0.014	5.78	0.001	0.003	0.000	0.002	0.010	6.44	0.094	
Detection limit				0.020	0.026	0.095	0.004	0.010	0.003	0.010	0.006	0.006	0.004

Abbreviation: n.d. = not determined and std. dev. = standard deviation.

## **7.1. Spidergrams and binary diagrams**

### *7.1.1. Pyrrhotite*

Pyrrhotites from all assemblages (matrix + breccia, Fe-rich and Cu-rich) have flat trace element patterns and overall similar shapes (Fig. 29). They have negative Zn, Cd and Cu anomalies, of which zinc represents the most depleted metal in all the assemblages.

Matrix + breccia and Fe-rich assemblages have similar concentrations for all elements, whereas the composition of the pyrrhotite from the Cu-rich assemblage is slightly different. The pyrrhotite in the Cu-rich assemblage is poorer in Ni and richer in incompatible elements such as Se, Ag, Cd and Te than the pyrrhotite of the other assemblages. The concentration of the other elements Sn, As, Sb, Pb, Bi, Re, Pd, Pt, Rh and Ir are generally similar in the pyrrhotite from all assemblages.

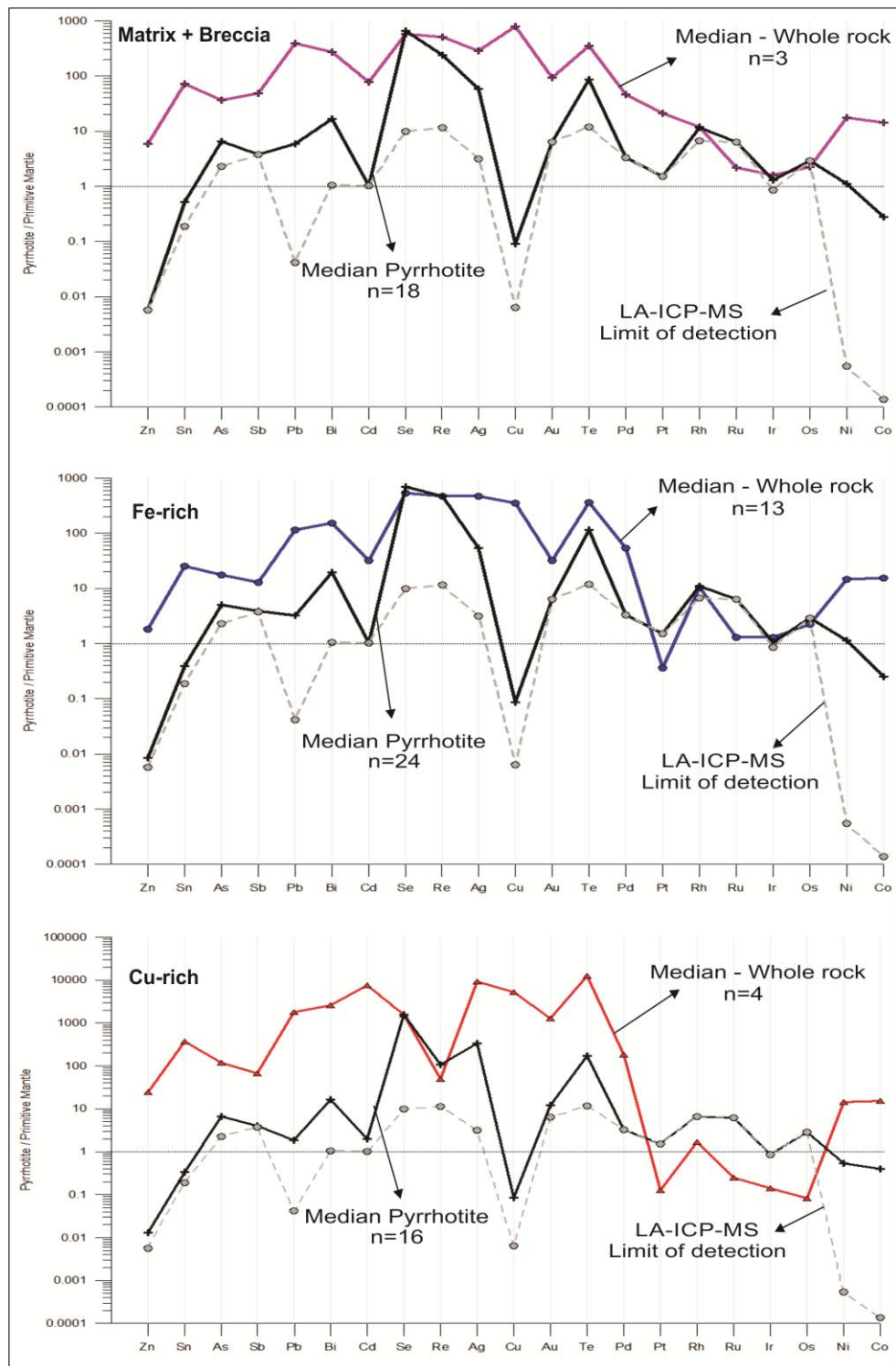


Fig. 29: Primitive mantle normalized multi-element diagram of pyrrhotite, LA-ICP-MS and whole rock data, from different assemblages. **A:** Matrix + breccia; **B:** Fe-rich; **C:** Cu-rich, compared to whole rock data. Dashed line represents the detection limit of LA-ICP-MS data. The normalization values are from Lyubetskaya and Korenaga (2007).

### *7.1.2. Pentlandite*

Pentlandite from matrix + breccia, Fe-rich, Cu-rich assemblages have flat trace element patterns and similar concentrations for most of the elements and are below or close of the detection limit for Os, Ir and Rh. Matrix + breccia assemblage is the most enriched in Ru, followed by Fe-rich assemblage. Pentlandites have negative Zn, Cd and Cu anomalies (Fig. 30).

Palladium, Ni and Co are enriched in all pentlandites, however, pentlandite from the matrix + breccia assemblage is the least enriched in Pd and the Cu-rich assemblage is the least enriched in Ni and Co. All assemblages have an even distribution for incompatible elements such as Sn, As, Sb, Pb, Bi, Se, Au and Te. Pentlandite from the Cu-rich assemblage is the richest in Ag and Pd.

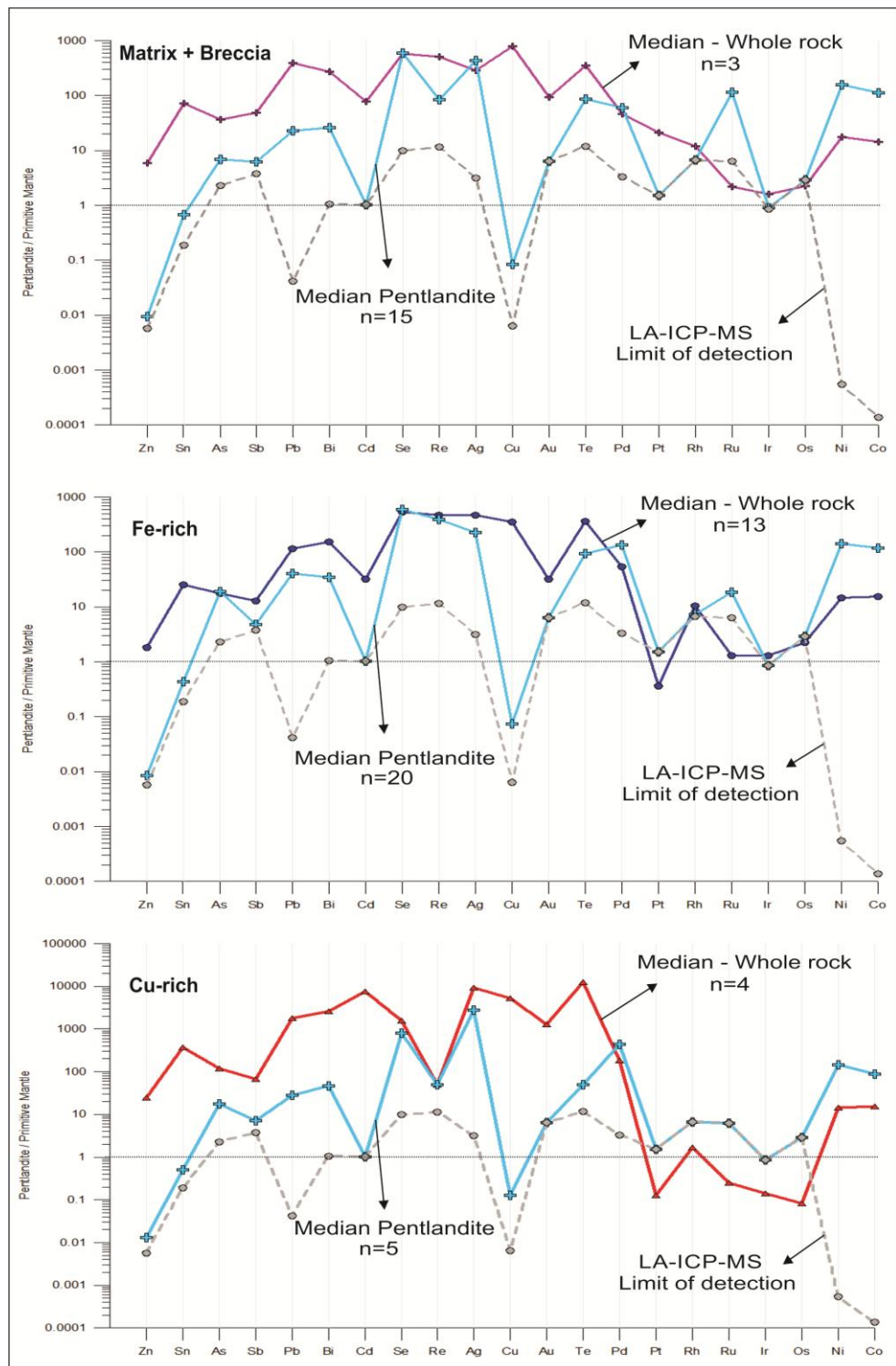


Fig. 30: Primitive mantle normalized multi-element diagram of pentlandite, LA-ICP-MS and whole rock data, from different assemblages. **A:** Matrix+breccia; **B:** Fe-rich; **C:** Cu-rich compared to whole rock data. Dashed line represents the detection limit of LA-ICP-MS data. The normalization values are from Lyubetskaya and Korenaga (2007).

### 7.1.3. *Palladium in pentlandite*

Different types of pentlandite were analyzed in the Fe-rich and Cu-rich assemblages to constrain their Pd contents. In the Fe-rich assemblage, coarse grained pentlandite in contact with pyrrhotite, and pentlandite flames within pyrrhotite were analyzed. In Cu-rich assemblage, coarse grained pentlandite in contact with pyrrhotite and coarse grained pentlandite in contact with cubanite were analyzed. Palladium contents were observed to vary between pentlandite textures and with assemblage types. Figure 31 A shows that Pd is almost absent in pentlandite flames. Coarse-grained pentlandite in contact with pyrrhotite in Fe-rich assemblage, also has low content of Pd compared to pyrrhotite in Cu-rich assemblage, as shown in figure 31 B, but it does contain more Pd than the pentlandite flames.

For the Cu-rich assemblage, Pd content varies according to the mineralogy, if the pentlandite is in contact with pyrrhotite (Fig. 31 C), the amount of Pd is lower compared to pentlandite that is in contact with cubanite (Fig. 31 D). Pentlandite in the Cu-rich assemblage is also richer in Pd than the Fe-rich assemblage. Table 8 shows the content of S, Co, Ni and Pd of each case presented above.

Table 8: Sulfur, Co, Ni and Pd content for different pentlandite.

Sample	Mineral	S (%)	Co (%)	Ni (%)	Pd (ppb)
A) VB36	Pn flame (Fe-rich)	18.7	0.88	23.8	< 12.0
B) VB29	Pn in contact with Po (Fe-rich)	25.4	1.37	27.8	24.6
C) VB27	Pn in contact with Po (Cu-rich)	19.1	1.78	29.0	350
D) VB6	Pn in contact with Cub (Cu-rich)	19.1	0.98	28.3	792

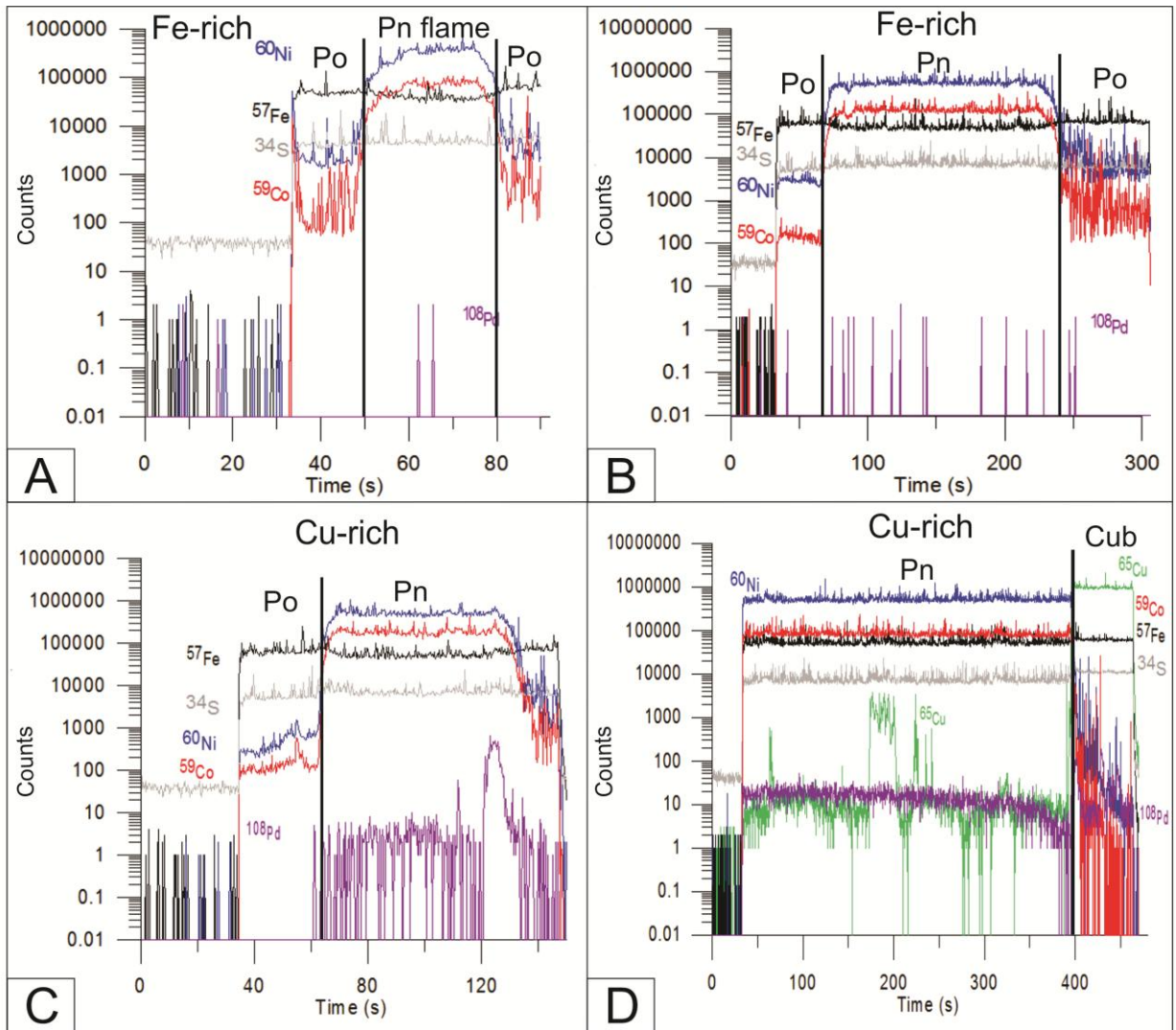


Fig. 31: Time-signal diagrams (time (s) vs counts) of Pd content in different textures of pentlandite. **A:** Palladium content in pentlandite flames (Fe-rich assemblage – VB36); **B:** Palladium content in coarse grained pentlandite in contact with pyrrhotite (Fe-rich assemblage – VB29); **C:** Palladium content in coarse grained pentlandite in contact with pyrrhotite (Cu-rich assemblage – VB27); **D:** Palladium content in coarse grained pentlandite in contact with cubanite (Cu-rich assemblage – VB6).

#### 7.1.4. Chalcopyrite

Trace element patterns for chalcopyrite from all assemblages are flat from Sn to Pd, except for the negative Re and Au anomalies, and the positive Cu anomaly. From Pd onwards there is a steep decrease in the mantle normalized concentrations of the elements. Copper followed by Te are the richest metals in all assemblages (Fig. 32).

Chalcopyrite from the Cu-rich assemblage is the richest in incompatible elements such as Zn, Se, Bi, Pd, Ag, Cd, Sn, Au and Pb. Sphalerite exsolutions which host the remainder of the Zn in the rocks and some Cd, occur mainly in chalcopyrite. These exsolutions are more frequent in the Cu-rich assemblage than in the others assemblages.

Figure 33 A shows a good correlation between Cd and Zn in chalcopyrite, in the Cu-rich assemblage. Galena also occurs in all assemblages, but as in the case of sphalerite, it is more frequent in Cu-rich assemblage.

Silver and Pb telluride minerals were the most common telluride varieties (altaite (PbTe)) and PMM (hessite (Ag<sub>2</sub>Te)) observed during SEM work. Figure 33 B binary diagram Ag vs Te (for Cu-rich assemblage) shows a strong positive correlation between these elements, except three analyses of pentlandite that are enriched in Ag and depleted in Te.

Chalcopyrite is richer in incompatible elements compared to the other sulfide minerals, whereas pyrrhotite is richer in some PGE (Os, Ir, Ru, Rh) and Re, and pentlandite is richer in Ni, Co and Pd. The binary diagram Ni vs Co (Fig. 34), for matrix + breccia and Fe-rich assemblages, shows a strong positive correlation between these elements and this correlation is observed in all of the other assemblages.

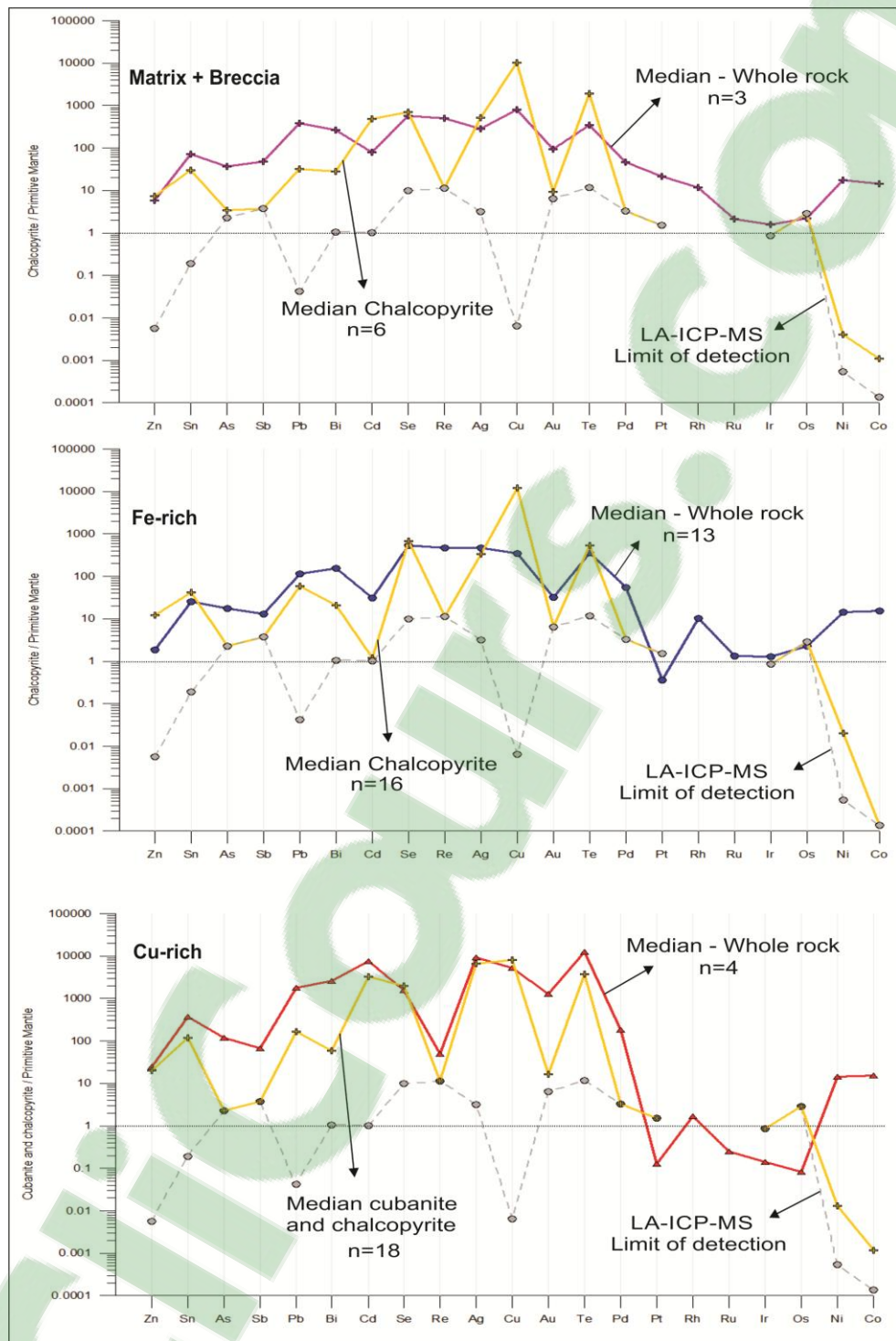


Fig. 32: Primitive mantle normalized multi-element diagram of chalcopyrite, LA-ICP-MS and whole rock data, from different assemblages. **A:** Matrix + breccia; **B:** Fe-rich; **C:** Cu-rich, compared to whole rock data. Dashed line represents the detection limit of LA-ICP-MS data. The normalization values are from Lyubetskaya and Korenaga (2007).

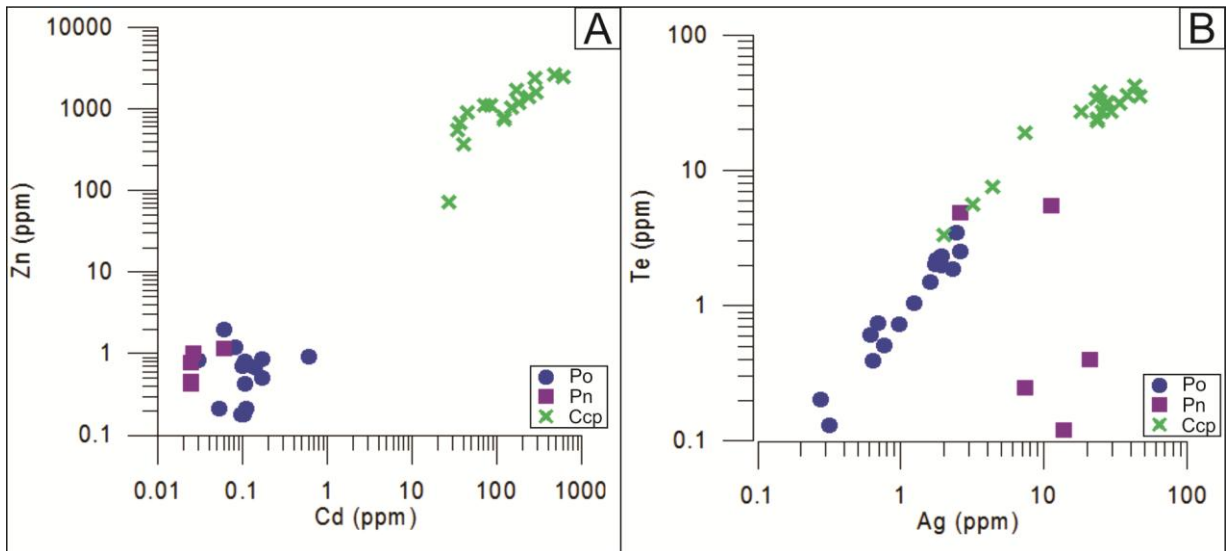


Fig. 33: Binary diagrams. **A:** Zn vs Cd shows a strong positive correlation for chalcopyrite. **B:** Ag vs Te shows a strong positive correlation between the BMS minerals for Cu-rich assemblage.

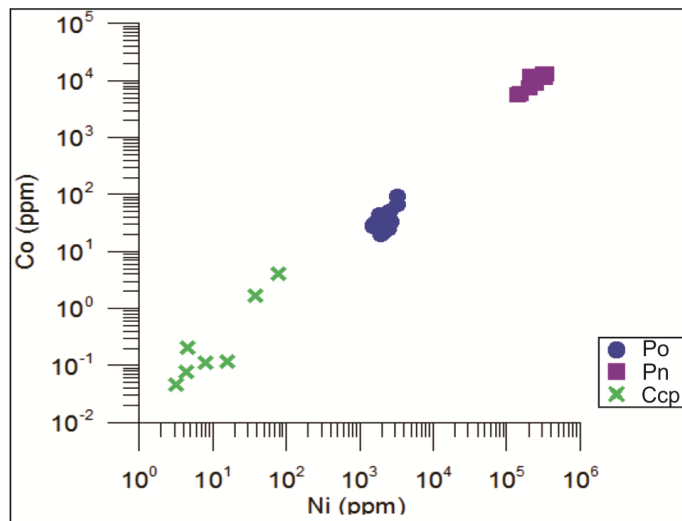


Fig. 34: Binary diagram, Ni vs Co shows a strong positive correlation between BMS minerals for matrix + breccia and Fe-rich assemblages.

## 7.2. Comparison with other deposits

Laser ablation inductively coupled plasma mass spectrometry analysis from the Ovoid ore body are compared with other magmatic sulfide deposits around the world such as Sudbury (Dare et al. 2011, 2014), Lac des Îles (Duran et al. 2016b) and Aguablanca (Piña et al. 2012). Comparison of ore bodies was undertaken using the following subdivided ore assemblages: Matrix + breccia, Fe-rich and Cu-rich. As shown earlier in this chapter, substantial variations in trace elements can exist between the same minerals from different ore assemblages, thus the need to compare minerals of the same ore assemblages from different deposits against one another, rather than bulk mineral chemistry from the deposits.

### 7.2.1. Matrix + breccia sulfide

Pyrrhotite, pentlandite and chalcopyrite trace element data from the matrix + breccia assemblage of Voisey's Bay were compared with matrix assemblage from Aguablanca (Piña et al. 2012) (Fig. 35). For pyrrhotite, both deposits have similar concentrations of Cd, Se, Au, Te and Pt. For the Ru, Os, Ni and Co, both have similar shaped trace element patterns, but Aguablanca is slightly enriched. For the other elements, the sulfides from Aguablanca are richer than Voisey's Bay.

For pentlandite, Voisey's Bay and Aguablanca have similar amounts of Se, Au, Te, Pt and Ni, both deposits also have negative Cd and Pt anomalies. Pentlandite from Voisey's Bay is richer in Co and Aguablanca is richer in the other elements such as As, Bi, Re, Ru, Pd, Rh, Ir and Os.

For chalcopyrite, both deposits have similar concentrations of Se, Pt, Ir and Os and have negative Ni anomalies. All the other metals are richer in Aguablanca, except Cd and Te. Of note is the large difference in Co between the two deposits, chalcopyrite from Aguablanca is clearly enriched in Co compared to chalcopyrite from Voisey's Bay.

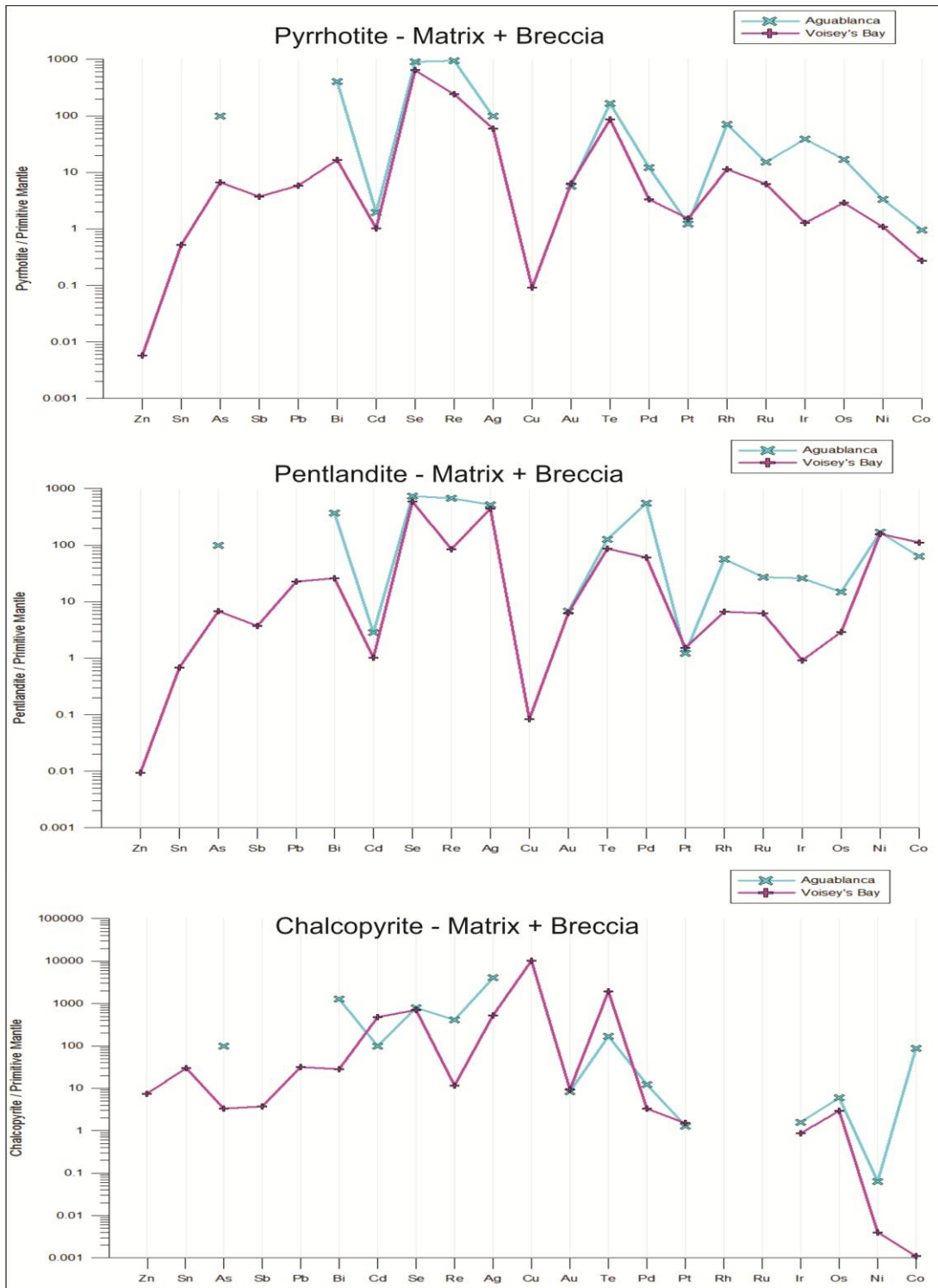


Fig. 35: Primitive mantle normalized multi-element diagram of matrix + breccia assemblage, from Voisey's Bay and matrix assemblage from Aguablanca deposits. **A:** Pyrrhotite; **B:** Pentlandite; **C:** Chalcopyrite. The normalization values are from Lyubetskaya and Korenaga (2007).

### 7.2.2. *Fe-rich sulfide*

Pyrrhotite, pentlandite and chalcopyrite trace element data from the Fe-rich assemblage of Voisey's Bay were compared with Sudbury (Dare et al. 2011) and Lac des Îles (Duran et al. 2016b) deposits (Fig. 36). Aguablanca is not presented, because the Fe-rich massive sulfide data is not available.

For pyrrhotite, all deposits have similar flat patterns and negative anomalies in Zn and Cu, with Voisey's Bay being the richest in Re and Te, and depleted in Co compared to the Lac des Îles and Sudbury. Lac des Îles being the most depleted in Zn and Cu, and Sudbury is the richest in As and Bi. All the other elements have similar concentrations.

Pentlandite trace element patterns from all the deposits have relatively flat patterns that have negative Zn, Cd and Cu anomalies. Pentlandite is enriched in Ni and Co compared to pyrrhotite and chalcopyrite. Voisey's Bay is the richest deposit in Re and Te, Sudbury is the richest in Sn, As, Cu and Ru and Lac des Îles is the richest in Ag, Pd and Rh. All the other elements have a similar concentration in these deposits.

For chalcopyrite, all deposits have flat pattern trace elements up to Cu, then negative sloping from Cu to Co, with negative anomalies in Re, Au, Pt, Ir, Ni and Co. Voisey's Bay has negative anomalies in Cd and Pd compared to the Sudbury and Lac des Îles, however it is the richest in Pb and Te. Sudbury is the richest in incompatible elements (Sn, As, Sb and Cd) and Lac des Îles is the richest in Ag, Ni and Co. Bismuth, Se, Re, Cu, Au, Pt, Ru, Ir and Os concentrations in all the deposits are similar.

Platinum-group elements are depleted in Voisey's Bay compared to the other deposits presented in this study, however they have a similar shape of Lac des Îles and Sudbury, except for Pd in pentlandite and chalcopyrite which has a negative anomaly.

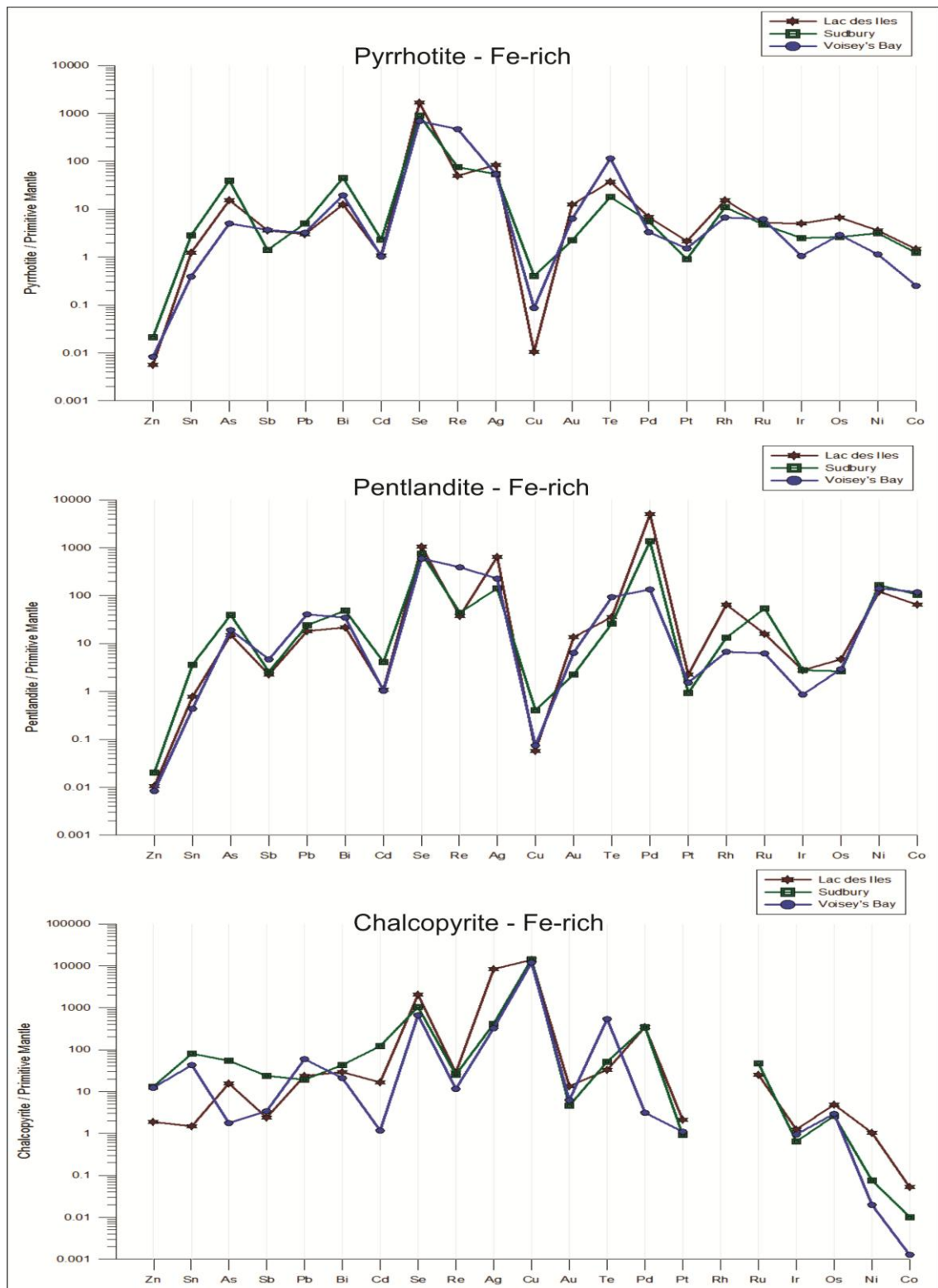


Fig. 36: Primitive mantle normalized multi-element diagram of Fe-rich assemblage, from Voisey's Bay, Lac des îles and Sudbury deposits. **A:** Pyrrhotite; **B:** Pentlandite; **C:** Chalcopyrite. The normalization values are from Lyubetskaya and Korenaga (2007).

### 7.2.3. *Cu-rich sulfide*

Pyrrhotite, pentlandite and chalcopyrite trace element data from the Cu-rich assemblage of Voisey's Bay are compared with the Sudbury (Dare et al. 2014) deposit (Fig. 37). Lac des Iles is not presented, because the Cu-rich massive sulfide data is not available. Piña et al. (2012) reported some chalcopyrite veinlet analysis for Aguablanca, however most elements are below the detection limit, and these data are not presented.

For pyrrhotite, both deposits have flat and similar trace element patterns. They both also have negative Zn and Cu anomalies. Platinum-group elements in the Voisey's Bay deposit were below the detection limit, therefore the detection limit was used as the maximum concentration for them in the diagram. Sudbury is the richest in incompatible elements such as Sn, As, Pb, Bi, Cd, Ag, Te and Pd, and Voisey's Bay is the richest in Re and Co. Both have similar Se and Ni concentrations.

For pentlandite, Sudbury and Voisey's Bay have similar shapes and both contain similar concentrations of Pd, Pt, Ir, Os and Ni. Voisey's Bay and Sudbury have negative Zn, Cd, Re and Pt anomalies. The Voisey's Bay pentlandite is the richest in Re and Co and has a large negative Cu anomaly. Sudbury is the richest in all the other metals.

For chalcopyrite, Voisey's Bay and Sudbury have steep and similar trace element patterns, with negative Ni and Co anomalies. Both deposits are observed to have similar concentrations for many elements, such as Pb, Bi, Se, Re, Ag, Cu, Au, Pt, Ir and Os. Voisey's Bay is the richest in Zn, Cd and Te, and Sudbury is the richest in Sn, As, Sb, Pd, Ni and Co.

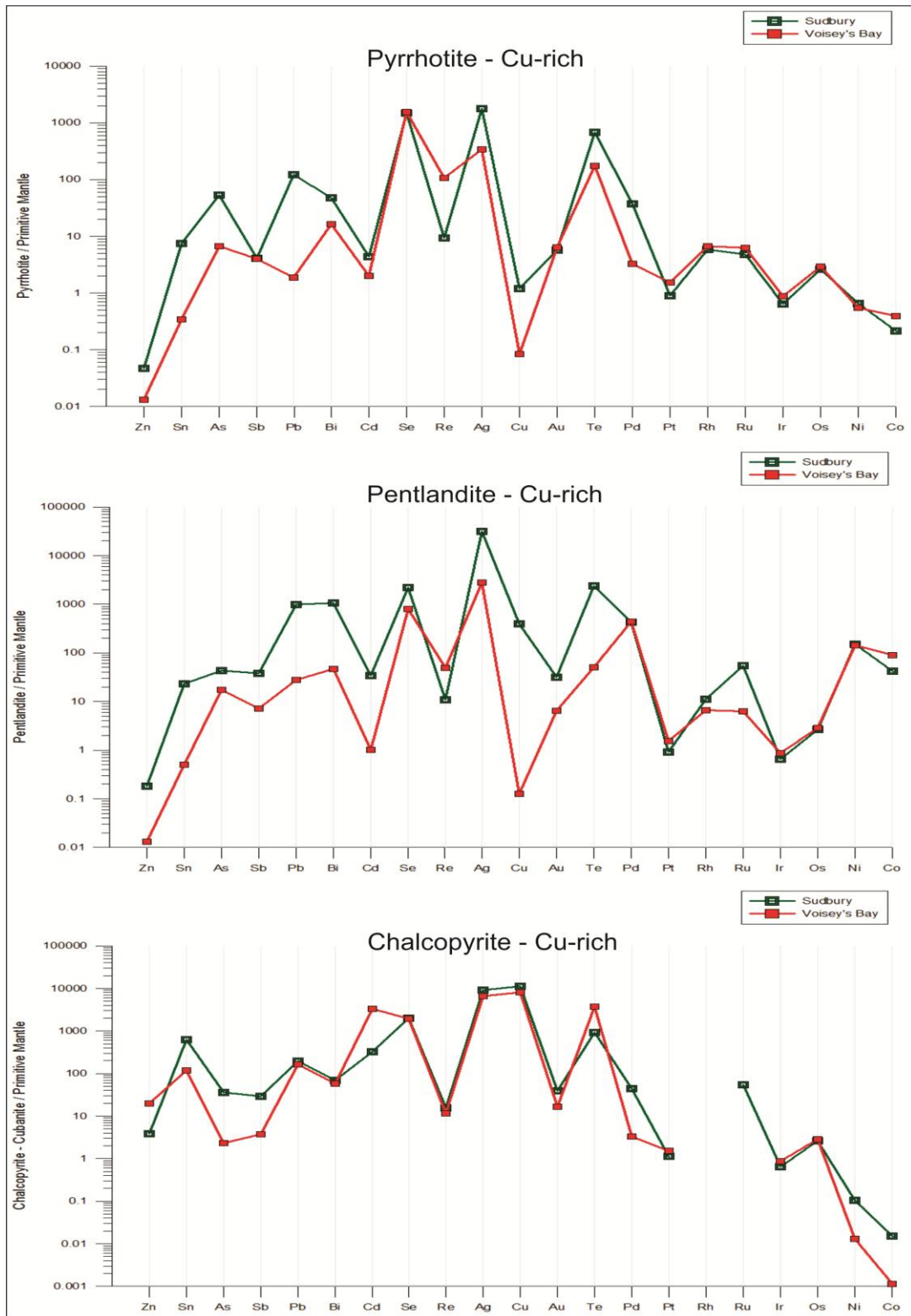


Fig. 37: Primitive mantle normalized multi-element diagram of Cu-rich assemblage, from Voisey's Bay and Sudbury deposits. **A:** Pyrrhotite; **B:** Pentlandite; **C:** Chalcopyrite. The normalization values are from Lyubetskaya and Korenaga (2007).

## CHAPTER 8

### 8. LA-ICP-MS INTERPRETATION

#### 8.1. Mass balance

Mass balance calculations are performed to evaluate the proportion of each element in each BMS mineral to assess whether the BMS minerals are the principal host of the chalcophile elements and PGE. Mass balance calculation was carried out as follows:

Wt fraction Pn =

$$(\text{Ni in 100 \% sulfides} - \text{Ni in Po}) / \text{Ni in Pn} \quad (4)$$

Wt fraction Cu-rich phase in the Fe-rich assemblage, in the breccia and the matrix sulfides treated as Ccp =

$$(\text{Cu in 100 \% sulfides}) / \text{Cu in Ccp} \quad (5)$$

Wt fraction Cu-rich phase in the Cu-rich sulfides treated as cub =

$$(\text{Cu in 100 \% sulfides}) / \text{Cu in Cub} \quad (6)$$

Wt fraction Po =

$$1 - (\text{wt fraction Pn} - \text{wt fraction Cu-rich phase}) \quad (7)$$

To calculate the weight fraction of each element present in each base metal sulfide the formula used:

Wt fraction element X in mineral Y =

(concentration X in mineral)\*(wt fraction mineral Y) / (concentration X in 100%

sulfides)

(8)

Median rather than average values were used for the concentrations to avoid the effects of outliers.

For some elements the median concentrations were less than detection limit. In these cases the detection limit was used to calculate the maximum amounts of the elements that could be present in the sulfide minerals (Table 9 – **outline in pink**).

Table 9: Result of mass balance calculation for Fe-rich, Cu-rich and matrix + breccia assemblages. The elements **outlined in pink** represent the median concentrations that are less than the detection limit. In these cases the detection limit was used to calculate the maximum amount of the elements that could be present in the sulfide minerals.

	Fe-rich			Cu-rich			Matrix + Breccia		
	Po	Pn	Ccp	Po	Pn	Cb	Po	Pn	Ccp
Zn (%)	0.344	0.055	17.2	0.010	0.018	48.9	0.103	0.024	7.32
Sn (%)	1.20	0.179	4.94	0.029	0.021	23.0	0.572	0.110	2.44
As (%)	31.3	26.9	<1.049	1.33	5.40	<1.238	10.9	2.46	0.586
Sb (%)	23.2	3.92	<0.776	<1.151	3.76	<3.30	<4.557	2.14	<0.434
Pb (%)	1.43	4.66	1.46	0.113	1.62	4.50	0.741	0.683	1.26
Bi (%)	10.0	5.47	0.241	0.174	2.76	2.19	5.44	3.39	0.611
Cd (%)	<2.76	<0.311	36.5	0.007	<0.011	27.5	<1.196	0.142	15.2
Se (%)	86.4	10.3	2.40	23.6	13.2	68.2	72.6	8.64	5.56
Re (%)	76.5	7.58	<0.100	57.2	18.4	<14.66	51.5	3.75	<0.1347
Ag (%)	17.0	10.6	2.25	0.96	15.2	43.7	15.1	13.0	7.41
Cu (%)	0.024	0.002	90.9	0.001	0.001	100	0.015	0.001	98.83
Au (%)	<21.5	<2.94	0.832	<0.14	<0.96	1.101	<5.830	<0.744	0.674
Te (%)	24.63	2.63	3.14	0.460	0.483	19.7	16.6	1.71	23.7
Pd (%)	<4.00	26.2	<0.117	<0.497	66.0	<1.059	<6.02	38.2	<0.429
Pt (%)	<302	<45.3	<14.4	<234	<93.8	<801	<6.0	<4.99	<0.428
Rh (%)	72.0	<7.29	n.d.	<76.71	<46.8	n.d.	72.6	<9.44	n.d.
Ru (%)	360	<121	n.d.	<686	<7532	n.d.	<243	<836	n.d.
Ir (%)	94.9	<9.98	<1.81	<140	<107	<324	118	10.94	<3.25
Os (%)	<134	<14.25	<3.19	<9420	<614	<2269	<166	<22.79	<7.80
Ni (%)	5.27	89.1	0.003	1.01	97.9	0.062	5.30	102	0.001
Co (%)	1.16	73.7	0.000	0.518	66.8	0.005	1.415	89.82	0.000

Abbreviation: n.d. = not determined.

In all 3 assemblages (Fe-rich, Cu-rich and matrix + breccia) considered in this mass balance, some elements Se, Re, Cu, Rh, Ir, Ni and Co are largely present in the sulfide minerals (Table 9, Fig. 38, 39 and 40). Rhodium, Re and Ir are predominantly present in pyrrhotite, Co and Ni in pentlandite and Cu in chalcopyrite or cubanite. These elements, except Cu would have originally partitioned into MSS during crystallization of the sulfide liquid. At temperature <650 °C pyrrhotite and pentlandite exsolve from MSS and Co, Ni, Rh, Re and Ir in the MSS partitioned into the pyrrhotite and pentlandite. Copper has originally partitioned into ISS during crystallization. At low temperature, chalcopyrite and cubanite exsolve from ISS and the Cu in the ISS partition in the chalcopyrite or cubanite. In addition, Se is present in all the base metal sulfides. Selenium is slightly incompatible with MSS (Table 10) and slightly compatible with ISS, however pyrrhotite hosts the largest amount of Se in Fe-rich and matrix + breccia assemblages because pyrrhotite is the dominant mineral in these assemblages. In the Cu-rich assemblage most of the Se is hosted in the cubanite.

As has been reported for other deposits (Barnes et al. 2006; Godel and Barnes, 2008; Dare et al. 2010b, 2011; Piña et al. 2012; Duran 2015) pentlandite in the Fe-rich and breccia sulfides hosts a significant amount of the Pd (20 to 40 %). For the Cu-rich assemblage, pentlandite hosts 66% of the Pd, but given that only one sample contained pentlandite grains large enough to analyze, this may not be representative.

Zinc, Ag, Cd, Sn and Te concentrations are highest in chalcopyrite and cubanite (Fig. 38, 39 and 40 and Table 9). These elements are strongly incompatible with MSS and mildly incompatible to slightly compatible with ISS (Table 10). Thus the high concentrations in chalcopyrite and cubanite are reasonable. In the mass balance calculation much (20 to 50%) of the Zn, Sn, Cd, Ag and Te was found in these minerals in the Cu-rich assemblage. For the Fe-rich and matrix + breccia samples chalcopyrite is

remains the base-metal sulfide which hosts the most Zn, Sn and Cd. In contrast pyrrhotite and pentlandite contain ~ 20 % of the Ag and Te. The high proportion of Ag and Te in pyrrhotite and pentlandite is surprising given that the partition coefficient into MSS for these elements is low  $<0.1$  (Table 10). The relatively high proportion of Ag and Te in pyrrhotite and pentlandite in the Fe-rich assemblage could arise because Fe-rich rocks are adcumulates. The trapped liquid phase has largely been removed from the rocks and thus any incompatible elements present are the small quantity that originally partitioned into MSS.

Table 10: Partition coefficient from chalcophile elements. Modified from Barnes and Ripley (2016).

	MSS/sulfide liquid			ISS/sulfide liquid	
	Experimental		Empirical	Experimental	
	Min	Max		Min	Max
<b>Ag</b>	0.01	0.11	0.38	0.19	1.2
<b>As</b>	0.02	0.5		0.11	0.24
<b>Au</b>	0.0038	0.09	0.1	0.21	1
<b>Bi</b>	0.003	0.0074		0.026	0.13
<b>Cd</b>			0.3-0.5		
<b>Co</b>	0.92	1.6	1.6		
<b>Cu</b>	0.06	0.36	0.07	1	2
<b>Ir</b>	2.3	14.7	3.8-13	0.05	0.22
<b>Mo</b>	2.1	2.9			
<b>Ni</b>	0.36	1.72	1.1	0.1	0.9
<b>Os</b>	2	23	3.4-11	0.06	0.53
<b>Pb</b>	0.001	0.049		0.05	
<b>Pd</b>	0.06	0.24	0.13	0.3	0.7
<b>Pt</b>	0.04	0.03	0.004	0.125	0.487
<b>Re</b>	1.6	8.5	4.3-9	0.054	0.11
<b>Rh</b>	1	11	2.7-8.3	0.055	0.15
<b>Ru</b>	1	19	0.96	0.083	0.84
<b>Sb</b>	0.002	0.017		0.029	0.142
<b>Se</b>	0.5	0.75	0.4	0.83	1.2
<b>Sn</b>	<0.03	0.009		0.16	
<b>Te</b>	0.0015	0.07		0.31	0.822
<b>Zn</b>	0.36	0.62	0.02	3.9	

Some elements such as Sn, Pb, Au, and Bi are present in the BMS but not in significant amounts <16 %. These elements are mostly hosted and controlled by other minerals such as magnetite, galena, arsenides, tellurides, bismuthides, PGM or PMM.

For some elements Ru, Os, and Pt it is not possible to make a meaningful mass balance calculation because most of these elements are present at less than detection levels and assuming the detection limit as the maximum level of the element present permits up to 100 % of the element to be present in the sulfides.

In their study Kelvin et al. (2011) calculated a mass balance for four elements (Pd, Pt, Au and Ag) for their Pb, Pd and Pt rich rocks. They calculated that 22.5% Pd, 1.0% Pt, 13.7% Au and 5.1% Ag are found to be hosted by BMS. Palladium and Au are in agreement with our study and host similar amounts compared to Fe-rich assemblage. In our study more Ag was found to be present in the BMS ~30 vs 5.1 % Ag. Kelvin et al. (2011) studied exceptional samples that were enriched in PGM and PMM phases and Ag concentrates mostly in these phases. It has not been possible to compare Pt concentration mass balance, because this element is below the detection limit in our study. Also Kelvin et al. (2011) has calculated the mass balance just for a few elements as discussed above.

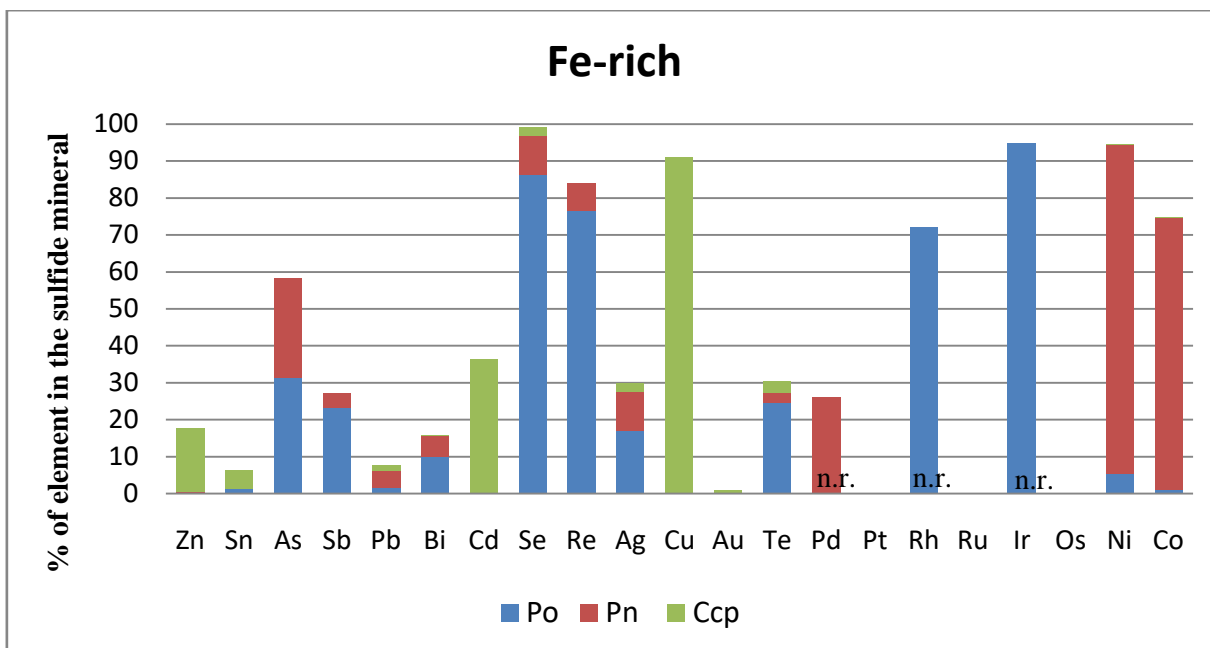


Fig. 38: Mass balance of chalcophile and platinum-group elements for Fe-rich assemblage from the Ovoid. The elements are ordered relative to their compatibility during partial melting of the mantle, from the most incompatible to the left to the most compatible to the right. For this graph we used the the median proportion (percent) of each element in pyrrhotite, pentlandite and chalcopyrite. Abbreviation: n.r. = not reported.

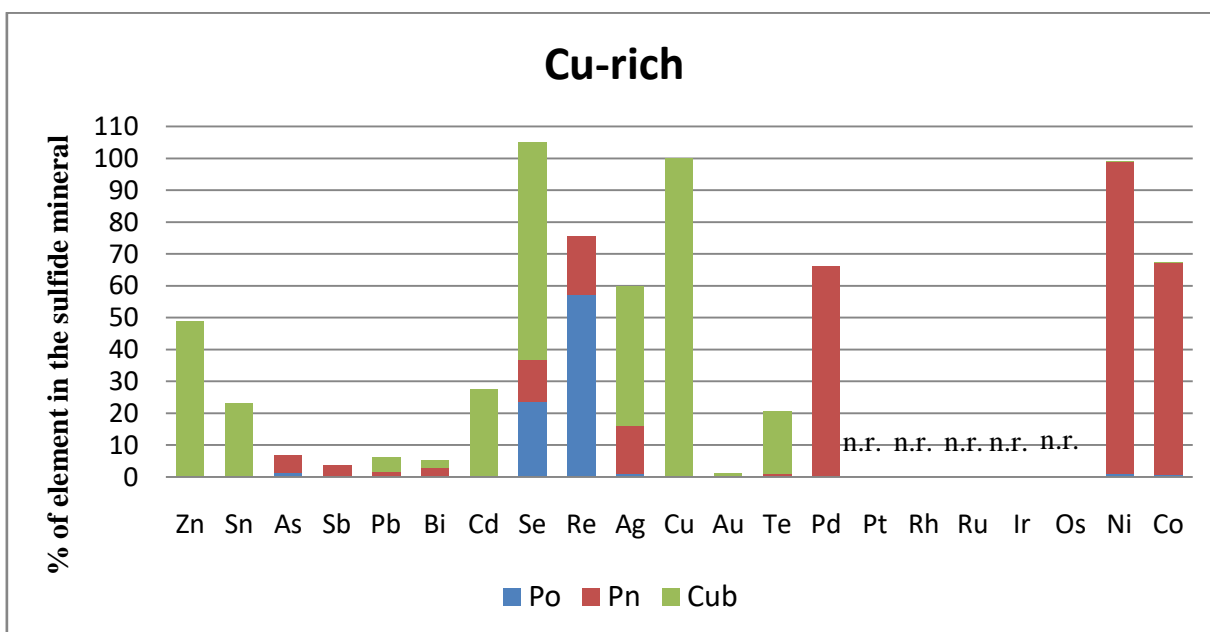


Fig. 39: Mass balance of chalcophile and platinum-group elements for Cu-rich assemblage from the Ovoid. The elements are ordered relative to their compatibility during partial melting of the mantle, from the most incompatible to the left to the most compatible to the right. For this graph we used the median proportion (percent) of each element in pyrrhotite, pentlandite and cubanite. Abbreviation: n.r. = not reported.

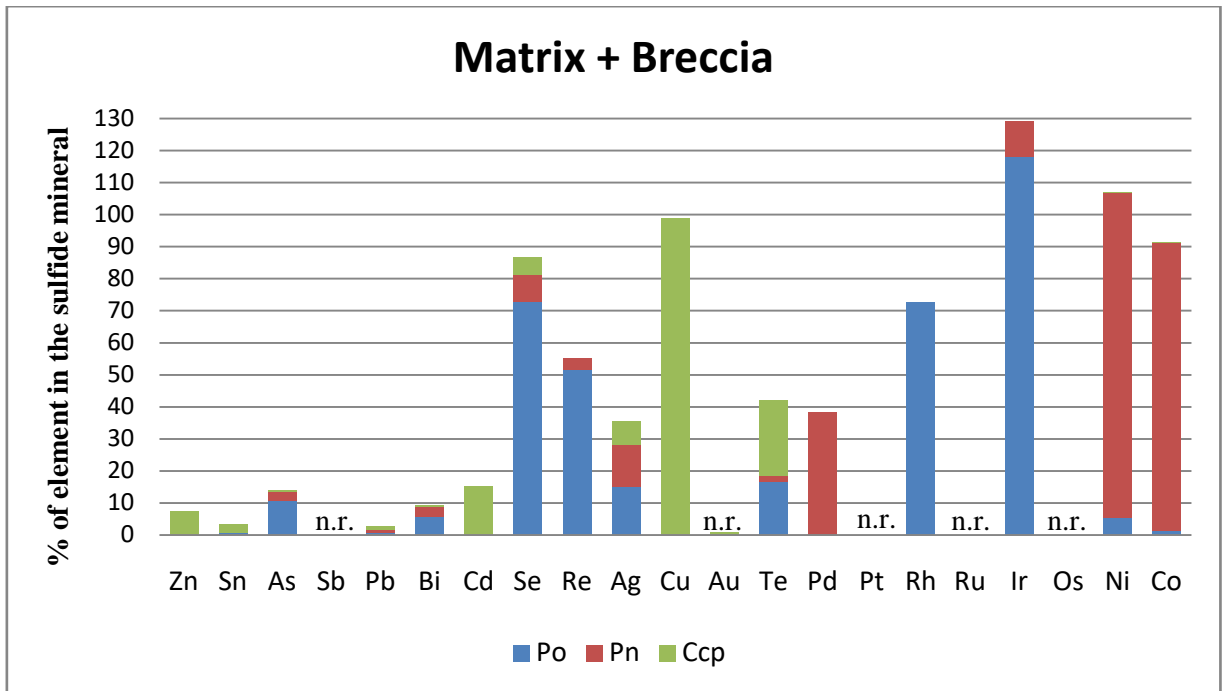


Fig. 40: Mass balance of chalcophile and platinum-group elements for matrix + breccia assemblage from the Ovoid. The elements are ordered relative to their compatibility during partial melting of the mantle, from the most incompatible to the left to the most compatible to the right. For this graph we used the median proportion (percent) of each element in pyrrhotite, pentlandite and chalcopyrite. Abbreviation: n.r. = not reported.

## CHAPTER 9

### 9. DISCUSSION

#### 9.1. Sulfide fractionation

##### *9.1.1. Sulfide fractionation and chalcophile elements distribution among base-metal sulfide minerals*

It is well known from experimental work (Distler et al. 1977; Fleet et al. 1993; Li et al. 1996; Barnes et al. 1997, 2001; Brenan, 2002; Mungall et al. 2005; Liu and Brenan 2015) that the composition of magmatic sulfide liquid changes during fractional crystallization. These changes produce variations in mineral assemblages and chemistry observed in different ore types of magmatic sulfide ore deposits (Barnes and Lightfoot 2005; Barnes et al. 2008; Dare et al. 2010a, 2011; Naldrett 2011). Variations observed in the Ovoid ore body of the Voisey's Bay deposit may be ascribed to the fractional crystallization process and can be summarized as follows:

When the temperature is  $<1190$  °C, the MSS (represented by the Fe-rich massive sulfide ore) starts to crystallize and Fe, Ir, Rh and Re partition into cumulus MSS as they are the most compatible elements. At high temperatures the partition coefficient of Ni into MSS is slightly  $<1$ , but Ni becomes compatible with MSS as temperature decreases (Li et al. 1996; Barnes et al. 2001). Experimental work (Naldrett 1969) suggests that at  $1050$  °C, MSS and magnetite crystallize together. This is because the oxygen content of the sulfide liquid increases during MSS crystallization until the magnetite-MSS cotectic point is reached at  $1050$  °C (Fig. 41 A). Elements incompatible

with MSS Cu, Zn, As, Pd, Ag, Cd, Sn, Te, Pt, Au, Pb and Bi, remain in the fractionated liquid from which ISS crystallizes as the temperature cools to ~900 °C.

When the ISS crystallizes (Craig and Kullerud 1969; Fleet and Pan 1994) Cu, Zn, Ag, Cd and Sn partition into ISS (represented by the Cu-rich massive sulfide ore, Fig. 41 B), whereas the other incompatible metals remain in the residual liquid (As, Pd, Te, Sb, Pt, Au and Bi). The distribution of the elements between Fe-rich and Cu-rich ores of the Ovoid is consistent with this model and suggests that the mineralization observed is the result of crystal fractionation of a magmatic sulfide liquid. The mass balance presented in the chapter 8 (LA-ICP-MS interpretation), supports the distribution of trace elements among the base-metal sulfides minerals.

As the temperature drops to ~650 °C, pyrrhotite, pentlandite and minor chalcopyrite start to exsolve from the MSS and continue exsolving until 250 °C (Kelly and Vaughan 1983; Naldrett et al. 2000b). In addition chalcopyrite, minor pentlandite and pyrrhotite start exsolving from the ISS and at temperature of <335 °C cubanite exsolves and coexists with the other sulfide minerals (Yund and Kullerud 1966; Naldrett et al. 2000b; Lusk and Bray 2002) (Fig. 41 C). Cubanite is the predominant sulfide mineral exsolved from ISS during fractional crystallization due to the high metal / sulfur ratio in the sulfide liquid favoring cubanite exsolving over chalcopyrite exsolving (Naldrett et al. 2000b). Troilite exsolves from pyrrhotite in MSS when the temperature is <145 °C (Kissin and Scot, 1982; Naldrett et al. 2000b; Huminicki, 2007; Naldrett, 2011) (Fig. 41-D). Troilite has a high metal / sulfur ratio in the sulfide liquid and develops from the pyrrhotite (Naldrett et al. 2000b; Naldrett 2011).

Finally, PGM, PMM arsenide-bismuthide-telluride phases can either crystallize or exsolve. If they crystallize (what occurs rarely) the temperature believed to this process is <550 °C and these phases are evidences of crystallization from late-stage,

trapped semi-metal rich melt as at Sudbury Dare et al. (2014). Most common process is the exsolution of PGM, PMM, arsenide-bismuthide-telluride phases. They exsolve from the residual liquid, but can also exsolve from ISS and rarely MSS. Few of these phases are included in pyrrhotite from Fe-rich assemblage and most of these phases are included in cubanite and galena from Cu-rich assemblage. These exsolutions represent the composition of the ultimate residual liquid, because elements such as Bi, Te, Au and Sb represent the most incompatible metals and rest in the of the sequence of exsolution where, for example, native bismuth laths and electrum exsolve. All the mineralogical assemblages and textures from Fe-rich and Cu-rich assemblages described above are consistent with this sequence of exsolution for the Ovoid ore body, suggesting that the MSS and ISS crystallized from a sulfide liquid.

Furthermore, galena and sphalerite observed in Fe-rich and Cu-rich ores display exsolution textures as well suggesting that these minerals exsolved from MSS and mainly from ISS along with pyrrhotite, pentlandite, chalcopyrite and cubanite. Little amounts of galena and sphalerite control part of the budget of Pb, Zn and Cd (Barnes et al. 2006; Dare et al. 2014). However, the timing of exsolution of galena and sphalerite is difficult to constrain, as little is presently known about how and when galena and sphalerite form in magmatic sulfide systems (Dare et al. 2014). Experimental data are currently not available for Pb, but the experiments of Kojima and Sugaki (1984) and the study of Dare et al. (2014) propose that moderate amounts of Zn, is soluble in ISS, but this solubility decreases with decreasing in temperature. The Zn solubility results in the exsolutions of skeletal star-shaped sphalerite.

The model proposed for Voisey's Bay is similar to other deposits such as Aguablanca, Lac des Îles and Sudbury. It follows the typical model for distribution of trace elements by fractional crystallization.

### 9.1.2. Palladium diffusion into pentlandite

Mass balance calculation showed that pentlandite from Fe-rich ore accounts for ~26 % of whole rock Pd budget which is counterintuitive as Pd is incompatible in MSS. Palladium concentrates in the fractionated liquid and should partition into residual liquid and finally form PGM. The Pd diffusion into pentlandite has previously been observed in sulfide droplets at Noril'sk, Sudbury and Aguablanca (Barnes et al. 2006; Dare et al. 2010b; Piña et al. 2012). These authors propose that Pd might diffuse from MSS and the majority of Pd diffuse from Cu-rich rich or residual liquid into pentlandite.

Experimental work by Kelly and Vaughan (1983) showed that different textures of pentlandite are exsolved from MSS depending on factors such as temperature and diffusion time. Later work by Dare et al. (2010b) and by Piña et al. (2012) observed three different textures of pentlandite during progressive cooling. The coarse granular pentlandite starts exsolving at ~650 °C, forming rims that grow as the temperature cools. The veinlets which wrap around the grain boundaries of other minerals exsolves at ~300 °C and the pentlandite flames form last when the temperature is <250 °C.

To assess the amount of Pd in pentlandite, LA-ICP-MS analyses were conducted in coarse grained and flames textures in both the Fe-rich ore and Cu-rich ore. These results are presented in the chapter 7 (LA-ICP-MS results). It was observed that the amount of Pd in pentlandite varies according to the pentlandite texture, the amount of cubanite or chalcopyrite in the sample, as well as, if the pentlandite is in contact with cubanite or pyrrhotite.

For Fe-rich ore, the majority of Pd diffuses at temperatures of 650 °C and 400 °C, when the cores of pentlandite form and the Pd diffuse together with Ni and Co to

form coarse-granular pentlandite (Dare et al. 2010b; Piña et al. 2012). The coarse-granular pentlandite hosts most of the Pd diffused from MSS. Pentlandite flames are almost absent of Pd, this is attributed to their formation at low temperatures where only a small amount of Pd is available to diffuse into flames. For Cu-rich ore, there is more Pd available compared to Fe-rich ore, as the partition coefficient for Pd into ISS is higher. As a result, the coarse-granular pentlandite in contact with pyrrhotite hosts a considerable amount of Pd compared to pentlandite from Fe-rich ore. However, the pentlandite in contact with cubanite in the Cu-rich ore hosts the largest amount of Pd, this results because cubanite exsolves from ISS at the end of the process of sulfide fractionation, and the liquid from which it forms is more evolved and tend to concentrate Pd.

Finally, the amount of Pd to diffuse into pentlandite depends on (1) the original concentration of Pd in the sulfide liquid; (2) the rate of cooling; (3) the degree of fractionation of Cu-rich liquid (Dare et al. 2010b; Piña et al. 2012). In the case of the Ovoid ore body, slow cooling coupled with fractionated Cu-rich liquid, provides more Pd into the coarse-granular pentlandite of Cu-rich ore than in coarse-granular pentlandite of Fe-rich ore. However, the original concentration of Pd at Ovoid is not that rich compared to other deposits such as Noril'sk, Sudbury and Lac des Iles.

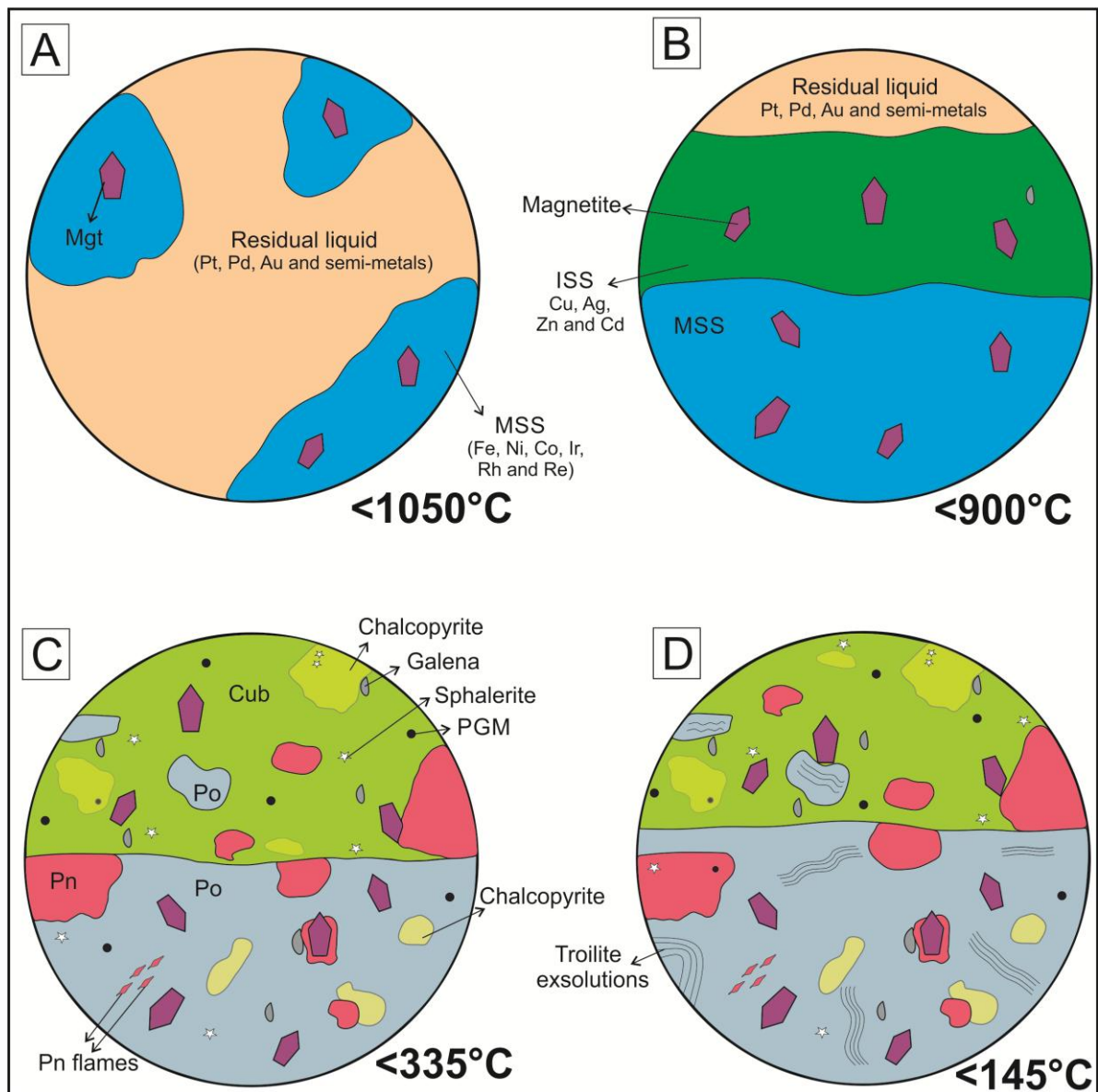


Fig. 41: Schematic model of the crystallization history of the Ovoid ore body and the distribution of PGE and other trace elements among the mineral phases. **A:** At  $T < 1050^{\circ}\text{C}$ , crystallization of MSS and magnetite. **B:** At  $T < 900^{\circ}\text{C}$ , crystallization of ISS. **C:** MSS and ISS exsolve to sulfide minerals. MSS: pyrrhotite represents the matrix, pentlandite and minor chalcopyrite; and ISS: cubanite represents the matrix, minor chalcopyrite, pentlandite and pyrrhotite. Galena and sphalerite are also exsolved. Exsolution of PGM, PMM, arsenide-bismuthide-telluride phases are developed. Also there is no residual liquid remaining when  $T < 335^{\circ}\text{C}$ . **D:** At  $T < 145^{\circ}\text{C}$ , troilite exsolved from pyrrhotite.

## 9.2. Evolution of sulfide liquid during the fractional crystallization in the Ovoid

It is known that during progressive fractional crystallization of sulfide liquid, it becomes more evolved and enriched in incompatible elements such as Pd, Pt, Bi, Te, As and Sb, which remain in the residual liquid and crystallize last.

Naldrett et al. (2000a) support the idea that fractional crystallization at the Ovoid occurs from the base to the top and from the margins toward the center in a closed system. This hypothesis from Naldrett et al. (2000a) is supported by a variation of Rh / Cu vs Rh. Lightfoot et al. (2012) and Boutroy et al. (2014) corroborate this argument when they show a decrease in Ir and Rh and an increase of (Pt+Pd) / (Os+Ir+Ru+Rh) ratio from the margins toward to the center where Cu-rich ore is concentrated.

The current study supports the idea that a trend of fractional crystallization exists from the margin to the center of the Ovoid because the Pd / Ir ratio increases toward the Cu-rich core as well as the amount of incompatible elements (Bi+Te+As+Sb) which are higher in the Cu-rich core compared to the Fe-rich rim (Fig. 42). However as shown in the model in chapter 6 (whole rock interpretation), there are two possibilities for the sulfide fractional crystallization: (1) two different liquids crystallized in Ovoid, one forming the Fe-rich ore and the other one forming the Cu-rich ore which was enriched in incompatible elements; (2) the Ovoid was formed by one liquid and another event(s) occur to enrich the Ovoid ore body in Bi and Te.

Therefore, it is clear that fractional crystallization is an important process in Ovoid and that the Cu-rich ore is more evolved than the Fe-rich ore. However the Cu-rich ore is coming from a different liquid to the the Fe-rich ore, or another event(s) is necessary to explain the enrichment of Te and Bi and this is indicative of an open system.

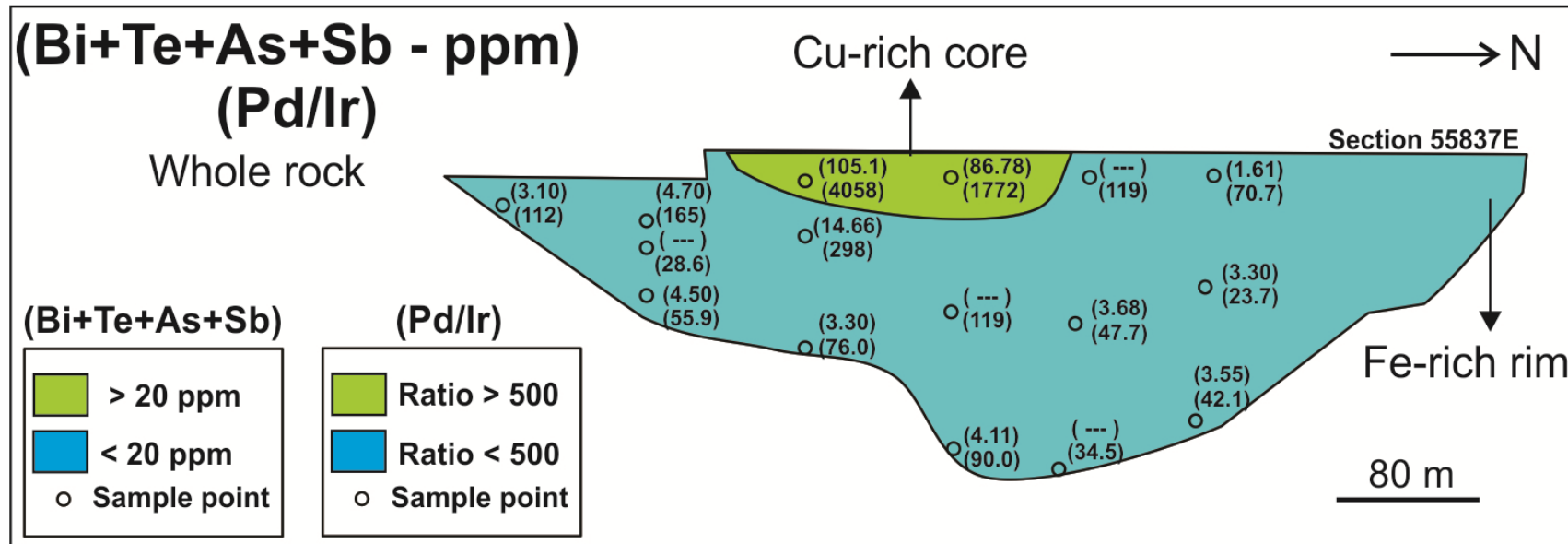


Fig. 42: West facing geologic section through the Ovoid ore body showing (Bi+Te+As+Sb) and Pd / Ir ratio. The sum of incompatible elements (Bi+Te+As+Sb) and Pd / Ir ratio increase from the Fe-rich rim to the Cu-rich core.

### 9.3. Implications of depth emplacement

The first depth of emplacement for Voisey's Bay was estimated by Foster (2006), at ~14 km depth. This consideration was based on a geothermobarometric study of contact aureoles of the nearby Nain plutonic suite by Berg (1977) and McFarlane et al. (2003). Later work by Saumur et al. (2015) estimated the original pressure for the Nain plutonic suite (Berg, 1979 Bohlen and Boettcher 1981; Morse 1982) at a depth of emplacement of ~9-11 km.

Figure 43 shows different depths of emplacement for different Ni-Cu-PGE deposits and Voisey's Bay is the deepest. At this depth, the rocks from Voisey's Bay cooled slowly and there was enough time to form coarse grained minerals, and extensive exsolutions such as troilite, skeletal star-shaped sphalerite and native bismuth laths. It is important to observe that the slow cooling does not affect the amount of PGM formed, because the amount of PGM formed is directly related to the amount of PGE present in rocks, which in this case is very low. The PGM found is a Pd-mineral, which is in agreement with the mass balance calculation because Os, Ir, Ru and Rh are hosted mainly in the base-metal sulfide minerals and Pt is very depleted. The depletion of PGE in the Ovoid might be related to magma emplacement, when the PGE were lost during transport in the conduit by formation of sulfides or were stucked in the conduit, or might be related to the magma source that was originally depleted in these elements. On the other hand, the Ovoid is enriched in incompatible elements such as bismuth and tellurium. The importance of these elements is that they play a role forming anions for PGM (Peregoedova 1998; Huminicki et al. 2008; Dare et al. 2014; Liu and Brenan 2015).

The high concentration of bismuth in the Ovoid rocks is anomalous. Two possibilities may have occurred in the Ovoid to explain the enrichment in bismuth: (1) Magma contamination from Bi-rich country rocks, such as graphitic gneiss or paragneiss at depth; (2) The initial bismuth concentration from the parental magma was not volatilized and did not escape as a gas nor was remobilized by fluids during the genesis of Ovoid. Given the great depth of emplacement, either processes or a combination of both are possible. Here is discussed bismuth because it represents one of the most enriched semi-metals in the Ovoid ore body, however other semi-metals such as Sb, Te and As could occur the same process.

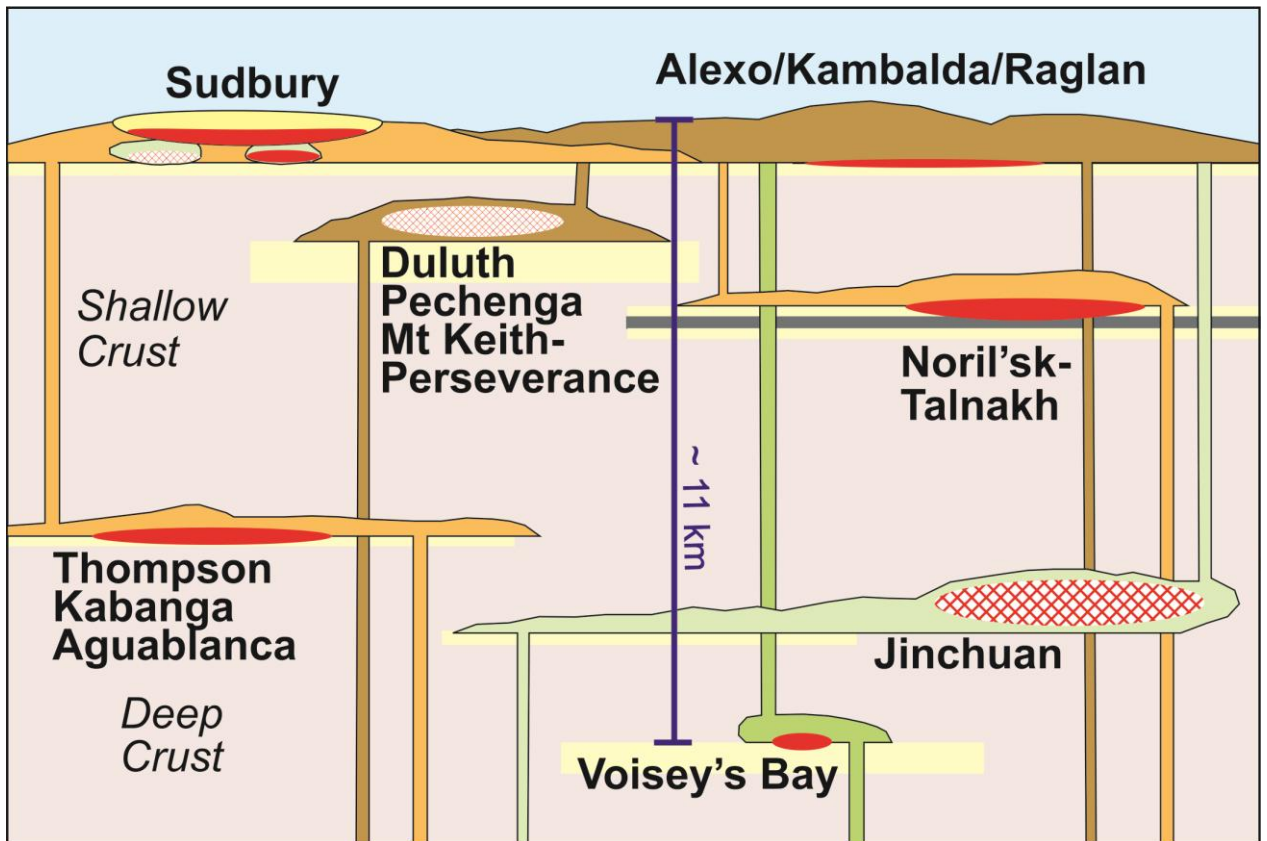


Fig. 43: Nickel-Cu-PGE deposits settings showing the depth of formation in each one. Voisey's Bay is the deepest and was emplaced at ~11 km. Modified from Michael Lesher (personal communication).

#### 9.4. Where are the platinum-group elements?

Huminicki et al. (2008) studied a hornblende gabbro dyke in the southeast extension zone of the Ovoid ore body (Fig. 44 A), where there are considerable concentrations of PGE (up to Pt = 1.95 g/t; Pd = 1.41 g/t; Au = 6.59 g/t) and incompatible elements such as Pb, Ag, Sn, Te, Bi and Sb. The budget of PGE in their study is controlled by the PGM that were formed when Pd and Pt formed PGM by combining with the incompatible elements. The PGM are hosted in chalcopyrite, bornite and galena.

Huminicki et al. (2008) presents three lines of evidence that the intrusion of the hornblende gabbro dyke is correlated with the Ovoid ore body: (1) lead isotopes were used to test if the galena found in the dyke has the same source of the galena from the Ovoid, and the Pb isotopes ratio indicates that they were produced through similar processes; (2) geological and spatial relationships show that the dyke is spatially connected as a splay off the main troctolite conduit (Fig. 44 B), which hosts the Ovoid ore body; (3) the geochemical signature of REE indicates that the dyke is related to the main conduit troctolite.

Based on the above evidence, the hornblende gabbro dyke has probably segregated early sulfides and should be the rock most appropriate to find higher concentrations of PGE at Voisey's Bay. This rock could have depleted the magma in PGE, that then formed the Ovoid, explaining why the Ovoid is PGE depleted.

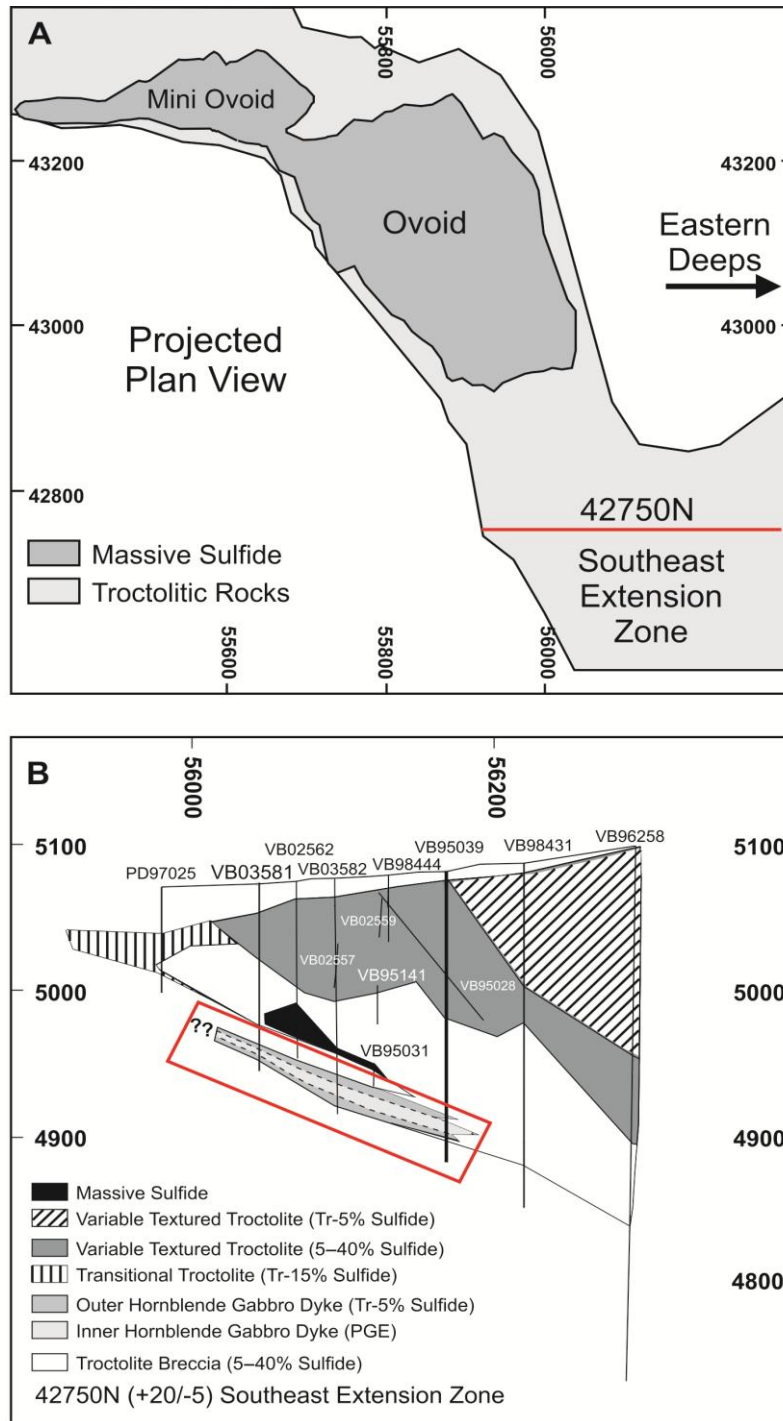


Fig. 44: **A:** Plan view of the Ovoid, Mini-Ovoid and Southeast Extension Zone projected to the surface. The red line corresponds where the (42750N) cross-section was carried out. **B:** North-facing (42750N) cross-section through the Southeast Extension Zone indicating the lithologies and the spatial relationship between the hornblende gabbro dyke (red square) that hosts the PGE mineralization and the Ovoid. Modified from Huminicki et al. (2008).

## 9.5. Application to exploration

During the last 10 years, LA-ICP-MS has been used as a new technique to estimate and calculate the proportion of each element in base metal sulfides mineral in order to understand whether the BMS minerals are the principal host of the chalcophile elements, specially the PGE. Pentlandite is an important base-metal sulfide mineral, because it hosts IPGE (Os, Ir, Ru), Rh and Pd. Based on this mineral a Rh vs Pd diagram was first proposed by Duran et al. (2016b) as a new tool to identify exploration target. This diagram was updated during this study to include Voisey's Bay pentlandite (Fig. 45).

Figure 45 suggests that a different composition of pentlandite can be distinguished between Ni-Cu sulfide deposits and PGE-dominated deposits. Nickel-Cu sulfide deposits (Sudbury: Dare et al. (2011); Aguablanca: Piña et al. (2012); Jinchuan: Chen et al. (2014); Rosie Nickel Prospect: Godel et al. (2012); Voisey's Bay in this study) have Pd concentrations in pentlandite of  $\leq 9$  ppm and Rh concentrations in pentlandite of  $\leq 0.4$  ppm. On the other hand, PGE-dominated deposits Bushveld Complex - Platreef: Holwell and McDonald, (2007), - Merensky Reef: Godel et al. (2007), Osbahr et al. (2013) and GNPA: Smith et al. (2014); Stillwater Complex: Godel and Barnes, (2008); Great Dyke: Barnes et al. (2008); Noril'sk: Barnes et al. (2006); Lac des Iles: (Djon and Barnes, (2012) and Duran et al. (2016b)) have Pd concentrations in pentlandite of  $> 9$  ppm up to 50.000 ppm as J-M reef at Stillwater Complex and Rh concentrations in pentlandite of  $> 0.4$  ppm up to 700-100 ppm as Merensky reef at Bushveld Complex. It is important to note that pentlandite from Lac des Iles has low concentrations of Rh, however it is enriched in Pd, making Lac des Iles distinguishable from other Ni-Cu sulfide deposits (Duran et al. 2016b).

For many years, different techniques such as classic geologic mapping, soil sampling, channel and chip sampling and geophysics have been used in an attempt to discover new Ni-Cu-PGE magmatic deposits. Nowadays, new discoveries of these deposits close to the surface are becoming increasingly difficult. Perhaps it is time to develop a new technique to guide the exploration towards new discoveries of magmatic deposits at depth.

Other studies have been developing tools to improve the exploration of ore deposits such as McClenaghan (2005) and McClenaghan et al. (2014) who studied indicator minerals from glacial terrains to use as pathfinders for buried mineral deposits. Preserved sulfides can be found in glacial terrains where chemical weathering is weak and they are buried fast due to the glacial flow, avoiding mechanical abrasion. McClenaghan et al. (2011) recovered a considerable amount of pentlandite in glacial till samples from the Thompson Nickel Belt in Canada. This case study shows that it is possible to recover sulfide minerals and opens the doors for exploration in other glacial terrains with promising potential for Canada, Siberia, Greenland and Scandinavia. At the moment, what has been proposed is to recover the pentlandite from the heavy minerals fraction of till samples and to mount them in epoxy allowing for fast analysis of a large number of grains at low cost using LA-ICP-MS. Finally, results can be plotted on the diagram Rh vs Pd (in pentlandite) (Fig. 45). This allows one to distinguish if the analyzed pentlandite plots in the Ni-Cu sulfide deposits field or in the PGE-dominant deposits field (Duran et al. 2016b).

The importance of this diagram is to guide and to select the appropriate exploration technique, because the tools to discover a layered intrusion deposit (such as Bushveld, Stillwater and Noril'sk) are different than the tools used to discover a magma

conduit deposit (such as Jinchuan and Voisey's Bay), including the geophysics, drilling and geochemistry sampling programs.

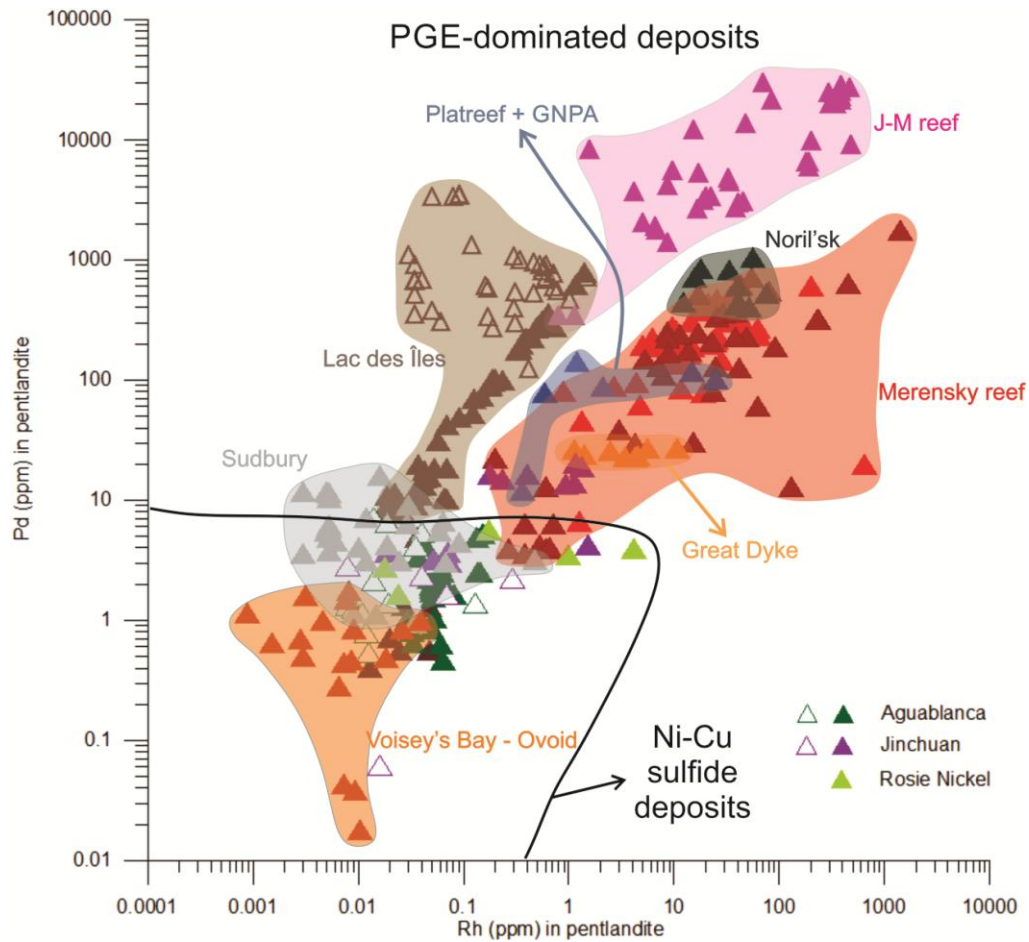


Fig. 45: Binary diagram of Rh vs Pd (in pentlandite). Modified from Duran et al. (2016b). Pentlandites from Ni-Cu sulfide deposits can be discriminated from pentlandite from PGE-dominated deposits. The data sources are: PGE-dominant deposits: Bushveld Complex (Platreef): Holwell and McDonald, (2007), (Merensky Reef) Godel et al. (2007), Osbahr et al. (2013) and (GNPA) Smith et al. (2014); Stillwater Complex: Godel and Barnes, (2008); Great Dyke: Barnes et al. (2008); Noril'sk: Barnes et al. (2006); and Lac des Îles: Djon and Barnes, (2012) and Duran et al. (2016b). Ni-Cu sulfide deposits: Sudbury: Dare et al. (2011); Aguablanca: Piña et al. (2012); Jinchuan: Chen et al. (2014); and Rosie Nickel Prospect: Godel et al. (2012); and Voisey's Bay: this study. For all open triangles = disseminated ore; closed triangles = massive ore.

## CHAPTER 10

### 10. CONCLUSION

The samples studied from the Ovoid in the Voisey's Bay deposit are separated into five different assemblages: disseminated sulfide, breccia sulfide, matrix sulfide, Fe-rich massive sulfide and Cu-rich massive sulfide. The sulfides from disseminated sulfide contain <1 % S, breccia sulfide and matrix sulfide contain between 10-25 % S and have different textures. The troctolite with disseminated assemblage contains minor fine-grained (0.2 mm) patches of sulfides, the breccia assemblage contains interlocking patches (3-4 cm) of sulfides and troctolite and matrix sulfides form an interconnected network surrounding troctolite. Opaque minerals present in these assemblages are pyrrhotite, pentlandite and chalcopyrite with additional magnetite and minor ilmenite. The Fe-rich massive sulfide is composed of coarse-grained pyrrhotite, pentlandite, chalcopyrite and magnetite. The Cu-rich massive sulfide is composed of coarse-grained cubanite / chalcopyrite, pentlandite, pyrrhotite, and magnetite.

Recalculated to 100 % sulfides the whole rock geochemistry indicates that breccia, matrix and Fe-rich assemblages have similar compositions whereas the Cu-rich assemblage has a different composition. The Fe-rich, breccia and matrix assemblages are richer in Re, Rh, Ru, Ir and Os than the Cu-rich assemblage. The Cu-rich assemblage is enriched in Zn, Sn, As, Sb, Pb, Bi, Cd, Ag, Cu, Au, Te, and Pd. The disseminated assemblage is the richest in almost all metals compared to the other assemblages, except for Bi, Cd, Re, Ag, Cu and Te. The Ovoid ore body is generally depleted in platinum-group elements and richer in other elements such as Zn, Pb, Bi, Pb, Cd and Te compared to other Ni-Cu magmatic sulfide deposits.

Crystal fractionation modelling of sulfides shows that the Fe-rich ore represents a monosulfide solid-solution (MSS) cumulate that started to crystallize together with magnetite at ~1050 °C. Based on plot of Cu versus Pd the Cu-rich ore cannot represent the fractionated liquid as it does not contain sufficient Pd. Cu-rich ore could be the cumulate of the intermediate solid-solution (ISS) with its crystallization starting at ~900 °C. However plots of Cu vs Bi and Te vs Bi show that the ore is too rich in these elements for it to represent an ISS cumulate from the same liquid that formed the MSS cumulate. A second liquid or some other processes are required to form the Cu-rich ore.

Platinum-group minerals, PMM, arsenide-bismuthide-telluride phases can either crystallize or exsolve. Most common process is the exsolution of PGM, PMM, arsenide-bismuthide-telluride phases. They exsolve from the residual liquid, but can also exsolve from ISS and rarely MSS. The distribution of chalcophile elements among the BMS is controlled by their partition coefficient during the fractional crystallization of MSS and ISS. Most of incompatible elements (Bi, Te, Sb, As) play an important role forming anions (ligands) for the formation of PGM, if there is PGE available in the system.

When T attained ~650 °C, MSS starts to exsolve pyrrhotite, pentlandite and minor chalcopyrite. Similarly, ISS started to exsolve chalcopyrite, minor pentlandite and pyrrhotite, and when the temperature reached <335 °C cubanite exsolved and coexists with other sulfide minerals that have already exsolved from ISS. Cubanite is the predominant mineral exsolved from ISS. The exsolution of MSS and ISS continued until 250 °C and troilite exsolved from pyrrhotite when T <145 °C.

The metal distribution among the BMS minerals shows that pyrrhotite and pentlandite host >70 % of the Ir, Rh and Re. Pentlandite also hosts significant amount of Ni, Co and >20% of the Pd. These observations suggest that these elements were initially concentrated in MSS and have partitioned by exsolution of pyrrhotite and

pentlandite. Cubanite and chalcopyrite host significant amounts of Cu, Ag, Zn, Sn and Cd; however, they are depleted in IPGE, Sb, As and Au, suggesting that cubanite and chalcopyrite exsolved from ISS. Skeletal star-shaped sphalerite exsolutions occur and host the remainder of the Zn, and a small amount of Cd. Galena hosts most of the Pb. Gold, Pd, Bi, Te, Pb and Ag also exsolve as electrum, PGM, PMM, telluride and native bismuth minerals.

The presence of Pd, an incompatible element, in pentlandite cannot be explained solely by sulfide fractionation. Palladium diffuses into pentlandite early during the exsolution of MSS. Most of the Pd diffused in pentlandite is hosted in the coarse-granular pentlandite.

Petrology and geochemical data shows the sulfide liquid that formed the Ovoid ore body has undergone extensive fractionation, and cooled slowly forming coarse-grained minerals and exsolutions.

Finally, the Rh vs Pd diagram (in pentlandite) Duran et al. (2016b) represents a new exploration tool where it is possible to distinguish PGE-dominated deposits and Ni-Cu sulfide deposits. This diagram can be useful for base metal and PGE exploration in order to discriminate the possible sources of pentlandite in glaciated terrains.

## CHAPTER 11

### 11. REFERENCES

- Allegre, C.J., and Minister, J. F. 1978. Quantitative models of trace element behavior in magmatic processes. *Earth and Planetary Science Letters*, **38**:1–25.
- Amelin, Y., Li, C., and Naldrett, A.J. 1999. Geochronology of the Voisey's Bay intrusion, Labrador, Canada, by precise U–Pb dating of coexisting baddeleyite, zircon and apatite. *Lithos*, **47**:33–51.
- Barnes, S.-J. 2016. Chalcophile elements. *Encyclopedia of Geochemistry*. Springer, 220p, DOI:10.1007/978-3-319-39193-9\_220-1.
- Barnes, S.-J., and Lightfoot, P.C. 2005. Formation of magmatic nickel-sulfide ore deposits and processes affecting their copper and Platinum-Group Elements contents. *Economic Geology*, **100th Anniversary Volume**:179–213.
- Barnes, S.-J., and Ripley E.M. 2016. Highly siderophile and strongly chalcophile elements in magmatic ore deposits. *Reviews in Mineralogy and Geochemistry*, **81**:725–774.
- Barnes, S.-J., Cox, R.A., and Zientek, M. 2006. Platinum-group element, gold, silver and base metal distribution in compositionally zoned sulfide droplets from the Medvezky Creek Mine, Noril'sk, Russia. *Contributions to Mineralogy Petrology*, **152**:187–200.
- Barnes, S.-J., Acterberg, E., Makovicky, E., and Li, C. 2001. Proton probe results for partitioning of platinum group elements between monosulphide solid solution and sulphide liquid. *South African Journal of Geology*, **104**:337–351.

- Barnes, S.-J., Makovicky, E., Karup-Moller, S., Makovicky, and M., Rose- Hanson, J. 1997. Partition coefficients for Ni, Cu, Pd, Pt, Rh and Ir between monosulfide solid solution and sulfide liquid and the implications for the formation of compositionally zoned Ni-Cu sulfide bodies by fractional crystallization of sulfide liquid. *Canadian Journal of Earth Sciences*, **34**:366–374.
- Barnes, S.-J., Prichard, H.M., Cox, R.A., Fisher, P.C., and Godel, B. 2008. The location of the chalcophile and siderophile elements in platinum-group element ore deposits (a textural, microbeam and whole rock geochemical study): Implications for the formation of the deposits. *Chemical Geology*, **248**:295–317.
- Bédard, L.P., Savard, D.D., and Barnes, S.-J. 2008. Total sulphur concentration in geological reference materials by elemental infrared analyzer. *Journal of Geostandards and Geoanalysis*, **32**:203–208.
- Berg, J.H. 1977. Regional geobarometry in the contact aureoles of the anorthositic Nain complex, Labrador. *Journal of Petrology*, **18**:399–430.
- Berg, J.H. 1979. Physical constraints and tectonic setting of the Nain complex. *Geological Association of Canada Abstracts*, **4**:1–39.
- Bohlen, S.R., and Boettcher, A.L. 1981. Experimental investigations and geological applications of orthopyroxene geobarometry. *American Mineralogist*, **61**:29–37.
- Boutroy, E., Dare, S.A.S., Beaudoin, G. Barnes, S.-J., and Lightfoot, P.C. 2014. Magnetite composition in Ni-Cu-PGE deposits worldwide and its application to mineral exploration. *Journal of Geochemical Exploration*, **145**:64–81.
- Brenan, J.M. 2002. Re–Os fractionation in magmatic sulphide melt by monosulfide solid solution. *Earth Planetary Science Letters*, **199**:257–268

- Chen, L.M., Song, X.Y., Danyushevsky, L.V., Wang, Y.S., Tian, Y.L., and Xiao, J.F. 2014. A laser ablation ICP-MS study of platinum-group and chalcophile elements in base metal sulfide minerals of the Jinchuan Ni–Cu sulfide deposit, NW China. *Ore Geology Reviews*, **65**:955–967.
- Craig, J.R., and Kullerud, G. 1969. Phase relations in the Cu-Fe-Ni-S system and their application to magmatic ore deposits. *Economic Geology*, **4**:344–358.
- Dare, S.A.S., Barnes, S.-J., and Beaudoin, G. 2012. Variation in trace element contents of magnetite crystallized from a fractionating sulphide liquid, Sudbury, Canada: implications for provenance discrimination. *Geochimica et Cosmochimica Acta*, **88**:27–50.
- Dare, S.A.S., Barnes, S.-J., and Prichard, H.M. 2010b. The distribution of platinum group elements (PGE) and other chalcophile elements among sulfides from the Creighton Ni–Cu–PGE sulfide deposit, Sudbury, Canada, and the origin of palladium in pentlandite. *Mineralium Deposita*, **45**:765–793.
- Dare, S.A.S., Barnes, S.-J., Prichard, H.M., and Fisher, P.C. 2010a. The timing and formation of platinum-group minerals from the Creighton Ni-Cu-platinum-group element sulfide deposit, Sudbury, Canada: Early crystallization of PGE-rich sulfarsenides. *Economic Geology*, **105**:1071–1096.
- Dare, S.A.S., Barnes S.-J., Prichard H.M., and Fisher P.C. 2011. Chalcophile and platinum-group element (PGE) concentrations in the sulfide minerals from the McCreedy East deposit, Sudbury, Canada, and the origin of PGE in pyrite. *Mineralium Deposita*, **46**:381–407.
- Dare, S.A.S., Barnes S.-J., Prichard H.M. and Fisher P.C. 2014. Mineralogy and Geochemistry of Cu-Rich Ores from the McCreedy East Ni-Cu-PGE Deposit (Sudbury, Canada): Implications for the behavior of platinum group and

- chalcophile elements at the end of crystallization of a sulfide liquid. *Economic Geology*, **109**:343–366.
- Distler, V.V., Malevsky, A.Y., and Laputina, I.P. 1977. Distribution of platinoids between pyrrhotite and pentlandite in crystallization of a sulphide melt. *Geochimica International*, **14**:30–40.
- Djon, M.L.N., and Barnes, S.-J. 2012. Changes in sulfides and platinum-group minerals with the degree of alteration in the Roby, Twilight, and high grade zones of the Lac des Iles Complex, Ontario, Canada. *Mineralium Deposita*, **47**:875–896.
- Duran, C.J. 2015. Origine des lentilles riches en sulfures des gisements de palladium du Lac des Iles, Ontario, Canada. PhD thesis, Université du Québec à Chicoutimi, Chicoutimi, Québec, 372p.
- Duran, C.J., Barnes, S.-J., and Corkery, J.T. 2016a. Geology, petrography, geochemistry, and genesis of sulfide-rich pods in the Lac des Iles palladium deposits, western Ontario, Canada. *Mineralium Deposita*, **51**:509–532.
- Duran, C.J., Barnes, S.-J., and Corkery, J.T. 2016b. Trace element distribution in primary sulfides and Fe-Ti oxides from the sulfide-rich pods of the Lac des Iles Pd deposits, Western Ontario Canada: Constraints on processes controlling the composition of the ore and the use of pentlandite compositions in exploration. *Journal of Geochemical Exploration*, **166**:45–63.
- Fleet, M.E., Chryssoulis, S.L., Stone, W.E., and Weisener, C.G. 1993. Partitioning of platinum-group elements and Au in the Fe - Ni - Cu - S system: experiments on the fractional crystallization of sulfide melt. *Contributions to Mineralogy and Petrology*, **115**:36–44.

- Fleet, M.E., and Pan, Y. 1994. Fractional crystallization of anhydrous sulfide liquid in the system Fe–Ni–Cu–S, with application to magmatic sulfide deposits. *Geochimica et Cosmochimica Acta*, **58**:3369–3377.
- Foster, J. 2006. Voisey's Bay: Geology, geochemistry and genesis. Abstract at Australian Earth Sciences Convention (AESC), Melbourne, Australia, 1–7.
- Godel, B., and Barnes, S.-J. 2008. Platinum-group elements in sulfide minerals and the whole rock of the J-M Reef (Stillwater complex): Implication for the formation of the reef. *Chemical Geology*, **248**:272–294.
- Godel, B., Barnes, S.-J., and Maier, W.D. 2007. Platinum-group elements in sulphide minerals, platinum-group minerals, and the whole rocks of the Merensky Reef (Bushveld Complex, South Africa): Implication for the formation of the reef. *Journal of Petrology*, **48**:1569–1604.
- Godel, B., González-Álvarez, I., Barnes, S.J., Barnes, S.-J., Parker, P., and Day, J. 2012. Sulfides and sulfarsenides from the Rosie Nickel Prospect, Duketon greenstone belt, Western Australia. *Economic Geology*, **107**:275–294.
- Holwell, D.A., and McDonald, I. 2007. Distribution of platinum-group elements in the Platreef at Overysel, northern Bushveld Complex: a combined PGM and LA-ICP-MS study. *Contributions to Mineralogy and Petrology*, **154**:171–190.
- Holwell, D.A., and McDonald, I. 2010. A review of the behavior of platinum group elements within natural magmatic sulfide ore systems. The importance of semimetals in governing partitioning behavior. *Platinum Metals Review*, **54**:26–36.
- Huminicki, M.A.E. 2007. A Comprehensive Geological, Mineralogical, and Geochemical Evaluation of the Voisey's Bay Ni–Cu–Co Sulfide Deposit: an

- Integration of Empirical Data and Process Mechanics. PhD thesis, Memorial University of Newfoundland, St. John's, Newfoundland, 386p.
- Huminicki, M.A.E., Sylvester, P.J., Cabri, L.J., Lesher, C.M., and Tubrett, M. 2005. Quantitative mass balance of platinum-group elements in the Kelly Lake Ni-Cu-PGE deposit, Copper Cliff offset, Sudbury. *Economic Geology*, **100**:1631–1646.
- Huminicki, M.A.E., Sylvester, P.J., Lastra, R., Cabri, L.J., Evans-Lamswood, D., and Wilton, D.H.C. 2008. First report of platinum-group minerals from a hornblende gabbro dyke in the vicinity of the Southeast extension zone of the Voisey's Bay Ni-Cu-Co deposit, Labrador: *Mineralogy and Petrology*, **92**:129–164.
- Hutchinson, D., and McDonald, I. 2008. Laser ablation ICP-MS study of platinum-group elements in sulphides from the Platreef at Turfspruit, northern limb of the Bushveld Complex, South Africa. *Mineralium Deposita*, **43**:695–711.
- Kelly, D.P., and Vaughan, D.J. 1983. Pyrrhotite-pentlandite ore textures: a mechanistic approach. *Mineralogical Magazine*, **47**:453–463.
- Kelvin, M.A., Sylvester, P.J., and Cabri, L.J. 2011. Mineralogy of rare occurrences of precious-metal-enriched massive sulfide in the Voisey's Bay Ni-Cu-Co Ovoid deposit, Labrador, Canada. *Canadian Mineralogist*, **49**:1505–1522.
- Kissin, S.A., and Scott, S.D. 1982. Phase relations involving pyrrhotite below 350°C. *Economic Geology*, **77**:1739–1754.
- Kojima, S., and Sugaki, A. 1984. Phase relations in the central portion of the Cu-Fe-Zn-S system between 800° and 500°C. *Mineralogical Journal*, 1215–28.
- Kullerud, G., Bell, P.M., and England, J.L. 1965. High pressure differential thermal analysis. *Carnegie Institute Washington Yearbook*, **64**:197–199.
- Kullerud, G., Yund, R.A., and Moh, G.H. 1969. Phase relations in the Cu-Fe-S, Cu-Ni-S and Fe-Ni-S systems. *Economic Geology*, **4**:323–343.

- Li, C., and Naldrett, A.J. 1999. Geology and petrology of the Voisey's Bay intrusion: reaction of olivine with sulfide and silicate liquids. *Lithos*, **47**:1–32.
- Li, C., Naldrett, A.J., Coats, C.J.A., and Johannessen, P. 1992. Platinum, palladium, gold, and copper-rich stringers at the Strathcona mine, Sudbury: Their enrichment by fractionation of a sulfide liquid. *Economic Geology*, **87**:1584–1598.
- Li, C., Naldrett, A.J., and Ripley, E.M. 2007. Controls on the Fo and Ni contents of olivine in sulfide-bearing mafic/ultramafic intrusions: principles, modeling and examples from Voisey's Bay. *Earth Science Frontiers*, **14**:177–185.
- Li, C., Naldrett, A.J., Rucklidge, J.C., and Kilius, L.R. 1993. Concentration of platinum-group elements and gold in sulfides from the Strathcona deposit, Sudbury, Ontario. *Canadian Mineralogist*, **31**:523–531.
- Li, C., Barnes, S.-J., Makovicky, E., Rose-Hansen, J., and Makovicky, M. 1996. Partitioning of Ni, Cu, Ir, Rh, Pt and Pd between monosulfide solid solution and sulfide liquid: effects of composition and temperature. *Geochimica et Cosmochimica Acta*, **60**:1231–1238.
- Lightfoot, P.C., Keays, R.R., Evans-Lamswood, D.E., and Wheeler, R. 2012. Crustal contamination and multiple S-saturation events in Nain Plutonic Suite magmas: evidence from Voisey's Bay, Labrador, Canada. *Mineralium Deposita*, **47**:23–50.
- Liu, Y., and Brenan, J. 2015. Partitioning of platinum-group elements (PGE) and chalcogens (Se, Te, As, Sb, Bi) between monosulfide-solid solution (MSS), intermediate solid solution (ISS) and sulfide liquid at controlled  $fO_2$ - $fS_2$  conditions. *Geochimica et Cosmochimica Acta*, **159**:139–161.

- Lusk, J., and Bray, D.M. 2002. Phase relation and the electrochemical determination of sulfur fugacity for selected reaction in the Cu-Fe-S and Fe-S systems at 1 bar and temperatures between 185 and 460 °C. *Chemical Geology*, **192**:222–248
- Lyubetskaya T., and Korenaga, J. 2007. Chemical composition of Earth's primitive mantle and its variance: 1. Method and results. *Journal of Geophysical Research*, **112**:B03211- DOI:10.1029/2005JB004223.
- McFarlane, C.R.M., Carlson, W.D., and Connelly, J.N. 2003. Prograde, peak, and retrograde P-T paths from aluminium in orthopyroxene: High temperature contact metamorphism in the aureole of the Makhavinekh Lake Pluton, Nain Plutonic Suite, Labrador. *Journal of Metamorphic Geology*, **21**:405–423
- McClenaghan, M.B. 2005. Indicator mineral methods in mineral exploration. *Geochemical Exploration Environment Analysis*, **5**:233–245.
- McClenaghan, M.B., Averill, S.A., Kjarsgaard, I.M., Layton-Matthews, D., and Matile, G. 2011. Indicator mineral signatures of magmatic Ni–Cu deposits, Thompson Nickel Belt, central Canada. In: McClenaghan, B., Peuraniemi, V., Lehtonen, M. - Indicator Mineral Methods in Mineral Exploration Workshop. 25th International Applied Geochemistry Symposium, Rovaniemi-Finland, 22–26.
- McClenaghan, M.B., Plouffe, A., and Layton-Matthews, D. 2014. Application of indicator mineral methods to mineral exploration. *Geologic Survey Canada Open File 7553*, 74p.
- Mall, A.P., and Sharma, R.S. 1988. Coronas in olivine metagabbros from the Proterozoic Chotanagpur terrain at Mathurapur, Bilhar, India. *Lithos*, **21**:291–300.
- Morse, S. 1982. A partisan review of Proterozoic anorthosites. *American Mineralogist*, **67**:1087–1100.

- Mungall, J.E., Andrews, R., Cabri, L.J., Sylvester, P.J., and Tubrett, M. 2005. Partitioning of Cu, Ni, Au, and platinum-group elements between monosulfide solid solution and sulfide melt under controlled oxygen and sulfur fugacities. *Geochimica et Cosmochimica Acta*, **69**:4349–4360.
- Naldrett, A.J. 1969. A portion of the system Fe-S-O between 900 and 1080°C and its application to sulfide ore magmas. *Journal of Petrology*, **10**:171–201.
- Naldrett, A.J. 1999. World-class Ni-Cu-PGE deposits: key factors in their genesis. *Mineralium Deposita*, **34**:227–240.
- Naldrett, A.J. 2004. *Magmatic sulfide deposits: Geology, geochemistry and exploration*. Berlin, Springer, 727p.
- Naldrett, A.J. 2011. Fundamentals of magmatic sulfide deposits. *Economic Geology*, **17**:1–50.
- Naldrett, A.J., and Duke, J.M. 1980. Platinum metals in magmatic sulfide ores. *Science*, **208**:1417–1428.
- Naldrett, A.J., and Li, C. 2007. The Voisey's Bay deposit, Labrador, Canada. In: *Mineral deposits of Canada: a synthesis of major deposit-types. District metallogeny, the evolution of geological provinces, and exploration methods*. Geological Association of Canada, Mineral Deposits Division, Special Publication, **5**:387–407.
- Naldrett, A.J., Innes, D.G., Sowa, J., and Gorton, M.P. 1982. Compositional variations within and between five Sudbury ore deposits. *Economic Geology*, **77**:1519–1534.
- Naldrett, A.J., Asif, M., Krstic, S., and Li, C. 2000a. The composition of mineralization at the Voisey's Bay Ni–Cu sulfide deposit, with special reference to platinum-group elements. *Economic Geology*, **95**:845–865.

- Naldrett, A.J., Singh, J., Krstic, S., and Li, C. 2000b. The mineralogy of the Voisey's Bay Ni–Cu–Co deposit, Northern Labrador, Canada: influence of oxidation state on textures and mineral compositions. *Economic Geology*, **95**:889–900.
- Osbahr, I., Klemd, R., Oberthür, T., Brätz, H., and Schouwstra, R. 2013. Platinum-group element distribution in base-metal sulfides of the Merensky Reef from the eastern and western Bushveld Complex, South Africa. *Mineralium Deposita*, **48**:211–232.
- Paton, C., Hellstrom, J., Paul, B., Woodhead, J., and Hergt, J. 2011. Iolite: freeware for the visualization and processing of mass spectrometric data. *Journal of Analytical Atomic Spectrometry*, **26**:2508–2518.
- Peregoedova, A.V. 1998. The experimental study of the Pt-Pd partitioning between monosulfide solid solution and Cu-Ni-sulfide melt at 900–840°C. Geological Society of South Africa and South African Institute of Mining and Metallurgy Symposium Series, **S18**:325–327.
- Piña, R., Gervilla, F., Barnes, S.-J., Ortega, L.M., and Lunar, R. 2012. Distribution of platinum-group and chalcophile elements in the Aguablanca Ni-Cu sulfide deposit (SW Spain): Evidence from a LA-ICP-MS study. *Chemical Geology*, **302–303**:61–75.
- Ryan, B. 2000. The Nain Churchill boundary and the Nain plutonic suite: a regional perspective on the geologic setting of the Voisey's Bay Ni–Cu–Co deposit. *Economic Geology*, **95**:703–724.
- Ripley, E.M., Park, Y.-R., Li, C., and Naldrett, A.J. 1999. Sulfur and oxygen isotopic evidence of country rock contamination in the Voisey's Bay Ni-Cu- Co deposit, Labrador, Canada. *Lithos*, **47**:53–68.

- Saumur, B.M., Cruden, A.R., Evans-Lamswood, and Lightfoot, P.C. 2015. Wall-rock structural controls on the genesis of the Voisey's Bay intrusion and its Ni-Cu-Co magmatic sulfide mineralization (Labrador, Canada). *Economic Geology*, **110**:691–711.
- Savard, D., Barnes, S.-J., and Meisel, T. 2010. Comparison between nickel- sulfur fire-assay Te-co-precipitation and isotopic-dilution with high pressure asher techniques for determination of platinum-group elements, rhenium and gold. *Geostandards and Geoanalytical Research*, **34**:281–291.
- Song, X.-Y., Keays, R.R., Zhou, M.-F., Qi, L., Ihlenfeld, C., and Xiao, J.-F. 2009. Siderophile and chalcophile elemental constraints on the origin of the Jinchuan Ni-Cu-(PGE) sulfide deposit, NW China. *Geochimica et Cosmochimica Acta*, **73**:404–424.
- Smith, J.W., Holwell, D.A., and McDonald, I. 2014. Precious and base metal geochemistry and mineralogy of the Grasvally Norite Pyroxenite–Anorthosite (GNPA) member, northern Bushveld Complex, South Africa: implications for a multistage emplacement. *Mineralium Deposita*, **49**:667–692.
- Yund, R.A., and Kullerud, G. 1966. The Fe-Pb-S system. *Journal of Petrology*, **7**:454–488.
- Zientek, M.L., Likhachev, A.P., Kunilov, V.E., Barnes, S.-J., Meier, A.L., Carlson, R.R., Briggs, P.H., Fries, T.L., and Adrian, B.M. 1994. Cumulus processes and the composition of magmatic ore deposits: examples from the Talnakh District, Russia. In: *Proceedings of the Sudbury- Noril'sk Symposium*, Ontario Geological Survey, Special publication, **5**:373–392.

## CHAPTER 12

### 12. APPENDIX

#### 12.1. Correction factors for Ru<sup>101</sup>, Rh<sup>103</sup> and Pd<sup>108</sup>.

Calculation of the correction factor for the interference of Ru<sup>101</sup> with Ni<sup>61</sup>Ar<sup>40</sup> (varies according to the day of analysis).

$$\text{Ru}^{101} = \text{Ru}^{101} \text{ measured} - \left( \text{Ni}^{61} \times \frac{\text{Ru}^{101} \text{ in Ni blank}}{\text{Ni}^{61} \text{ in Ni blank}} \right)$$

$$\frac{\text{Ru}^{101} \text{ in Ni blank}}{\text{Ni}^{61} \text{ in Ni blank}} = 1.2 \times 10^{-6} \text{ or } 1.3 \times 10^{-6} \text{ or } 1.4 \times 10^{-6}$$

Calculation of the correction factor for the interference of Rh<sup>103</sup> with Cu<sup>63</sup>Ar<sup>40</sup> (varies according to the day of analysis).

$$\text{Rh}^{103} = \text{Rh}^{103} \text{ measured} - \left( \text{Cu}^{63} \times \frac{\text{Rh}^{103} \text{ in ISS2}}{\text{Cu}^{63} \text{ in ISS2}} \right)$$

$$\frac{\text{Rh}^{103} \text{ in ISS2}}{\text{Cu}^{63} \text{ in ISS2}} = 1.82 \times 10^{-5} \text{ or } 2.0 \times 10^{-5}$$

Calculation of the correction factor for the interference of Pd<sup>108</sup> with Cd<sup>111</sup>.

$$\text{Pd}^{108} = \text{Pd}^{108} \text{ measured} - \left( \frac{\text{abundance } \% \text{ Cd}^{108}}{\text{abundance } \% \text{ Pd}^{108}} \right) \times \text{Cd}^{111}$$

$$\frac{\text{abundance } \% \text{ Cd}^{108}}{\text{abundance } \% \text{ Pd}^{108}} = 0.0336$$

## **12.2. Composition of pyrrhotite by LA-ICP-MS analysis**

Element		Co	Ni	Cu	Zn	As	Se	Ru	Rh	Pd	Ag	Cd	Sn	Sb	Te	Re	Os	Ir	Pt	Au	Pb	Bi
Isotope		59	61	65	66	85	82	101	103	108	109	111	120	121	128	185	190	193	195	197	208	209
VB7 (ppm)	1	24.6	2410	24	<0.334	0.750	52.7	0.0369	0.019	<0.012	0.151	<0.056	0.047	<0.026	0.271	0.037	<0.010	0.008	<0.010	<0.006	0.574	0.080
	2	91	3320	4.45	<0.334	0.370	48.9	<0.031	0.009	<0.012	0.233	<0.056	0.044	<0.026	0.750	0.013	<0.010	0.004	<0.010	<0.006	0.330	0.033
	3	21.6	2111	2.08	<0.334	0.660	48.1	<0.031	0.012	<0.012	0.238	<0.056	0.059	<0.026	0.560	0.019	<0.010	0.005	<0.010	<0.006	0.460	0.062
	4	20	1910	2.5	<0.334	0.340	47.9	<0.031	<0.006	<0.012	0.252	0.094	0.06	<0.026	0.440	0.017	<0.010	<0.003	<0.010	<0.006	0.309	0.045
	5	25.9	2260	3.54	<0.334	0.930	49.7	<0.031	0.008	<0.012	0.299	<0.056	0.09	0.0125	0.960	0.215	<0.010	0.003	<0.010	<0.006	1.05	0.072
	6	28.6	1990	1.23	<0.334	1.170	52.4	<0.031	<0.006	<0.012	0.262	<0.056	0.03	<0.026	0.740	0.131	<0.010	0.004	<0.010	<0.006	1.43	0.147
	7	26.1	2400	3.83	1.6	0.220	49.5	<0.031	0.008	<0.012	0.167	<0.056	0.21	0.049	0.442	0.016	<0.010	0.004	<0.010	<0.006	0.167	0.026
VB21 (ppm)	1	31.7	1671	0.29	<0.334	0.260	64.3	<0.031	0.012	<0.012	0.088	0.6	0.035	0.038	2.180	0.016	<0.010	0.016	<0.010	<0.006	0.139	0.023
	2	29.1	1542	0.166	<0.334	0.410	61.9	<0.031	0.006	<0.012	0.172	<0.056	0.098	<0.026	1.780	0.087	<0.010	<0.003	0.011	<0.006	0.522	0.069
	3	27.9	1496	0.104	0.69	0.317	65.2	<0.031	<0.006	<0.012	0.143	0.19	0.095	<0.026	0.790	0.093	<0.010	0.004	<0.010	<0.006	0.623	0.148
	4	32.2	1696	0.48	230	0.261	62.5	<0.031	0.011	<0.012	0.115	<0.056	0.086	0.036	1.120	0.067	0.0133	<0.003	<0.010	<0.006	0.550	0.063
VB8 (ppm)	1	67	3300	100	2.6	0.240	42.3	<0.031	0.009	<0.012	0.332	0.23	0.05	<0.026	0.290	0.056	<0.010	0.007	<0.010	<0.006	2.4	0.223
	2	30.2	2470	39	0.42	0.410	44.5	<0.031	0.014	<0.012	0.288	<0.056	0.033	<0.026	0.840	0.108	0.019	0.007	<0.010	<0.006	1.22	0.023
	3	44	1890	1.16	0.52	0.240	44.2	<0.031	0.012	<0.012	0.282	0.056	0.051	<0.026	0.650	0.100	0.021	0.004	<0.010	<0.006	1.57	0.130
	4	21.4	1960	19	<0.334	0.320	45	<0.031	0.011	<0.012	0.307	0.056	0.057	<0.026	0.450	0.084	0.015	0.008	<0.010	<0.006	1.08	0.072
	5	33.6	2650	1.41	23	0.420	48.4	<0.031	0.013	<0.012	0.179	<0.056	0.031	<0.026	0.450	0.161	0.02	0.007	<0.010	<0.006	1.11	0.058
	6	50	2600	1.6	<0.334	<0.116	43.7	0.0456	<0.006	<0.012	0.306	<0.056	0.056	0.027	0.260	0.070	0.014	0.005	<0.010	<0.006	2.48	0.108
	7	29	2420	39	<0.334	0.210	47.4	0.0349	0.014	<0.012	0.207	0.09	0.072	<0.026	0.870	0.150	<0.010	0.430	<0.010	<0.006	1.14	0.028
VB23 (ppm)	1	32.9	2510	5.52	0.88	0.520	57.6	<0.031	0.015	<0.012	0.181	<0.056	0.057	0.065	1.390	0.174	0.019	0.005	<0.010	<0.006	0.222	0.065
	2	21.6	2139	1.82	0.93	0.770	55.7	<0.031	0.007	<0.012	0.192	0.089	0.07	0.05	0.516	0.460	0.025	<0.003	<0.010	<0.006	0.318	0.181
	3	26.5	2185	1.87	1.6	0.310	58.1	0.0424	0.011	<0.012	0.25	<0.056	0.051	0.056	0.900	0.122	0.018	0.006	<0.010	<0.006	0.180	0.055
	4	38	3200	3.73	0.54	0.810	58	<0.031	0.009	0.020	0.178	<0.056	0.031	<0.026	1.400	0.211	0.021	0.008	<0.010	<0.006	0.247	0.082
	5	121	4100	1.41	0.8	0.840	57.2	<0.031	0.017	<0.012	0.209	0.062	0.041	0.115	1.690	0.128	<0.010	0.004	<0.010	<0.006	8	0.188

Element		Co	Ni	Cu	Zn	As	Se	Ru	Rh	Pd	Ag	Cd	Sn	Sb	Te	Re	Os	Ir	Pt	Au	Pb	Bi
Isotope		59	61	65	66	85	82	101	103	108	109	111	120	121	128	185	190	193	195	197	208	209
VB25 (ppm)	1	23.7	1839	1.72	0.51	0.341	56.8	<0.031	0.006	<0.012	0.217	<0.056	0.06	0.043	0.218	0.059	<0.010	0.005	<0.010	<0.006	0.421	0.040
	2	30.7	2260	1.25	0.48	0.230	58.3	<0.031	0.011	0.033	0.273	0.081	0.028	<0.026	0.464	0.072	0.018	0.006	<0.010	<0.006	0.498	0.081
	3	27.3	2225	2.13	0.9	0.150	58.4	<0.031	<0.006	<0.012	0.237	0.079	0.032	<0.026	0.333	0.068	0.017	<0.003	<0.010	0.0069	0.473	0.037
VB26 (ppm)	1	26.9	2426	2.73	0.48	0.295	53.1	<0.031	<0.006	<0.012	0.124	<0.056	0.045	<0.026	1.240	0.221	0.0102	0.005	<0.010	<0.006	0.623	0.180
	2	29.5	2700	51	0.37	0.270	52.8	<0.031	0.008	<0.012	0.254	<0.056	0.044	0.074	1.140	0.263	<0.010	0.005	<0.010	<0.006	3.60	0.139
	3	27.1	2790	2.27	0.66	0.179	52	<0.031	0.012	<0.012	0.097	<0.056	0.03	<0.026	0.640	0.263	0.01	0.008	<0.010	<0.006	0.337	0.097
	4	24.0	2530	1.91	0.48	0.224	48.6	<0.031	0.016	<0.012	0.174	<0.056	0.04	<0.026	1.120	0.168	<0.010	0.005	<0.010	<0.006	1.43	0.139
VB29 (ppm)	1	25.9	2350	12	0.71	0.126	55.6	<0.031	<0.006	<0.012	0.143	<0.056	0.051	0.042	1.310	0.203	<0.010	<0.003	<0.010	<0.006	0.103	0.052
	2	26.9	2370	10.9	0.67	0.270	51.3	<0.031	<0.006	<0.012	0.161	<0.056	0.04	<0.026	1.550	0.188	<0.010	<0.003	<0.010	<0.006	0.510	0.107
	3	23.46	2043	6.74	<0.334	0.255	50	<0.031	<0.006	<0.012	0.164	<0.056	0.065	<0.026	1.246	0.183	0.01	0.003	<0.010	<0.006	0.390	0.077
	4	32.1	2477	8.04	<0.334	0.300	48.4	<0.031	<0.006	<0.012	0.2	<0.056	0.039	<0.026	1.210	0.168	0.019	0.004	<0.010	<0.006	0.490	0.047
	5	21.3	1661	3.41	<0.334	0.284	50.1	<0.031	<0.006	0.016	0.174	<0.056	0.047	0.03	0.910	0.175	0.014	0.004	<0.010	<0.006	0.640	0.059
VB31 (ppm)	1	17.5	1469	2.16	1.6	0.260	52	<0.031	0.006	<0.012	0.244	<0.056	0.035	0.054	0.156	0.119	0.01	0.005	<0.010	<0.006	0.480	0.074
	2	18.8	1569	1.84	<0.334	0.310	54.4	<0.031	0.010	<0.012	0.235	0.061	0.054	<0.026	0.299	0.117	0.02	0.005	<0.010	<0.006	0.462	0.052
	3	8.13	566	0.99	<0.334	<0.116	42.9	<0.031	0.012	<0.012	0.379	<0.056	0.032	0.035	0.165	0.035	0.032	<0.003	<0.010	<0.006	2.510	1.160
VB36 (ppm)	1	24.2	2020	2.33	0.58	0.144	51.7	<0.031	0.009	<0.012	0.33	<0.056	0.035	0.028	0.688	0.138	<0.010	<0.003	<0.010	<0.006	0.330	0.037
	2	23.2	2160	1.11	0.36	0.129	53.2	<0.031	0.009	<0.012	0.46	<0.056	0.042	0.064	0.455	0.077	<0.010	<0.003	<0.010	<0.006	5.6	0.108
	3	24.7	1907	4.49	0.42	0.168	49	<0.031	0.014	<0.012	0.471	<0.056	0.063	<0.026	0.780	0.178	0.0139	0.005	<0.010	<0.006	0.179	0.054
	4	24.8	2207	3.58	<0.334	0.138	50.3	<0.031	0.012	<0.012	0.289	<0.056	0.031	0.036	0.739	0.109	<0.010	<0.003	<0.010	<0.006	0.33	0.130
VB27 (ppm)	1	40.7	820	1.15	0.38	<0.116	143.6	<0.031	<0.006	<0.012	0.77	0.11	0.037	<0.026	0.512	0.030	0.011	<0.003	<0.010	<0.006	0.40	0.022
	2	58.5	1452	2.53	<0.334	0.370	146	<0.031	0.010	<0.012	1.6	0.095	0.043	0.044	1.510	0.045	0.0117	<0.003	<0.010	0.006	2.90	0.043
	3	34.5	690	2.29	0.67	0.660	132.4	<0.031	0.014	<0.012	1.93	0.138	0.035	<0.026	2.320	0.039	<0.010	0.010	<0.010	<0.006	0.870	0.060
	4	41.8	1210	2.13	<0.334	0.423	143.1	<0.031	0.008	<0.012	2.6	0.096	0.074	<0.026	2.540	0.032	<0.010	<0.003	<0.010	<0.006	1.17	0.177
	5	48.4	1060	1.34	0.43	0.420	149	<0.031	0.017	<0.012	2.3	0.105	0.032	<0.026	1.880	0.031	<0.010	<0.003	0.012	<0.006	0.380	0.061

Element		Co	Ni	Cu	Zn	As	Se	Ru	Rh	Pd	Ag	Cd	Sn	Sb	Te	Re	Os	Ir	Pt	Au	Pb	Bi
Isotope		59	61	65	66	85	82	101	103	108	109	111	120	121	128	185	190	193	195	197	208	209
VB34 (ppm)	1	39.2	1085	1.45	0.86	0.440	118	<0.031	<0.006	<0.012	1.22	0.17	0.037	0.034	1.040	0.052	<0.010	0.004	<0.010	<0.006	0.128	0.079
	2	42.8	1227	2.77	0.51	0.470	118.8	<0.031	<0.006	<0.012	0.695	0.168	<0.020	<0.026	0.747	0.107	0.0135	<0.003	<0.010	0.011	0.199	0.078
	3	42.3	1277	7.7	0.93	0.540	125.5	<0.031	<0.006	<0.012	1.91	0.6	0.041	<0.026	1.960	0.075	<0.010	<0.003	<0.010	<0.006	0.450	0.139
	4	35.9	1114	1.23	0.76	0.210	116.2	<0.031	0.006	<0.012	0.613	0.104	0.03	<0.026	0.609	0.050	0.0106	<0.003	<0.010	<0.006	0.060	0.008
VB5 (ppm)	1	53.2	2089	5.34	1.2	0.431	129.2	<0.031	<0.006	<0.012	1.75	0.082	0.053	<0.026	2.040	0.041	<0.010	<0.003	<0.010	<0.006	0.247	0.092
	2	38.4	1330	0.92	0.71	0.163	111.2	<0.031	<0.006	<0.012	0.633	0.098	0.022	0.08	0.393	0.028	<0.010	<0.003	<0.010	<0.006	0.113	0.027
	3	61.1	1723	5.09	<0.334	0.250	114.2	<0.031	<0.006	<0.012	2.44	0.096	0.036	<0.026	3.460	0.036	<0.010	<0.003	<0.010	0.026	1.06	0.088
	4	59	1416	3.64	<0.334	0.154	115.3	<0.031	<0.006	<0.012	1.78	0.104	0.023	<0.026	2.190	0.039	<0.010	<0.003	<0.010	0.014	0.068	0.027
	5	42.2	729	2.27	0.82	0.470	114.8	<0.031	<0.006	0.012	0.965	<0.056	0.035	0.026	0.725	0.029	<0.010	<0.003	<0.010	0.0084	0.230	0.063
VB6 (ppm)	1	20.9	1486	1.46	2	<0.116	73.5	<0.031	<0.006	0.029	0.277	0.059	0.035	<0.026	0.204	0.020	<0.010	<0.003	<0.010	<0.006	0.376	0.113
	2	17	1070	1.55	0.8	0.206	71.3	<0.031	<0.006	<0.012	0.319	0.108	0.026	<0.026	0.131	0.029	<0.010	0.008	<0.010	0.008	0.232	0.048

### **12.3. Composition of pentlandite by LA-ICP-MS analysis**

Element		Co	Ni	Cu	Zn	As	Se	Ru	Rh	Pd	Ag	Cd	Sn	Sb	Te	Re	Os	Ir	Pt	Au	Pb	Bi
Isotope		59	61	65	66	85	82	101	103	108	109	111	120	121	128	185	190	193	195	197	208	209
VB7 (ppm)	1	12630	320000	1.18	<0.334	0.22	44.8	0.844	0.012	0.895	1.256	<0.056	0.026	<0.026	0.488	0.069	<0.010	<0.003	<0.010	<0.006	0.534	0.048
	2	12350	325000	2.2	<0.334	0.36	47	0.808	0.006	<0.012	2.09	<0.056	0.04	<0.026	0.78	0.022	<0.010	<0.003	<0.010	<0.006	5.34	0.039
	3	13020	327000	1.07	<0.334	0.31	48.6	0.955	<0.006	1.050	1.76	<0.056	0.045	<0.026	0.431	0.037	0.0104	<0.003	<0.010	<0.006	1.11	0.236
	4	12620	318000	1.3	0.54	0.33	45.4	0.857	<0.006	1.270	0.392	<0.056	0.032	<0.026	0.311	0.040	<0.010	0.0056	<0.010	<0.006	3.49	0.094
	5	13290	319000	1.53	0.36	0.17	43.3	0.895	<0.006	0.345	0.613	<0.056	0.072	<0.026	0.254	0.042	<0.010	<0.003	<0.010	<0.006	3.29	0.103
	6	13090	311000	1.12	0.8	0.2	43.3	0.846	<0.006	0.218	6.66	<0.056	0.19	<0.026	0.423	0.020	<0.010	0.02	<0.010	<0.006	20.3	0.262
VB21 (ppm)	1	11750	209900	<0.159	<0.334	0.687	49.2	0.283	<0.006	1.121	0.294	<0.056	0.118	0.0315	0.948	0.032	<0.010	0.007	<0.010	<0.006	3.52	0.277
	2	11540	211800	<0.159	<0.334	0.768	49.4	0.299	0.024	1.531	0.236	<0.056	0.113	0.075	3.29	0.026	<0.010	0.0035	<0.010	<0.006	1.99	0.127
	3	11470	232600	6.3	0.56	0.8	49.4	0.247	<0.006	0.841	0.259	0.5	0.066	0.21	0.626	0.027	0.0106	<0.003	<0.010	<0.006	0.86	0.104
VB8 (ppm)	1	11580	320000	2.11	1.4	0.34	46	0.854	0.013	0.087	0.82	<0.056	0.093	0.041	0.63	0.040	0.018	0.0077	<0.010	<0.006	7.4	0.481
	2	13240	344000	220	8	0.53	43.1	0.883	0.035	0.096	2.21	0.095	0.27	0.045	0.69	0.113	0.015	<0.003	0.13	<0.006	8.9	0.553
VB23 (ppm)	1	12390	299000	1.13	<0.334	1.4	50.8	0.092	0.009	<0.012	3.75	<0.056	0.051	0.035	1.13	0.169	0.018	0.0031	<0.010	<0.006	3.8	0.080
	2	12830	281400	2.59	0.73	1.02	50.2	0.099	0.009	0.016	2.33	<0.056	0.043	0.33	0.865	0.104	0.0209	0.0048	<0.010	<0.006	24	0.118
	3	12880	288000	1.62	2.2	1.29	47.7	0.096	0.011	0.020	0.991	<0.056	0.073	0.058	1.02	0.181	0.0108	<0.003	<0.010	<0.006	9.6	0.211
VB25 (ppm)	1	12250	265600	1.14	0.94	1.11	47.4	0.046	0.019	0.961	0.82	<0.056	0.043	0.033	0.385	0.100	0.0149	0.0044	<0.010	<0.006	9.9	0.093
	2	12080	277000	1.08	0.54	1.2	46.1	0.054	<0.006	0.704	0.605	<0.056	0.051	0.038	0.414	0.171	0.013	<0.003	<0.010	<0.006	8.4	0.325
	3	12480	275500	0.95	0.86	1.02	48.2	<0.031	0.009	0.519	0.811	<0.056	0.041	<0.026	0.45	0.103	<0.010	<0.003	<0.010	<0.006	0.48	0.069
	4	11360	271800	2.64	0.65	0.92	45.2	0.033	0.008	0.665	3.69	<0.056	0.08	0.076	0.285	0.051	<0.010	0.0052	<0.010	<0.006	25.5	1.950
VB26 (ppm)	1	13750	287000	12	0.81	0.9	41.1	0.085	<0.006	0.485	0.844	<0.056	0.088	0.026	2.18	0.112	0.0114	<0.003	<0.010	<0.006	8.6	0.503
	2	14240	300000	1.17	0.53	0.99	47	0.112	0.007	0.283	0.642	<0.056	0.031	<0.026	0.409	0.168	<0.010	0.0073	0.017	0.0202	32.2	4.750
VB29 (ppm)	1	12430	280000	0.64	0.41	0.99	41.1	0.130	0.008	0.010	0.92	<0.056	0.044	0.36	0.416	0.111	<0.010	0.012	<0.010	<0.006	0.36	0.030
	2	13700	278500	6.9	0.335	1.29	44.4	0.091	0.006	0.024	0.51	<0.056	0.022	<0.026	0.45	0.113	0.012	<0.003	<0.010	<0.006	2.03	0.130

Element		Co	Ni	Cu	Zn	As	Se	Ru	Rh	Pd	Ag	Cd	Sn	Sb	Te	Re	Os	Ir	Pt	Au	Pb	Bi
Isotope		59	61	65	66	85	82	101	103	108	109	111	120	121	128	185	190	193	195	197	208	209
VB31 (ppm)	1	9940	278000	4.3	<0.334	0.71	54.3	0.087	<0.006	1.520	1.54	<0.056	0.079	<0.026	7.24	0.005	<0.010	<0.003	<0.010	<0.006	0.74	0.290
	2	9840	282000	2.09	8	0.76	45.3	<0.031	<0.006	1.756	1.591	<0.056	0.044	0.033	3.18	<0.004	<0.010	<0.003	<0.010	<0.006	3.81	0.159
	3	9760	280000	1.99	<0.334	0.544	45.3	0.112	<0.006	1.540	1.067	<0.056	<0.020	<0.026	1.69	<0.004	<0.010	<0.003	<0.010	<0.006	0.64	0.109
VB36 (ppm)	1	11990	279200	1.26	0.88	0.761	44.9	0.098	<0.006	0.901	0.6	0.16	0.027	0.035	0.405	0.123	<0.010	0.0072	<0.010	<0.006	1.99	0.374
	2	11130	276000	1.56	<0.334	0.76	43	0.109	<0.006	0.938	1.269	<0.056	0.03	<0.026	0.383	0.188	0.025	0.0045	<0.010	0.0078	10.4	1.290
	3	11390	275200	1.69	0.34	0.669	42.3	0.085	<0.006	1.081	0.865	0.11	0.035	0.037	0.565	0.088	<0.010	<0.003	<0.010	<0.006	6.9	0.145
	4	10690	281200	1.35	0.37	0.696	46.8	0.083	<0.006	0.866	1.318	<0.056	0.103	<0.026	8.37	<0.004	<0.010	<0.003	<0.010	<0.006	7.3	0.769
VB6 (ppm)	1	9360	277600	8.3	1.16	0.86	59.2	<0.031	<0.006	0.909	7.35	0.06	0.13	0.059	0.249	0.016	<0.010	<0.003	<0.010	0.0132	34	0.327
	2	8640	286000	5.03	0.77	0.6	57.2	<0.031	<0.006	1.054	11.2	<0.056	0.091	0.05	5.48	<0.004	<0.010	<0.003	<0.010	0.0062	9.9	0.185
	3	9170	288600	3.19	0.45	17.3	76.8	<0.031	<0.006	1.636	2.58	<0.056	0.041	0.106	4.83	0.013	<0.010	<0.003	<0.010	<0.006	1.86	0.162
	4	9930	280400	2.91	1	1.33	59.9	<0.031	<0.006	1.589	13.6	<0.056	0.052	<0.026	0.12	0.029	<0.010	<0.003	<0.010	<0.006	4.05	0.186
	5	10070	285000	2.35	0.43	0.868	61	<0.031	<0.006	1.745	20.8	<0.056	<0.020	0.042	0.401	0.018	<0.010	<0.003	<0.010	0.013	1.33	0.379

**Pentlandite in textural study (*Palladium in pentlandite*)**

Element		Co	Ni	Cu	Zn	As	Se	Ru	Rh	Pd	Ag	Cd	Sn	Sb	Te	Re	Os	Ir	Pt	Au	Pb	Bi
Isotope		59	61	65	66	85	82	101	103	108	109	111	120	121	128	185	190	193	195	197	208	209
VB27 (ppm)	Pn	17870	290000	9.90	0.540	1.010	113.7	1.120	0.743	0.350	3200	0.300	2.70	0.046	1900	<0.004	<0.010	<0.003	<0.010	0.097	11.7	3.93
VB29 (ppm)	Pn	13700	278700	0.148	<0.334	0.009	1.05	0.038	0.027	0.246	0.121	<0.056	0.009	<0.026	0.033	<0.004	<0.010	<0.003	<0.010	<0.006	0.299	0.005
VB6 (ppm)	Pn	9877	283700	7.60	0.350	3.830	57.2	1.154	0.792	0.792	7.970	<0.056	0.064	0.078	5.74	<0.004	<0.010	<0.003	<0.010	0.002	3.10	0.110
VB36 (ppm)	flame	8800	238000	4.1	<0.334	0.200	34.5	1.100	0.791	<0.012	15.4	<0.056	0.050	0.026	1.03	0.011	<0.010	<0.003	<0.010	0.001	8.20	0.100

#### **12.4. Composition of chalcopyrite by LA-ICP-MS analysis**

Element		Co	Ni	Cu	Zn	As	Se	Ru	Rh	Pd	Ag	Cd	Sn	Sb	Te	Re	Os	Ir	Pt	Au	Pb	Bi
Isotope		59	61	65	66	85	82	101	103	108	109	111	120	121	128	185	190	193	195	197	208	209
VB21 (ppm)	1	4	79	13090	447	0.146	57.2	n.d.	n.d.	<0.012	0.895	5.79	7.04	<0.026	5.55	0.0063	<0.010	<0.003	<0.010	<0.006	4.64	0.021
	2	1.7	38	12180	460	0.177	70.1	n.d.	n.d.	<0.012	2.08	5.7	4.83	<0.026	19	<0.004	<0.010	0.016	<0.010	0.009	4.56	0.069
VB8 (ppm)	1	0.047	3.2	255700	434	0.168	51.5	n.d.	n.d.	<0.012	4.61	34.3	2.95	0.026	20.1	<0.004	<0.010	0.033	<0.010	0.008	4.53	0.256
	2	0.116	15.5	256200	403	<0.116	52.1	n.d.	n.d.	<0.012	3.64	30.3	3.08	<0.026	15.4	<0.004	<0.010	<0.003	<0.010	<0.006	2.9	0.129
	3	0.205	4.6	254700	930	0.4	55.6	n.d.	n.d.	<0.012	5.21	57	4.87	0.031	18.6	<0.004	<0.010	<0.003	<0.010	0.010	4.74	0.205
	4	0.113	7.9	255500	352	0.25	47.6	n.d.	n.d.	<0.012	2.07	24	3.02	<0.026	13	<0.004	<0.010	<0.003	<0.010	0.017	2.17	0.112
VB25 (ppm)	1	0.143	40.6	283500	334	<0.116	60.9	n.d.	n.d.	<0.012	1.32	11.9	6.09	0.157	7.29	<0.004	<0.010	<0.003	<0.010	<0.006	16.6	0.091
	2	0.086	36.6	283200	720	<0.116	55.7	n.d.	n.d.	<0.012	1.29	23.9	4.37	0.035	4.72	<0.004	<0.010	<0.003	<0.010	0.009	6.44	0.048
	3	0.102	37.5	282100	880	<0.116	64.4	n.d.	n.d.	<0.012	2.70	24.1	2.44	<0.026	10.6	<0.004	<0.010	<0.003	<0.010	0.008	8.56	0.042
VB26 (ppm)	1	0.177	42.1	294400	217	0.27	46.5	n.d.	n.d.	<0.012	0.395	4.95	3.33	<0.026	0.668	0.28	0.0154	0.0084	<0.010	<0.006	13.6	0.047
	2	0.066	37.7	293300	275	0.151	48.4	n.d.	n.d.	<0.012	0.323	5.93	1.98	<0.026	0.479	0.209	0.0154	0.0043	<0.010	<0.006	10.8	0.119
VB29 (ppm)	1	0.072	42.4	298900	351	<0.116	49.6	n.d.	n.d.	<0.012	1.17	12.9	4.96	<0.026	5.29	<0.004	<0.010	<0.003	<0.010	<0.006	3.39	0.075
	2	0.19	44.1	300300	350	0.101	53.9	n.d.	n.d.	<0.012	1.02	13.3	6.11	<0.026	4.92	0.027	<0.010	<0.003	<0.010	0.006	4.78	0.092
	3	0.26	45.5	307000	1080	0.129	50.3	n.d.	n.d.	<0.012	0.922	27.8	6.7	<0.026	3.59	<0.004	<0.010	<0.003	<0.010	0.010	4.83	0.119
	4	0.078	40.4	307500	1110	<0.116	48.6	n.d.	n.d.	<0.012	0.923	32.7	6.12	<0.026	3.76	<0.004	<0.010	<0.003	<0.010	<0.006	3.89	0.043
VB31 (ppm)	1	1.26	99	320400	540	<0.116	62.3	n.d.	n.d.	<0.012	1.87	21.9	8.09	0.53	8.65	<0.004	<0.010	<0.003	<0.010	0.015	50.4	0.211
	2	1.23	83	318700	290	<0.116	62.4	n.d.	n.d.	<0.012	2.28	14.5	8.62	0.037	8.56	<0.004	<0.010	<0.003	<0.010	0.031	32.8	0.329
	3	1.08	76	315400	520	<0.116	61.3	n.d.	n.d.	<0.012	1.90	21.7	7.91	<0.026	7.63	<0.004	<0.010	<0.003	<0.010	0.038	28.9	0.400
	4	13	458	311300	1100	<0.116	62.6	n.d.	n.d.	<0.012	2.91	40	7.68	0.031	8.38	<0.004	<0.010	<0.003	<0.010	0.020	50.8	0.251
VB36 (ppm)	1	0.054	39.1	317400	970	<0.116	50.2	n.d.	n.d.	<0.012	1.45	38.6	4.14	<0.026	1.16	0.0063	<0.010	0.012	<0.010	0.025	7.54	0.020
	2	0.13	48.9	317700	780	<0.116	57.7	n.d.	n.d.	<0.012	5.2	32.1	4.96	<0.026	12.4	<0.004	<0.010	<0.003	<0.010	0.023	12.3	0.029
		0.154	39.7	313400	620	<0.116	47.7	n.d.	n.d.	<0.012	0.858	22.5	3.16	<0.026	0.596	0.118	0.0168	<0.003	<0.010	0.013	5.39	0.043

## **12.5. Composition of cubanite by LA-ICP-MS analysis**

Element		Co	Ni	Cu	Zn	As	Se	Ru	Rh	Pd	Ag	Cd	Sn	Sb	Te	Re	Os	Ir	Pt	Au	Pb	Bi
Isotope		59	61	65	66	85	82	101	103	108	109	111	120	121	128	185	190	193	195	197	208	209
VB27 (ppm)	1	0.670	32.1	212900	2670	0.116	186	n.d.	n.d.	<0.012	27.6	473	10.3	0.175	31.9	<0.004	<0.010	<0.003	<0.010	<0.006	69.0	0.323
	2	0.158	25.1	214400	1380	<0.116	184	n.d.	n.d.	<0.012	43.0	236	11.2	<0.026	42.6	<0.004	<0.010	<0.003	<0.010	<0.006	43.0	0.480
	3	0.070	24.9	210500	1190	<0.116	177	n.d.	n.d.	<0.012	37.8	183	10.81	0.051	35.7	<0.004	<0.010	<0.003	<0.010	<0.006	31.4	0.249
	4	0.154	24.3	218800	2480	<0.116	188	n.d.	n.d.	<0.012	18.0	610	133	0.107	27.4	<0.004	<0.010	<0.003	<0.010	0.033	32.8	0.293
	5	0.781	56.9	215700	71.0	<0.116	178	n.d.	n.d.	<0.012	22.9	26.9	70.0	1.55	33.7	<0.004	<0.010	<0.003	<0.010	0.010	118	0.175
VB34 (ppm)	1	0.112	23.2	191100	1110	<0.116	148	n.d.	n.d.	<0.012	25.4	85	11.1	<0.026	27.0	<0.004	<0.010	<0.003	<0.010	0.029	16.8	0.157
	2	0.057	22.8	185600	1050	<0.116	143	n.d.	n.d.	<0.012	33.8	152	13.0	<0.026	31.2	<0.004	<0.010	<0.003	<0.010	0.015	25.8	0.259
	3	0.036	22.5	186500	790	<0.116	143	n.d.	n.d.	<0.012	23.4	120	12.9	<0.026	24.1	<0.004	<0.010	<0.003	<0.010	0.015	19.6	0.187
	4	2.51	59.8	186000	370	<0.116	147	n.d.	n.d.	<0.012	26.2	40.7	17.0	<0.026	30.3	<0.004	<0.010	<0.003	<0.010	0.013	14.4	0.139
VB5 (ppm)	1	1.99	51.0	185000	2390	0.19	148	n.d.	n.d.	<0.012	29.2	283	8.75	<0.026	27.0	<0.004	<0.010	<0.003	<0.010	0.014	39.8	0.330
	2	0.440	27.8	188200	740	0.119	153	n.d.	n.d.	<0.012	23.4	123	10.9	<0.026	23.3	<0.004	<0.010	<0.003	<0.010	0.019	30.8	0.447
	3	0.120	25.4	187400	1730	<0.116	152	n.d.	n.d.	<0.012	24.3	169	9.5	0.040	38.4	<0.004	<0.010	<0.003	<0.010	0.019	20.5	0.470
	4	0.115	22.3	185200	1610	<0.116	146	n.d.	n.d.	<0.012	46.0	287	13.2	<0.026	35.1	<0.004	<0.010	<0.003	<0.010	0.016	28.4	0.332
VB6 (ppm)	1	0.022	41.5	276400	633	<0.116	69.0	n.d.	n.d.	<0.012	4.01	33.3	22.8	0.051	8.87	<0.004	<0.010	<0.003	<0.010	0.062	0.812	0.102
	2	0.024	33.7	276100	680	<0.116	69.2	n.d.	n.d.	<0.012	2.02	36.5	43.2	0.030	3.33	<0.004	<0.010	<0.003	<0.010	0.047	5.97	0.068
	3	0.047	35.8	280200	920	<0.116	67.1	n.d.	n.d.	<0.012	3.18	44.2	45.4	<0.026	5.61	<0.004	<0.010	<0.003	<0.010	0.031	7.99	0.380
	4	0.019	38.9	274800	558	<0.116	70.4	n.d.	n.d.	<0.012	4.40	34.2	26.0	<0.026	7.63	<0.004	<0.010	<0.003	<0.010	0.059	8.05	0.080
	5	0.048	35.6	278400	1100	<0.116	81.9	n.d.	n.d.	<0.012	7.40	72.0	14.2	<0.026	18.9	<0.004	<0.010	<0.003	<0.010	0.025	3.12	0.192

## **12.6. Reference material for LA-ICP-MS analysis**

	Element	Co	Ni	Cu	Zn	As	Se	Ru	Rh	Pd	Ag	Cd	Sn	Sb	Te	Re	Os	Ir	Pt	Au	Pb	Bi	
	Isotope	59	61	65	66	85	82	101	103	108	109	111	120	121	128	185	190	193	195	197	208	209	
<b>JB-MSS5</b>	Working Value (ppm)		10487	205		79	47	21.72	61.4	61.4	53			61.3		20.7	45.52	43.98	39.9	35.9	71.5	76.1	
	Average (ppm) n=15		10485	171		63.5	58.8	20.0	60.1	54.5	44.5			54.8		20.7	51.6	38.1	38.6	35.6	64.3	68.7	
	Standard Deviation		159	76.6		22.8	7.81	0.922	3.38	1.34	2.93			6.06		0.178	6.14	2.30	1.57	1.82	3.30	5.68	
	RSD (%)		1.52	44.9		35.8	13.3	4.61	5.63	2.45	6.58			11.1		0.860	11.9	6.05	4.07	5.11	5.13	8.27	
<b>GSE</b>	Working Value (ppm)	380	440		460	260	20.0					200	160	280	450							378	320
	Average (ppm) n=9	338	438		784	342	115					143	221	314	346							350	293
	Standard Deviation	12.1	10.9		243	23.4	26.8					4.70	20.7	6.61	8.39							9.01	10.0
	RSD (%)	3.56	2.49		31.0	6.85	23.4					3.29	9.36	2.11	2.42							2.57	3.41
<b>Po-727</b>	Working Value (ppm)							36.4	41.6	43.8						46.9	47.8	35.4	45.8				
	Average (ppm) n=17							36.5	41.6	43.4						46.7	48.0	35.5	45.7				
	Standard Deviation							0.387	0.437	0.664						0.579	0.740	0.570	1.06				
	RSD (%)							1.06	1.05	1.53						1.24	1.54	1.61	2.31				
<b>MASS-1</b>	Working Value (ppm)	60.0		134000	210000	65.0	51.0				50.0	60.0	59.0	60.0	15.0							68.0	60.0
	Average (ppm) n=16	60.5		122069	210113	65.0	51.0				50.0	60.2	59.1	60.0	15.0							68.4	60.1
	Standard Deviation	1.62		11254	3651	1.02	1.06				0.831	2.05	0.760	0.879	0.276							1.85	0.975
	RSD (%)	2.68		9.22	1.74	1.57	2.07				1.66	3.41	1.29	1.47	1.84							2.70	1.62